**(Electronic Supporting Information)**

# Heterogeneous C─H Functionalization in Water *via* Porous Covalent Organic Framework Nano Films: A Case of Catalytic Sphere Transmutation

Himadri Sekhar Sasmal,[1,2] Saikat Bag,[1,2] Bittu Chandra,[1] Poulami Majumder,[1,2] Himangshu Kuiry,[1] Sayam Sen Gupta,[1,*] and Rahul Banerjee[1,2,*]

[1]*Department of Chemical Sciences, Indian Institute of Science Education and Research, Kolkata, Mohanpur 741246, India.*

[2]*Centre for Advanced Functional Materials, Indian Institute of Science Education and Research, Kolkata, Mohanpur 741246, India.*

*****Email: sayam.sengupta@iiserkol.ac.in; Tel: +033-6136-0000-1309.*

*****Email: r.banerjee@ncl.res.in; Tel: +033-6136-0000-1327.*

.

## Table of Contents

## Section S-1: General Information

**Powder X-ray diffraction (PXRD)** data were collected by using a Rigaku, MicroMax-007HF which was equipped with intensity microfocus rotating anode as the X-ray generator. The radiation used for diffraction was Cu $K_\alpha$ ($\alpha$ = 1.54 Å) with a Ni filter. A Rigaku, R-axis IV++ detector was employed for the wide-angle experiments. All the PXRD data of Covalent Organic Framework (COF) nano-spheres as well as COF thin films were recorded in the range of $2\theta$ = 2–35°. For polyester membranes and catalyst embedded TpDPP COF film fabricated on polyester membranes, PXRD data were also collected in the range of $2\theta$ = 2-35°. The scan speed and the step size were set to 1° $min^{-1}$ and 0.02° respectively. The corresponding data were collected with the help of Control Win software.

**Fourier transform infrared (FT-IR)** spectra of the solid samples were recorded on a Bruker Optics ALPHA II spectrometer with a universal Zn-Se ATR (attenuated total reflection) accessory. All the data have been reported in wavenumber ($cm^{-1}$) scale.

**Nitrogen adsorption experiments** (0 to 1 bar) were performed using Quantachrome Quadrasorb automatic and Autosorb iQ instrument. The nitrogen adsorption isotherms were collected at 77 K using a liquid nitrogen bath. Before performing gas adsorption experiments, TpDPP COF nano-spheres, TpDPP COF thin films (synthesized *via* covalent self-assembly of TpDPP nano-spheres at the water-DCM interface), and TpDPP COF crystallites in powder form (synthesized *via* salt mediated crystallization approach)[1] were degassed at 140°C for 12 hrs under vacuum. Surface areas were calculated using the Brunauer-Emmett-Teller (BET) model applied between $P/P_0$ values of 0.05 and 0.3 for microporous and mesoporous COFs. Corresponding pore size distributions were calculated using the non-localized density functional theory (NLDFT).

**Carbon dioxide adsorption experiments** (0 to 1 bar) were performed using Quantachrome Quadrasorb automatic instrument. The $CO_2$ adsorption isotherms were collected at 293 K. Prior to the $CO_2$ adsorption experiment, TpDPP COF nano-spheres and TpDPP COF thin film were degassed at 140°C for 12hrs under vacuum using FloVac degasser.

**Thermogravimetric analysis (TGA)** was carried out on a Mettler-Toledo TG50 and SDT Q600 TG-DTA analyzer under $N_2$ atmosphere from 30°C to 900°C along with a ramp rate of

10°C $min^{-1}$. Before carrying out the TGA, the samples were activated at 100°C for 30 minutes to eliminate the water from the samples.

**Scanning Electron Microscopy (SEM)** images were obtained using Zeiss DSM 950 and FEI QUANTA 200 3D microscope operating at 10 kV using tungsten filament as the electron source. Prior to the imaging, the samples were sputtered with gold (nano-sized film) using an SCD 040 Balzers Union sputterer to avoid charging during SEM analyses. The samples were prepared simply by putting a drop of dispersed samples (COF nano-spheres, COF films, and the intermediate states during the transmutation) in DCM on a clean piece of Silicon wafer. Elemental mapping of the TpDPP COF nano-spheres, TpDPP COF films, $Fe^{III}$(Cl)bTAML@TpDPP COF nano-spheres, $Fe^{III}$(Cl)bTAML@TpDPP COF films were also recorded using SEM with energy dispersive X-ray spectrometry (EDS).

**Transmission Electron Microscopy (TEM)** images were obtained using FEI Tecnai G2 F20 X-TWIN TEM at an accelerating voltage of 200 kV. The samples were prepared by direct drop-casting (dispersed in DCM) onto copper grids TEM Window (TED PELLA, INC. 200 mesh)

**Ultraviolet-Visible Spectroscopy (UV-Vis)** data were measured using Agilent's Cary 8454 UV-Visible spectroscopy system equipped with 10 mm pathlength quartz cuvette having the volume of 500 µl at room temperature.

**Dynamic Light Scattering (DLS)** experiments were performed using Litesizer™ 500 equipped with a 658 nm, 40mW laser at 20°C with 10 mm pathlength quartz cuvette. The data was analyzed using Kalliope™ software.

**Confocal Laser Scanning Microscopy (CLSM)** images were collected using Carl Zeiss LSM 710 confocal workstation. The as-synthesized TpDPP COF nano-spheres were treated with $Et_3N$ and then Rhodamine B dye was adsorbed within the porous scaffold. Further, the TpDPP COF nano-spheres were effectively utilized for the fabrication of COF thin film using multiple drop-casting technique and the transmutation of COF nano-spheres to the COF films *via* the generation of COF fibers were monitored by time-dependent confocal imaging.

**Raman Spectroscopy** experiments were performed were carried out using LabRam HR 800 micro-Raman spectrometer with a resolution of about 1.2 $cm^{-1}$. A grating of 1500 grooves

$mm^{-1}$ was used to collect the Raman spectrum. Samples were excited by a diode laser having the wavelength of 785 nm and Raman scattered signals were collected in the backscattering geometry.

**X-ray Photoelectron Spectroscopy (XPS)** analysis was carried out using Thermo Scientific's K-Alpha$^{+}$ spectrometer. The pass energy for the survey scan and the high-resolution scan was maintained at 100 eV and 50 eV respectively where the angle between the analyzer and sample surface was 90°.

**Electron Paramagnetic Resonance (EPR)** spectroscopy was studied on dispersed powdered products (catalyst immobilized TpDPP COF nano-spheres and catalyst loaded TpDPP COF thin film) in acetonitrile by a conventional Bruker spectrometer (Bruker, EMXmicro) operating at X-band frequency and magnetic field modulation of 100 kHz, with a microwave power of 2.25 mW and modulation amplitude of 1 G at 123 K. The resonance lines were simulated by the Bruker WINEPR SimFonia program.

**pH measurement** of the reaction mixture with respect to time was carried out at 25°C using a LABARD advance microprocessor pH meter having 5-point calibration.

**Gas Chromatography-Mass Spectrometry (GC-MS)** was performed on a Thermo Scientific ISQ QD Mass Spectrometer attached with Thermo Scientific TRACE 1300 gas chromatograph using an HP-5 ms capillary column (30 m × 0.25 mm × 0.25 μm, J&W Scientific) with helium as the carrier gas. GC−MS method: oven temperature program, 18 min; initial temperature, 60 °C, hold for 2.00 min; ramp-1, 15 °C $min^{-1}$ to 180°C, hold for 1 min; ramp-2, 20 °C C $min^{-1}$ to 280°C, hold for 1 min; injector temperature, 220 °C; detector temperature, 280 °C.

## Section S-2: Materials and Synthetic Procedures

### Materials

For the synthesis of TpDPP COF nano-spheres, the starting materials 1,3,5–triformylphloroglucinol (**Tp**) was synthesized following the previously reported literature protocols.[1] The commercially available 3,8-diamino-6-phenylphenanthridine (**DPP**), trifluoroacetic acid (**TFA**) were purchased from Thermo Fischer Scientific and Avra Synthesis. The first member of the fifth-generation biuret modified TAML, $(Et_4N)_2[Fe^{III}(Cl)bTAML]$ catalyst was synthesized following the reported literature.[2] All the commercially available substrates for functionalization C─H bond such as Adamantane, *cis*-1,2-dimethylcyclohexane, *trans*-1,2-dimethylcyclohexane, *cis*-decahydronaphthalene, ethylbenzene, diphenylmethane, fluorene, 9,10-dihydroanthracene, styrene, *cis*-cyclooctene, ambroxide, and cedryl acetate were bought from Sigma-Aldrich, TCI chemicals and were used after column purification. All the catalysis reactions were performed under open air at room temperature in acetonitrile and pure water as the reaction medium in heterogeneous conditions.

### Synthetic Procedure

**Synthesis of TpDPP COF nano-spheres.** In the first step, in a typical synthesis,[3] the diamine (0.045 mmol) (**DPP**) was added into 100 ml dry dichloromethane (DCM) at room temperature, which resulted in a transparent homogeneous solution (light greenish-yellow). Trifluoroacetic acid (10-15 µl) was added directly to the solution as the catalyst for Schiff base reaction which turned the colour of the solution from light greenish-yellow to orange. Finally, a solution of 0.03 mmol trialdehyde (**Tp**) in 100 ml dry DCM was added slowly with stirring at room temperature. The reaction mixture was refluxed in a 250 ml round bottom flask at 70°C under $N_2$ atmospheres. After 12-15 hours, when all the starting materials were consumed, the colloidal solution of TpDPP COF nano-spheres was obtained. The transparent reaction mixture started becoming opaque during the course of the reaction and gradually became a well-dispersed colloidal solution with a bright orange colour. The solution-processable COF nano-spheres were purified by dialysis tubing using a semipermeable cellulose membrane with pore size 12 kDa MWCO. The COF nano-spheres could easily be separated from solution as precipitate *via* centrifugation (or by addition of non-polar solvents like hexane). Consequently, the as-synthesized COF nano-spheres could also be easily purified by dispersing isolated COF nano-spheres in fresh DCM by mild sonication. After complete precipitation/isolation of all

the COF nano-spheres, the precipitate was collected and washed thoroughly with Dimethylacetamide (DMAc) followed by dry acetone and isolated as power after drying in an oven at 120°C. These isolated and purified TpDPP COF nano-spheres were characterized using PXRD, IR, $N_2$ and $CO_2$ adsorption analyses, DLS and zeta potential measurement, TEM, SEM, and AFM. The as-synthesized colloidal solution of COF nano-spheres are very much stable and durable for several months (more than 4 months) without any changes in the particle size, Ostwald ripening, or any other structural transmutation and deformation in DCM.

**Immobilization of $(Et_4N)_2[Fe^{III}(Cl)bTAML]$ catalyst within TpDPP COF nano-spheres scaffold.** After synthesis and thorough characterization of the TpDPP COF nano-spheres, we investigated their adsorption capacity. At first, we took 1 mg of the purified and isolated TpDPP COF nano-spheres and measured their adsorption capacity towards different concentrations of the anionic macrocyclic catalyst **$(Et_4N)_2[Fe^{III}(Cl)bTAML]$** in acetonitrile. We took 1 ml catalytic solution in acetonitrile of different concentrations (0.2 mM, 0.4 mM and, 0.8 mM) and for each solution, we dispersed 1 mg of TpDPP COF nanosphere into the solutions *via* mild sonication. After that, we stirred the solution for 15 minutes. After 15 minutes TpDPP COF nano-spheres were isolated from the solution *via* centrifugation and from measuring the UV of each batch of catalytic solutions, we determined the adsorption capacity of the TpDPP COF nano-spheres. 1.0 mg of solid COF nano-spheres can immobilize 95% and 94.8% $(Et_4N)_2[Fe^{III}(Cl)bTAML]$ catalyst from 1 ml 0.2 and 1 ml 0.4 mM solution in acetonitrile. The same amount of COF nano-spheres (1.0 mg) can adsorb 66.8% of the catalyst molecules from 1 ml 0.8 mM solution in acetonitrile.

Now for both the homogeneous and heterogeneous C─H functionalization we have fixed the catalytic concentration as $4 \times 10^{-4}$ M or 0.4 mM (5 mol%) and substrate concentration as $8 \times 10^{-3}$ M (20 equivalent of catalyst). We have carried out the catalysis reaction for all the substrates in 1 ml of acetonitrile (in the case of TpDPP nano-spheres) and 1 ml of pure water (in the case of TpDPP thin film). Hence, we had taken 1 ml of 0.4 mM catalytic solution and added 1 mg of purified TpDPP COF nano-spheres into it. After mild centrifugation, TpDPP nano-spheres dispersed into the acetonitrile and after 15 minutes when the immobilization of the catalyst molecules within the COF nano-spheres scaffold was completed we collected the $[Fe^{III}(Cl)bTAML]^{2-}$@1X TpDPP COF nano-spheres as the heterogeneous catalyst *via* centrifugation. After drying the $[Fe^{III}(Cl)bTAML]^{2-}$@1X TpDPP COF nano-spheres catalyst properly with vacuum we have thoroughly characterized the wt% loading of $[Fe^{III}(Cl)bTAML]^{2-}$ catalyst within the TpDPP COF nano-spheres *via* TGA and ICP-MS. Now

keeping the catalyst amount constant (1 ml 0.4 mM) and increasing the COF nano-spheres amount from 1 mg to 2 mg, 3 mg and, 4 mg we had immobilized catalysts within the TpDPP COF nano-spheres and isolated $[Fe^{III}(Cl)bTAML]^{2-}$@2X TpDPP COF nano-spheres, $[Fe^{III}(Cl)bTAML]^{2-}$@3X TpDPP COF nano-spheres and $[Fe^{III}(Cl)bTAML]^{2-}$@4X TpDPP COF nano-spheres respectively. For optimization, we have carried out hydroxylation of the 3° C─H of adamantane with all 4 sets of heterogeneous catalysts keeping all the other catalytic parameters constant. Among them $[Fe^{III}(Cl)bTAML]^{2-}$@2X TpDPP COF nano-spheres catalyst showcased the highest catalytic activity as well as selectivity. Hence we had carried out the rest of all substrate scope using the $[Fe^{III}(Cl)bTAML]^{2-}$@2X TpDPP COF nano-spheres as the heterogeneous catalyst.

**Fabrication of $[Fe^{III}(Cl)bTAML]^{2-}$@TpDPP COF thin film/nanofilm.** Initial attempts for C-H functionalization in water using $[Fe^{III}(Cl)bTAML]^{2-}$@TpDPP COF nano-spheres were unsuccessful since the TpDPP COF nano-spheres, which were very dispersible in $CH_3CN$, aggregated in water. However, the individual TpDPP COF nano-spheres undergo covalent self-assembly among themselves in the water-DCM bilayer or even while drop-casted on top of any support and eventually form uniform TpDPP COF nanofilm. The COF thin films or nanofilms (since the thickness is in the nanometer scale) are even more crystalline, porous than COF nano-spheres, and are quite stable (does not undergo any further transmutation) in water. Hence, we decided to construct TpDPP COF thin films from the catalyst immobilized TpDPP COF nano-spheres *via* covalent self-assembly. We had carried out the fabrication of $[Fe^{III}(Cl)bTAML]^{2-}$@TpDPP COF thin film in two different ways.

**Covalent self-assembly of COF nano-spheres at the liquid-liquid interface:** In the first method, we had taken $[Fe^{III}(Cl)bTAML]^{2-}$@TpDPP COF nano-spheres dispersed in DCM in a closed container, and on the top of the DCM layer, slowly we had added water to form the DCM-water bilayer. In the DCM-water bilayer, the $[Fe^{III}(Cl)bTAML]^{2-}$@TpDPP COF nano-spheres started assembling which was driven by surface tension and after 1 day a uniform film was formed. The film was collected from the interface, washed with DCM, and dried in vacuum before going through all the characterization and catalytic applications. The energy dispersive X-ray spectrometry (EDS) mapping showcased the presence of well-distributed immobilization of the $(Et_4N)_2[Fe^{III}(Cl)bTAML]$ catalyst within the TpDPP COF thin film. We had used TGA and ICP-MS to determine the wt% of the catalyst immobilized with the scaffold of TpDPP COF thin film and accordingly we had carried out the C─H functionalization of various substrates in water using $[Fe^{III}(Cl)bTAML]^{2-}$@TpDPP COF thin film.

**Covalent self-assembly *via* multiple drop-casting of COF nano-spheres:** On the other hand, the multiple drop-casting was effectively utilized for the self-assembly of $[Fe^{III}(Cl)bTAML]^{2-}$@TpDPP COF nano-spheres driven by the evaporation of the solvent molecules to form crystalline though flexible, uniform catalyst impregnated COF thin film. Herein, the drop-casting method was based on the solvent evaporation from the droplets of colloidal TpDPP COF nano-spheres suspension deposited on the macroporous polymeric support. The evaporation of solvent molecules induced the formation of the meniscus between two COF nano-spheres and therefore attractive capillary forces and convective transport of the COF nano-spheres drove their self-assembly. In the drop-casting technique, although controlling the uniformity is challenging usually resulting in the 'coffee-ring' effect i.e., the droplets on solid support gradually dry into a ring-like dense deposit along the perimeter. However multiple numbers of the successful casting of the COF colloidal droplets at predetermined regions on the polymeric support, the slow evaporation of the solvent (acetonitrile) and most importantly the further covalent self-assembly between the congregated COF nano-spheres eventually led to the formation of COF thin film with uniform thickness. The covalent self-assembly which was driven by the free amine and aldehyde functionality of the COF nano-spheres occurred in an unusual way that was previously hidden and unheard of. As the solvent molecules started evaporating the individual COF nano-spheres were energetically destabilized. As a consequence, when the two individual spheres came in contact, they started reacting *via* reversible Schiff base reaction, provoked, and initiated the protrusion of the fibers/threads at their interface. With time, the distribution of fibers was enhanced and after 2 days, most of the nano-spheres were transmuted into the interconnected fibers. Further, after the time interval of 3 days, the covalent self-assembly of the interconnected fibers accomplished the formation of COF thin film of thicknesses of 200-300 nm regulated from the SEM analyses. In order to fabricate self-standing $[Fe^{III}(Cl)bTAML]^{2-}$@TpDPP COF thin film *via* multiple drop-casting, we drop-casted the $[Fe^{III}(Cl)bTAML]^{2-}$@TpDPP COF nano-spheres on the sugar plate as a support which is insoluble in acetonitrile but soluble in water. Consequently, after the complete formation of the catalytic COF thin film on top of the sugar plate (having a smooth surface), we dissolved the sugar plate in water, isolated purified the $[Fe^{III}(Cl)bTAML]^{2-}$@TpDPP COF thin film from the aqueous medium. This catalytic COF thin film was also uniformly immobilized with the catalysts which were confirmed from the EDX analyses.

The fundamental difference between the two types of covalent self-assembly is that in the DCM-water interface the spheres undergo covalent self-assembly without forming any thread or fibers whereas, in the case of multiple drop-casting, the transmutation of spheres to film

occurs through the generation of threads or fibers as intermediates and eventually the fibers get connected *via* covalent self-assembly to form COF thin film.

## Section S-3: Structure Modelling, Powder X-Ray Diffraction Analysis, and Refinement Data

Atomic positions and cell sizes of modeled COF layers were optimized using the Self Consistent Charge-Density Functional Tight Binding (SCC-DFTB) method. The layer stacking is affected by the Coulomb repulsion between the partial atomic charges in adjacent layers.[4] Hence, several slipped AA stacking possibilities were considered for each COF by shifting adjacent layers with respect to each other in different directions up to 6Å. The predicted slipped structure has the lowest energy while maintaining the agreement with the experimental PXRD pattern. The TpDPP COF has been modeled in the triclinic space group (P1) by comparing the experimental and simulated PXRD patterns. Refinements of the PXRD pattern were done using the Reflex module of the Material studio.

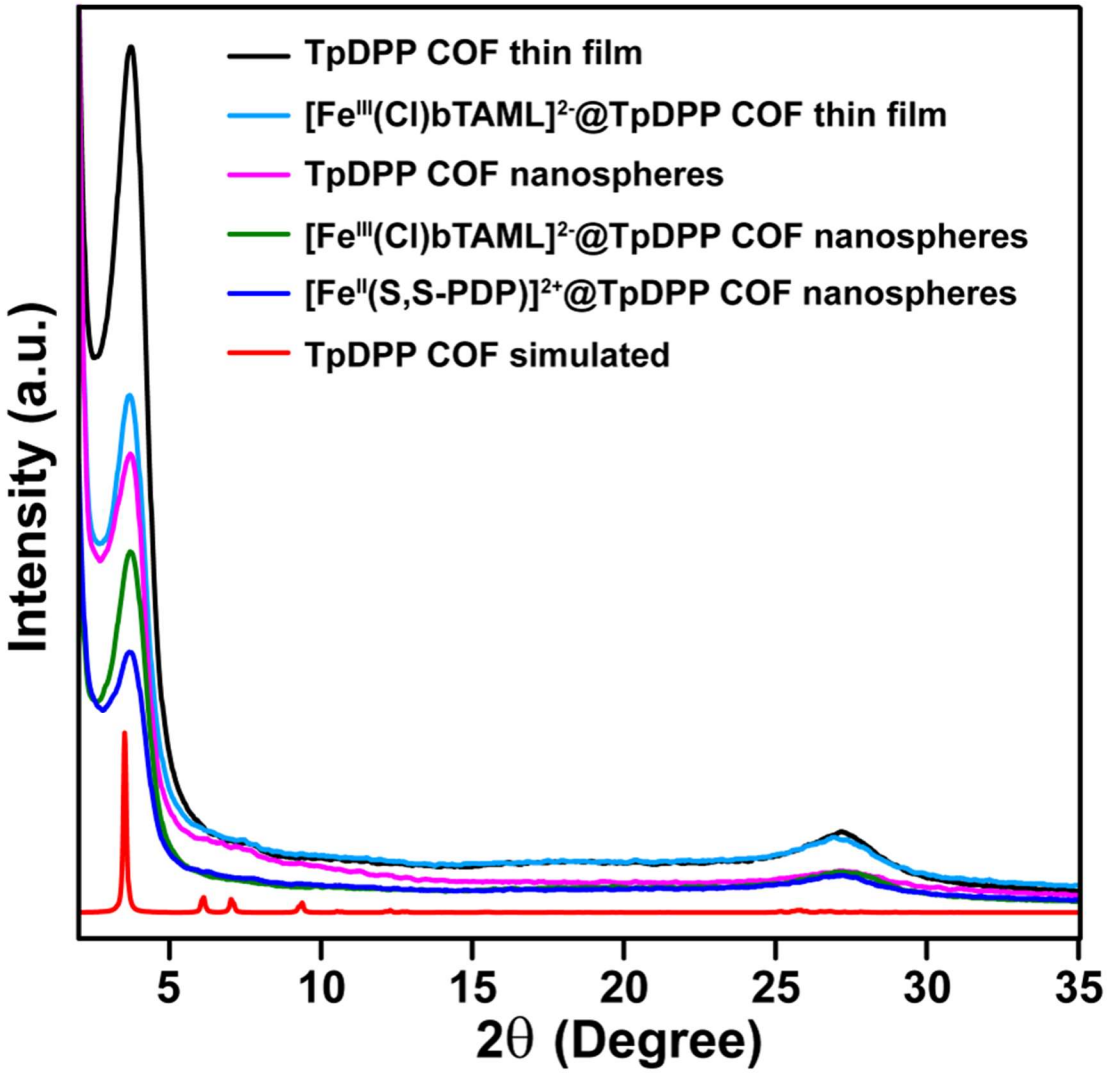

**Figure S1**. Experimental PXRD patterns of TpDPP COF nano-spheres, TpDPP COF thin film (synthesized by the self-assembly of TpDPP COF nano-spheres at the DCM-water interface), $[Fe^{III}(Cl)bTAML]^{2-}$@TpDPP COF nano-spheres, $[Fe^{III}(Cl)bTAML]^{2-}$@TpDPP COF thin film, and $[Fe^{II}(S,S\text{-}PDP)]^{2+}$@TpDPP COF nano-spheres in comparison with the simulated AA slipped (slipped eclipsed) pattern of the TpDPP COF.

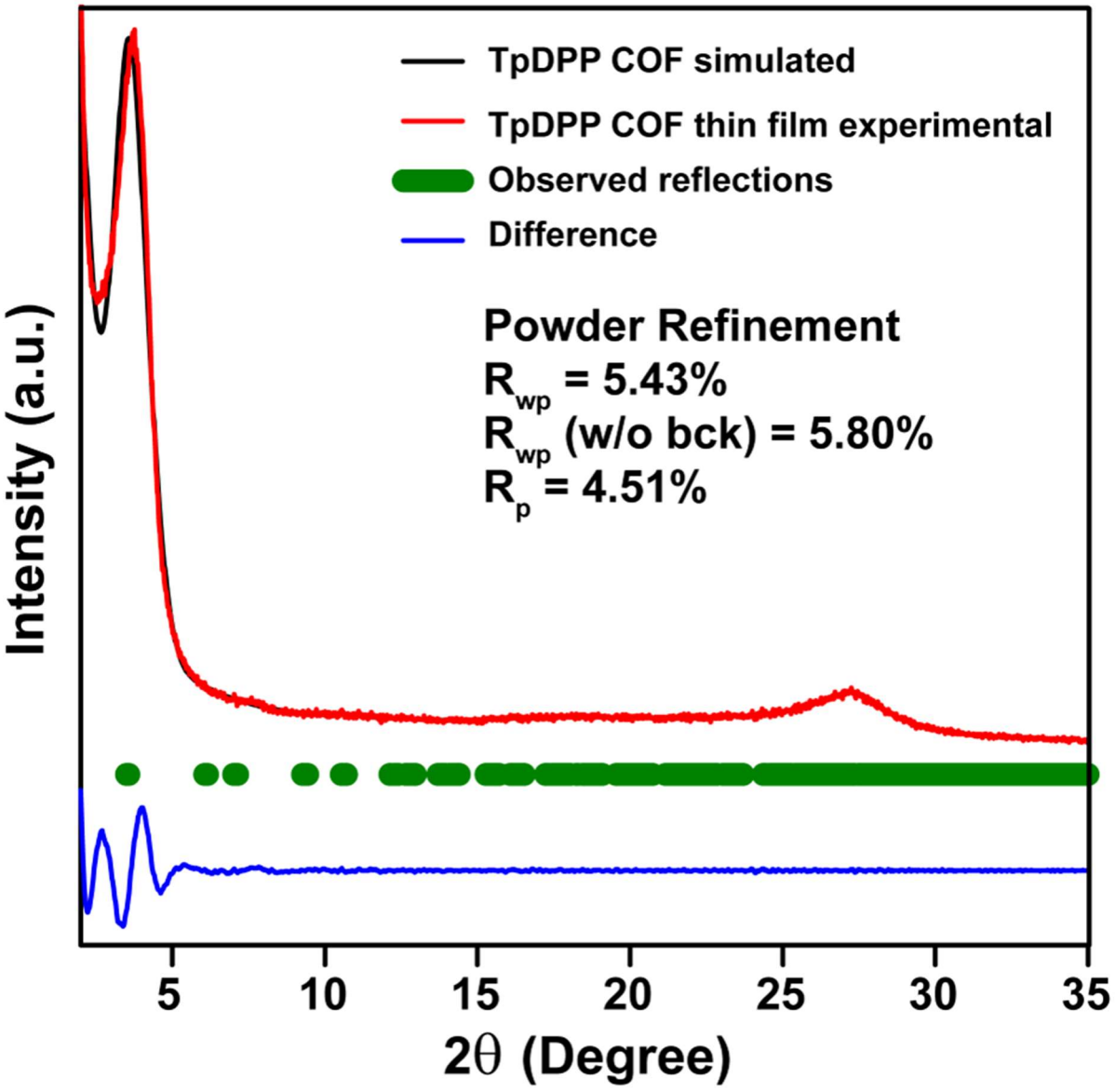


**Figure S2**. Pawley refinement patterns for TpDPP COF thin film indicate that the experimental and modeled (slipped eclipsed stacking) PXRD patterns are fairly matching.

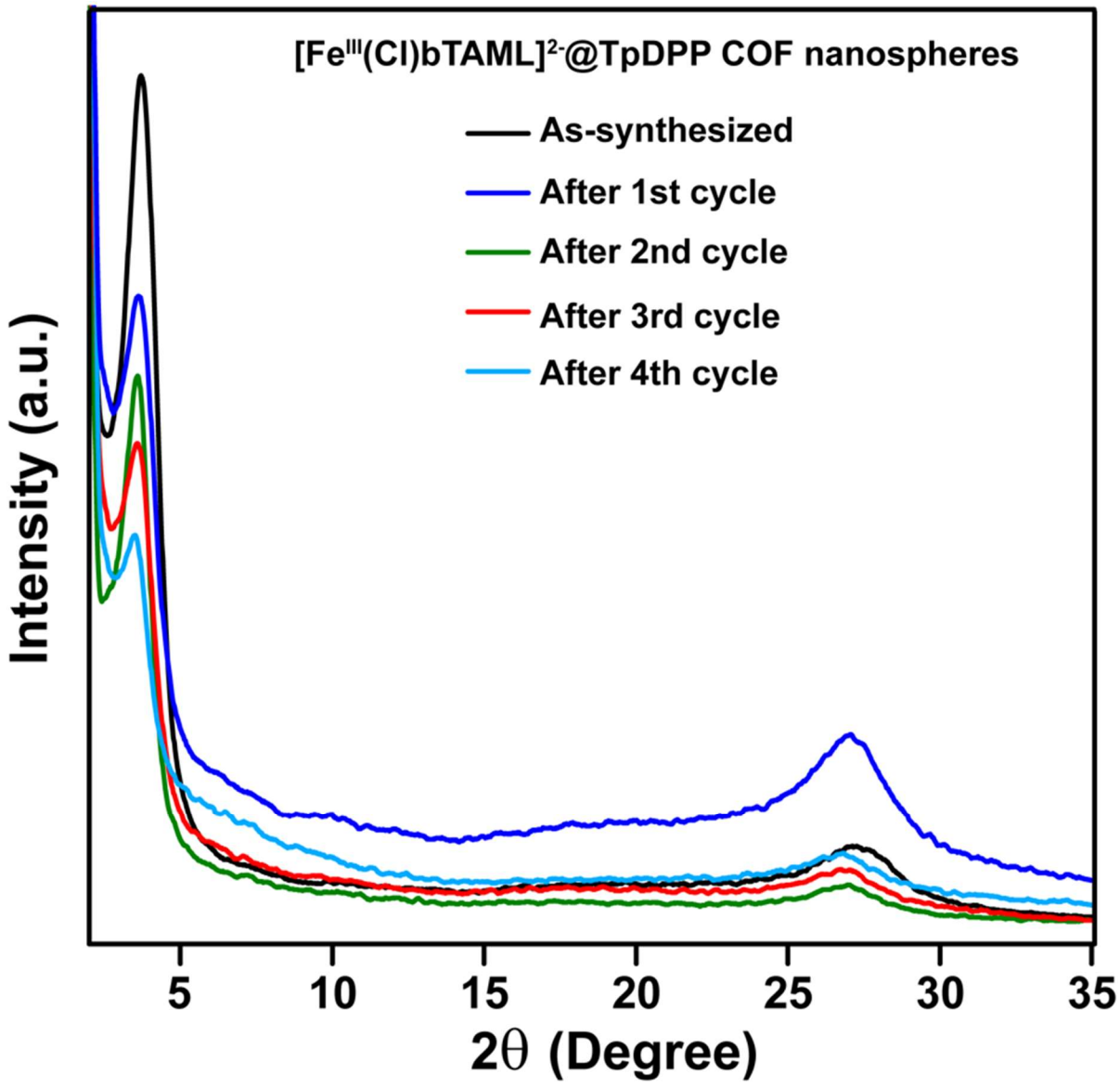


**Figure S3**. PXRD of the as-synthesized [Fe$^{III}$(Cl)bTAML]$^{2-}$@TpDPP COF nano-spheres and PXRD of the [Fe$^{III}$(Cl)bTAML]$^{2-}$@TpDPP COF nano-spheres after completing the catalytic 1$^{st}$, 2$^{nd}$, 3$^{rd}$, and 4$^{th}$ cycles of reactions (during the recyclability of [Fe$^{III}$(Cl)bTAML]$^{2-}$@TpDPP COF nano-spheres).

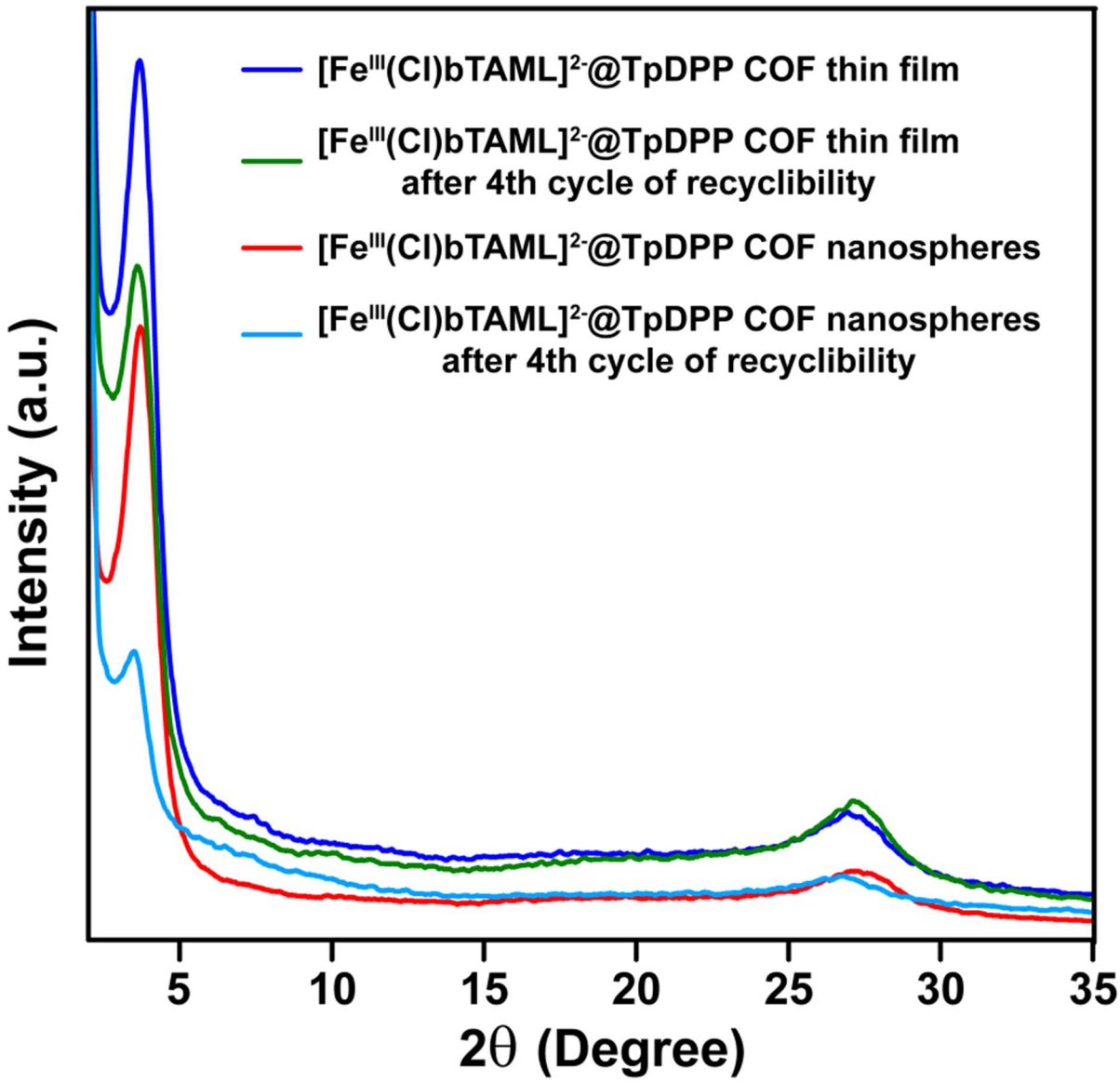


**Figure S4**. PXRD of the as-synthesized [Fe$^{III}$(Cl)bTAML]$^{2-}$@TpDPP COF nano-spheres and [Fe$^{III}$(Cl)bTAML]$^{2-}$@TpDPP COF thin film. After performing the catalytic reactions with recyclability up to 4 cycles, their structural backbones remain crystalline.

## Section S-4: FT-IR Spectra

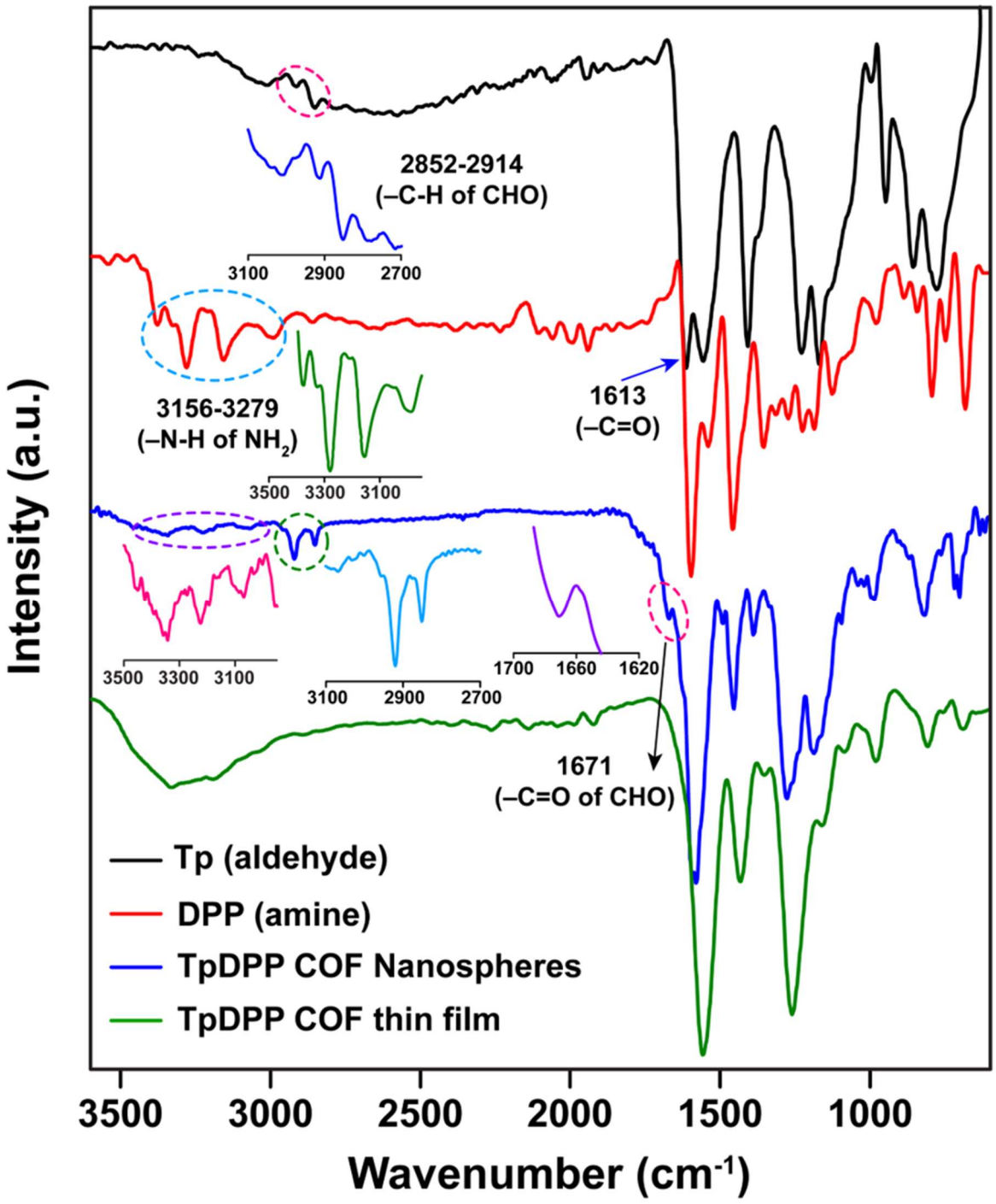


**Figure S5**. Comparison of FT-IR spectra between as-synthesized TpDPP COF nano-spheres, and TpDPP COF thin film with the starting materials (aldehyde and amine)/structural building units. FT-IR Spectra of TpDPP COF nano-spheres reveals the presence of free aldehyde and amine functionality presence within their structural backbone. Both the spectra of TpDPP COF nano-spheres and TpDPP COF thin film also show characteristic peaks corresponding to β-ketoenamine linked framework structure.

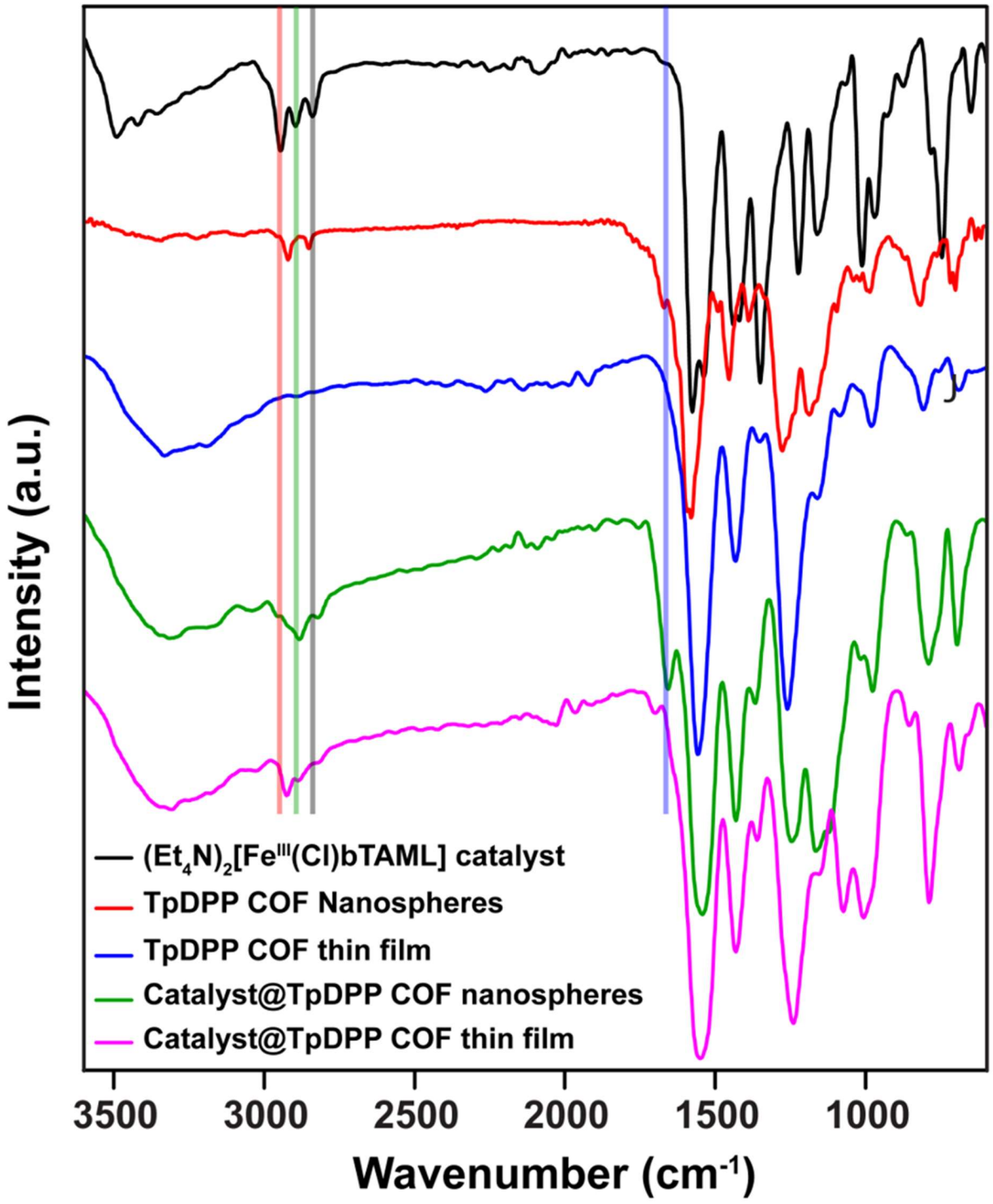


**Figure S6**. Comparison of FT-IR spectra between as-synthesized TpDPP COF nano-spheres, TpDPP COF thin film, $(Et_4N)_2[Fe^{III}(Cl)bTAML]$ catalyst, $[Fe^{III}(Cl)bTAML]^{2-}$@TpDPP COF nano-spheres, and $[Fe^{III}(Cl)bTAML]^{2-}$@TpDPP COF thin film. The spectral analysis showcases the incorporation/immobilization of catalyst within the TpDPP COF nano-spheres as well as TpDPP COF thin film scaffold.

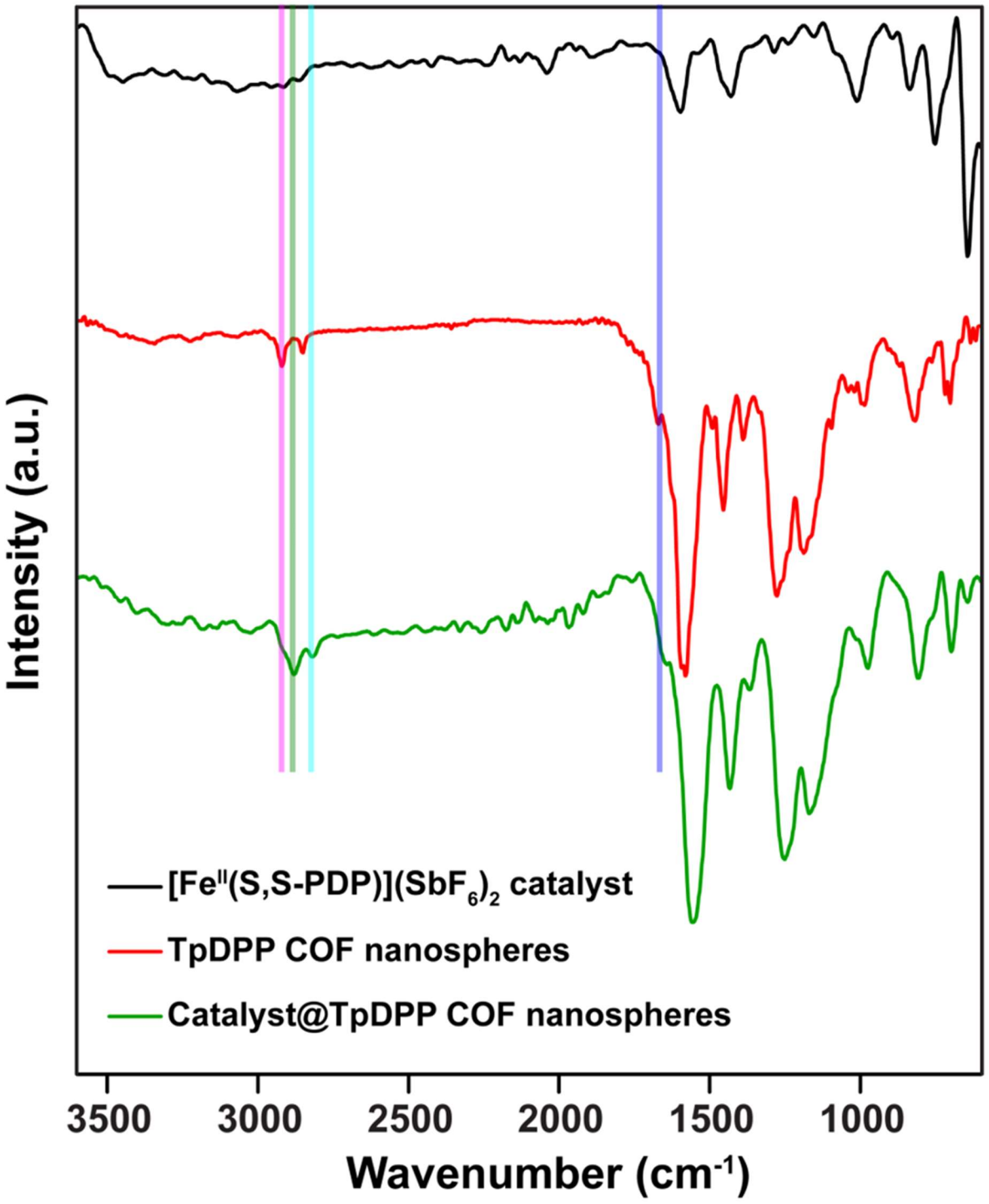


**Figure S7**. Comparison of FT-IR spectra between as-synthesized TpDPP COF nano-spheres, [$Fe^{II}$(S,S-PDP)]($SbF_6$)$_2$ catalyst, and [$Fe^{II}$(S,S-PDP)]$^{2+}$@TpDPP COF nano-spheres. The spectral analysis showcases the incorporation/immobilization of catalyst within the TpDPP COF nano-spheres scaffold.

## Section S-5: Nitrogen and Carbon Dioxide Adsorption Experiment

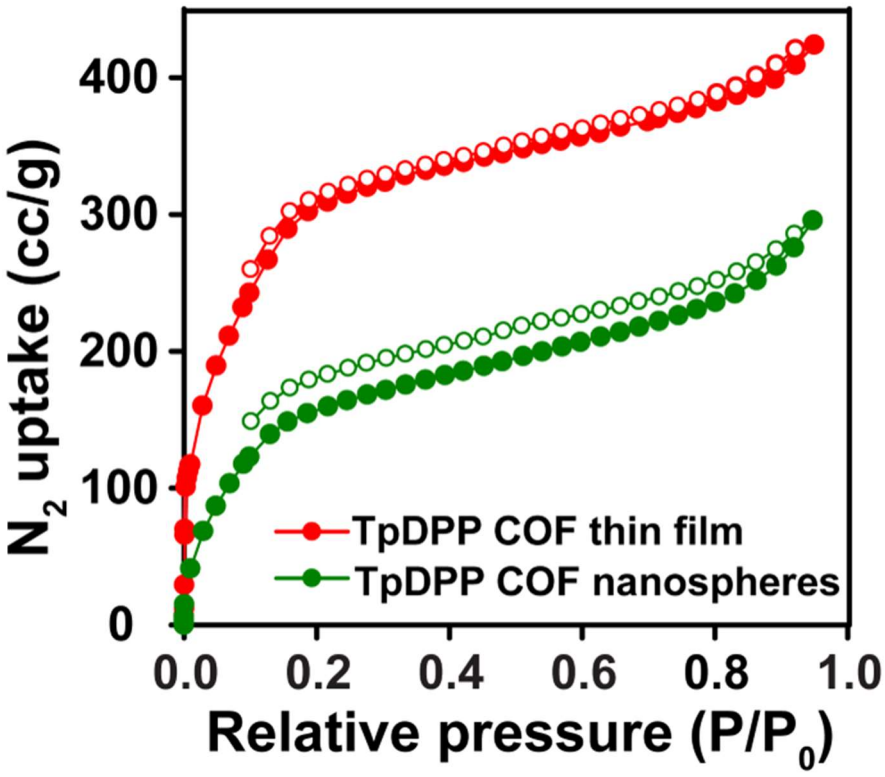


**Figure S8**. $N_2$ adsorption experiment of the purified and isolated TpDPP COF nano-spheres and TpDPP COF thin film. From the isotherm, the surface area ($S_{BET}$) of the TpDPP COF nano-spheres and TpDPP COF thin film were calculated to be 686 $m^2g^{-1}$ and 1265 $m^2g^{-1}$ respectively.

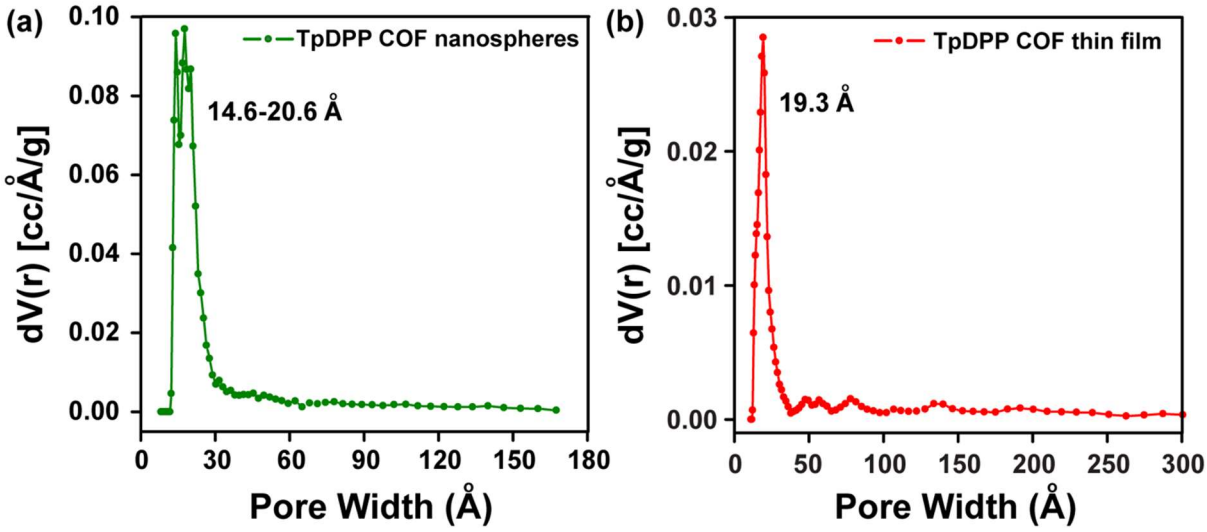


**Figure S9**. The pore size distribution of the (a) TpDPP COF nano-spheres and (b) TpDPP COF thin film obtained from the $N_2$ adsorption experiment. Pore size distributions were calculated using the density functional theory (NLDFT/QSDFT) model.

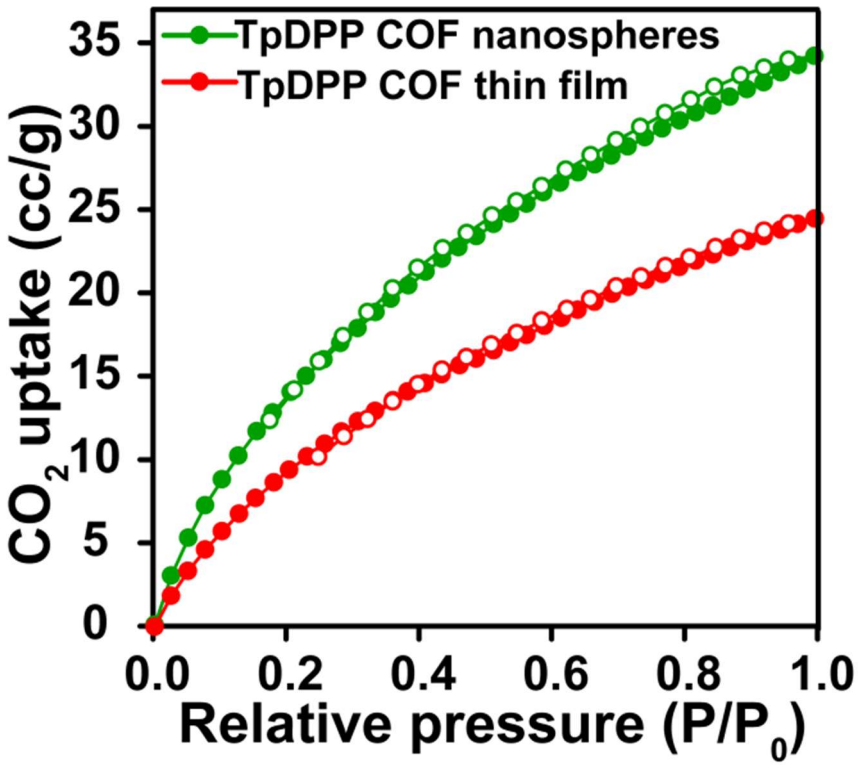


**Figure S10**. The TpDPP COF nano-spheres having the surface area of 686 $m^2g^{-1}$ showcased $CO_2$ uptake capacity of 34 $cm^3g^{-1}$ at 25 °C and 1 bar whereas the TpDPP COF thin film obtained from the covalent self-assembly TpDPP COF nano-spheres at DCM-water interface having a much higher surface area of 1265 $m^2g^{-1}$ could absorb only 24 $cm^3g^{-1}$ at 25 °C and 1 bar. The higher $CO_2$ adsorption capacity of TpDPP COF nano-spheres could be attributed to the presence of free -$NH_2$ functionality present in TpDPP COF nano-spheres.

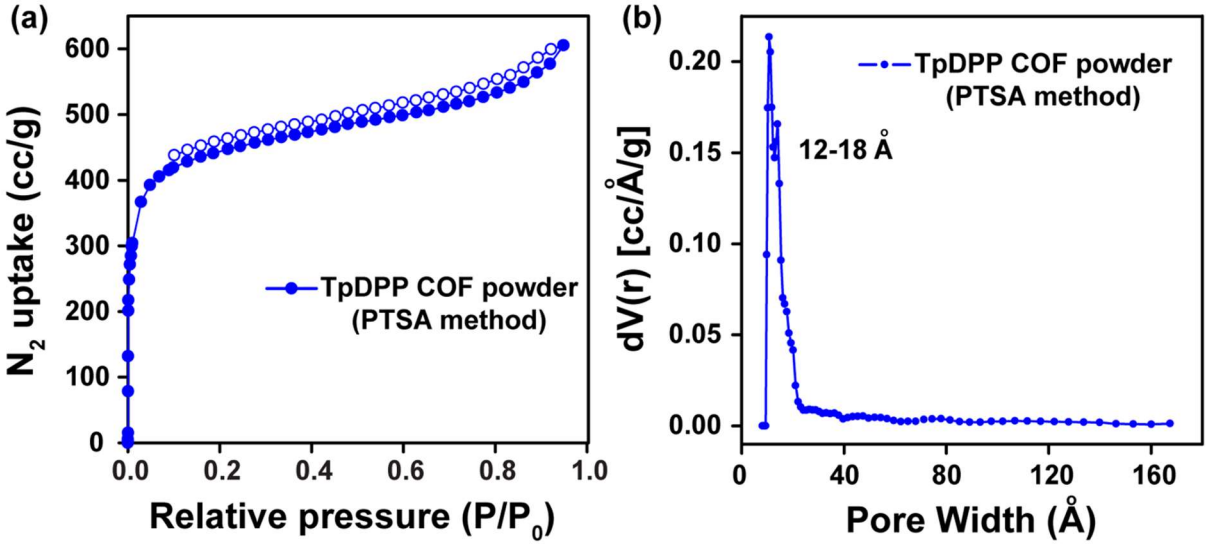

**Figure S11**. (a) $N_2$ adsorption isotherm of the TpDPP COF powder synthesized in salt (PTSA-DPP) mediated crystallization approach showcasing the surface area of 1565 $m^2g^{-1}$. (b) The pore size distribution of the TpDPP COF powder.

## Section S-6: UV/vis Absorption Spectra

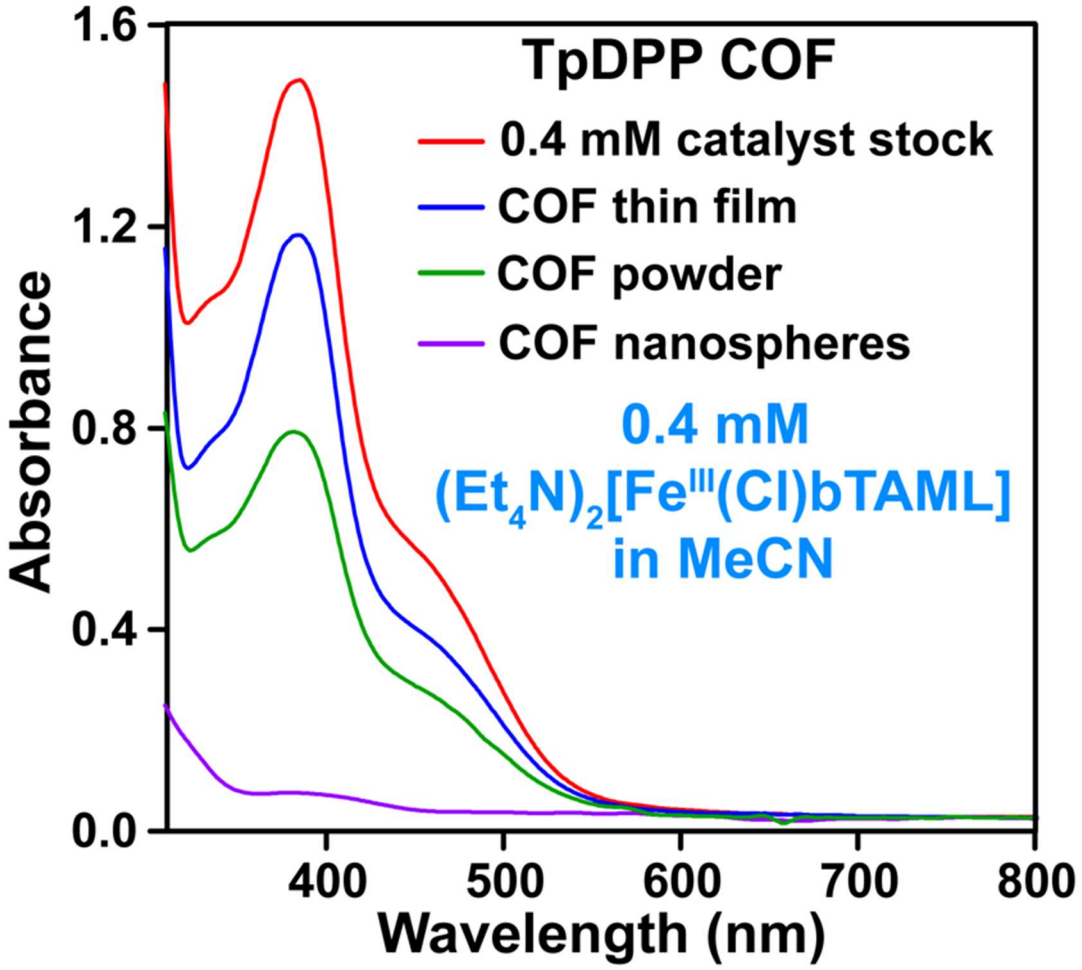


**Figure S12**. UV/vis Absorption Spectra before and after the adsorption of the $(Et_4N)_2[Fe^{III}(Cl)bTAML]$ catalyst by the 1 mg of TpDPP COF thin film (synthesized *via* covalent self-assembly of the TpDPP COF nano-spheres), TpDPP COF powder (synthesized *via* PTSA-amine salt mediated crystallization method), and TpDPP COF nano-spheres from the 1 ml 0.4 mM $(Et_4N)_2[Fe^{III}(Cl)bTAML]$ catalyst solution in acetonitrile. This experiment revealed 1 mg of the solid TpDPP COF thin film, TpDPP COF powder, and TpDPP COF nano-spheres could immobilize 94.8%, 47%, and 21% $(Et_4N)_2[Fe^{III}(Cl)bTAML]$ catalyst molecules from the 1 ml 0.4 mM of the catalytic solution in acetonitrile respectively within their porous crystalline scaffold.

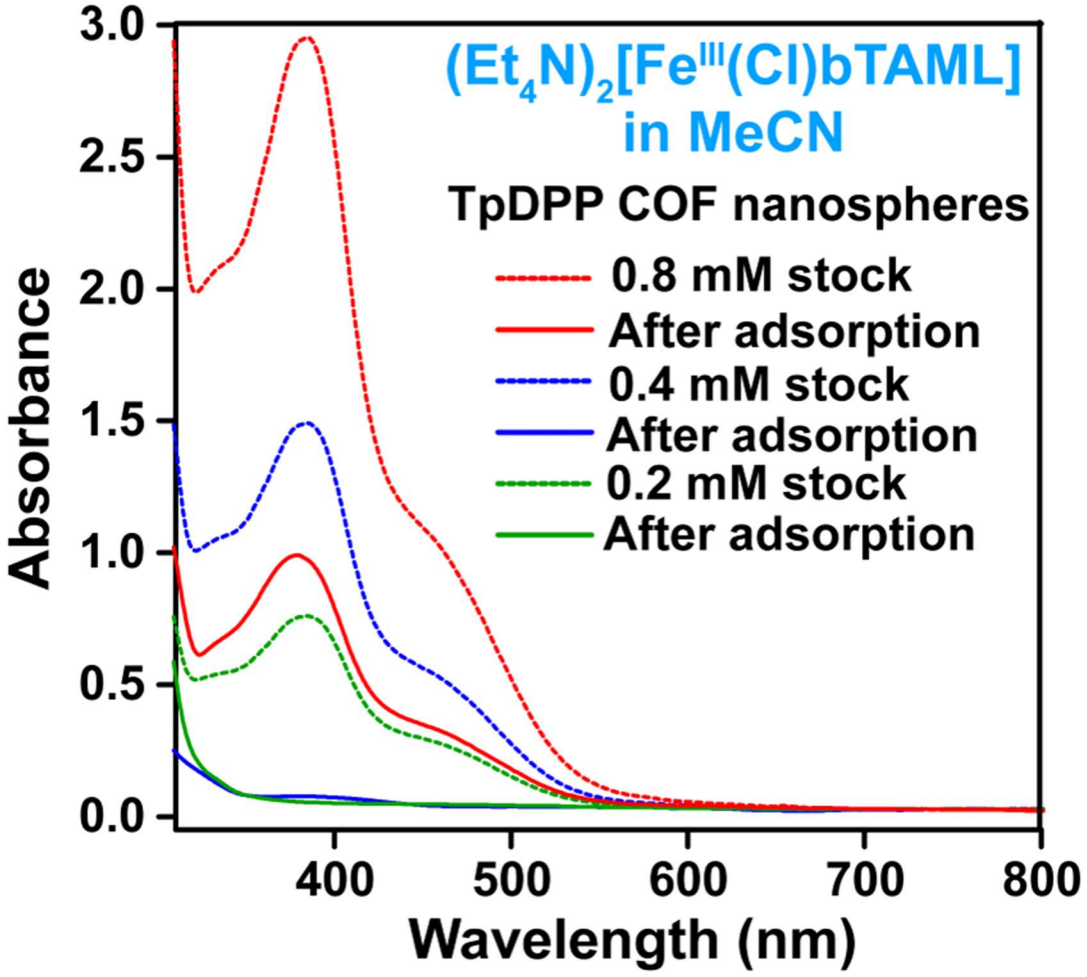


**Figure S13**. UV/vis Absorption Spectra before and after the adsorption of the $(Et_4N)_2[Fe^{III}(Cl)bTAML]$ catalyst by the TpDPP COF nano-spheres from the 1 ml acetonitrile solution of different concentrations of 0.2 mM, 0.4 mM, and 0.8 mM. In the case of 0.4 mM and the 0.8 mM catalytic stock solutions, we have represented the UV spectra obtained by extrapolation of the 0.2 mM catalytic stock since the Lambert-Beer law is not obeyed at a higher concentration. This experiment revealed after dispersing 1 mg of the solid COF nano-spheres into the 1 ml of the catalytic solution in acetonitrile, catalyst molecules from the solution of 0.2 mM and 04 mM got immobilized almost entirely (95% and 94.8% respectively) within the porous crystalline scaffold of the COF nano-spheres. Whereas for 0.8 mM catalytic concentration, the same amount of COF nano-spheres absorbed 66.8% of the catalyst molecules from the solution.

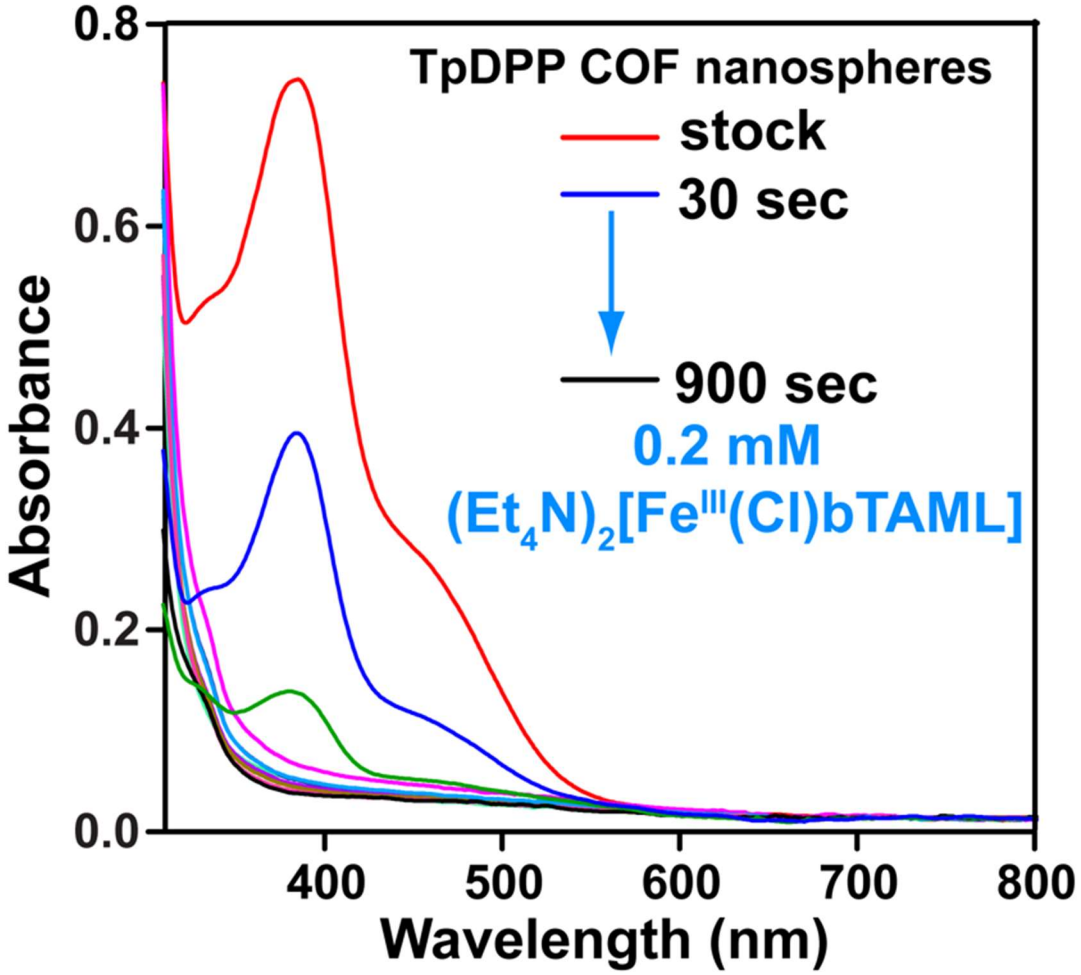


**Figure S14**. Time-dependent adsorption study of 0.2 mM $(Et_4N)_2[Fe^{III}(Cl)bTAML]$ catalytic solution in acetonitrile by as-synthesized TpDPP COF nano-spheres. After 15 min the neutralized COF nano-spheres (1 mg) could able to absorb the $(Et_4N)_2[Fe^{III}(Cl)bTAML]$ catalyst 95% from the 1 ml 0.2 mM catalytic solution in acetonitrile.

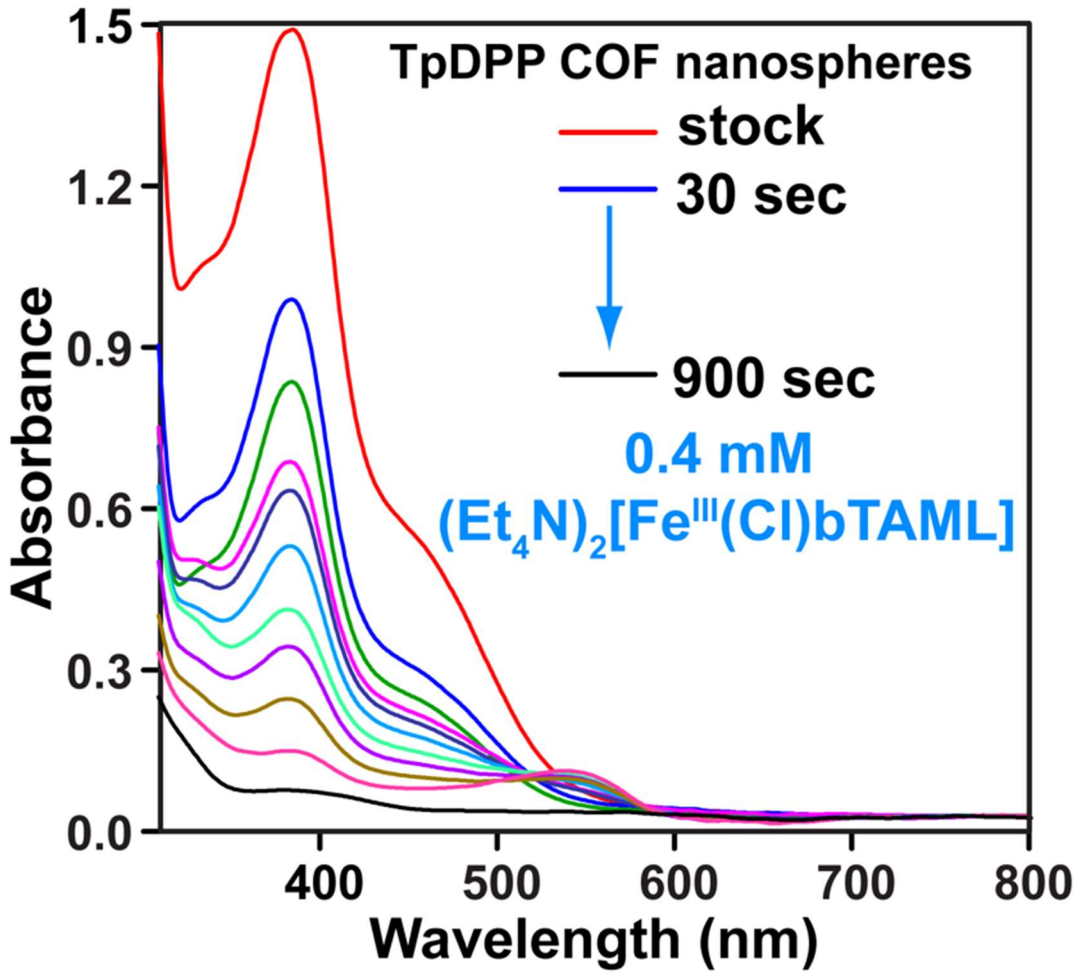


**Figure S15**. Time-dependent adsorption study of 0.4 mM $(Et_4N)_2[Fe^{III}(Cl)bTAML]$ catalytic solution in acetonitrile by as-synthesized TpDPP COF nano-spheres. After 15 min the neutralized COF nano-spheres (1 mg) could able to absorb the $(Et_4N)_2[Fe^{III}(Cl)bTAML]$ catalyst 94.8% from the 1 ml 0.4 mM catalytic solution in acetonitrile.

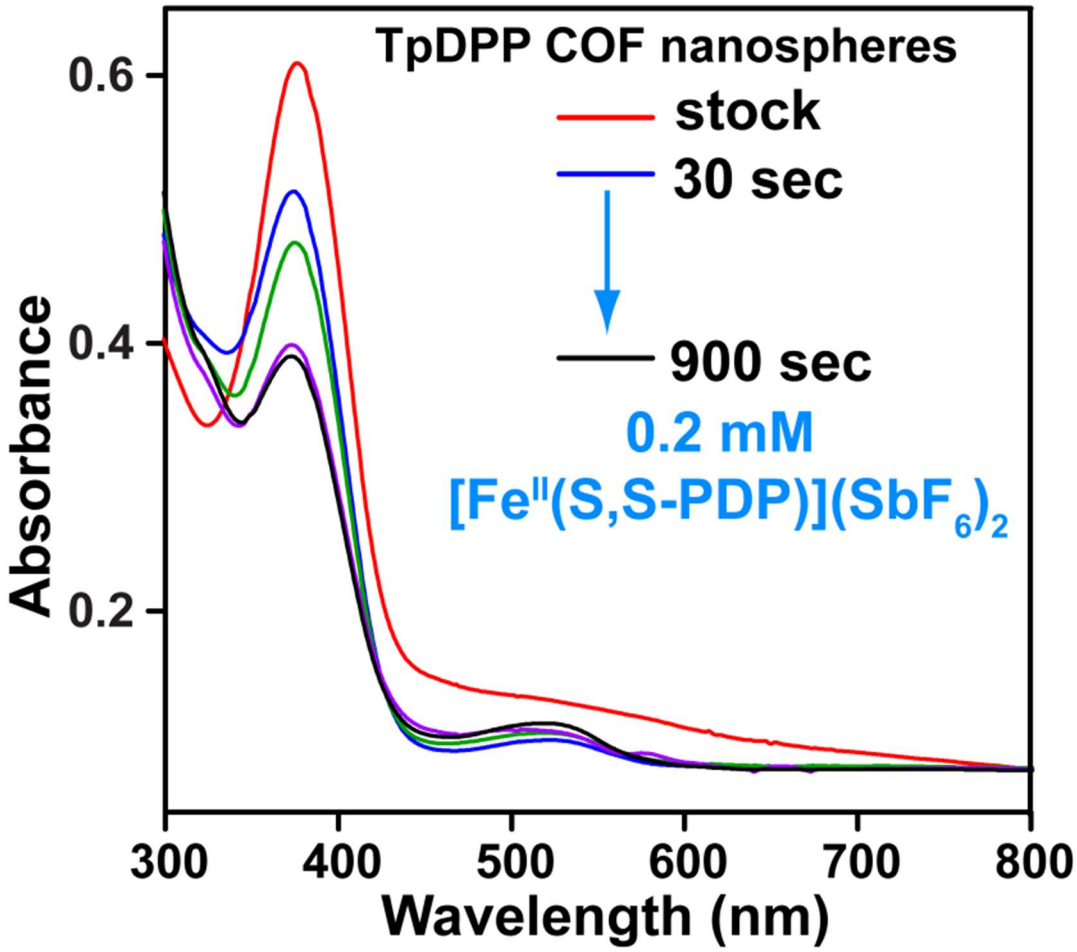


**Figure S16**. Time-dependent adsorption study of 0.2 mM $[Fe^{II}(S,S\text{-}PDP)](SbF_6)_2$ catalytic solution in acetonitrile by as-synthesized TpDPP COF nano-spheres. After 15 min the COF nano-spheres (1 mg) could able to absorb the $[Fe^{II}(S,S\text{-}PDP)](SbF_6)_2$ catalyst only 36% from the 1 ml 0.2 mM catalytic solution in acetonitrile due to the ionic repulsion between two cationic species.

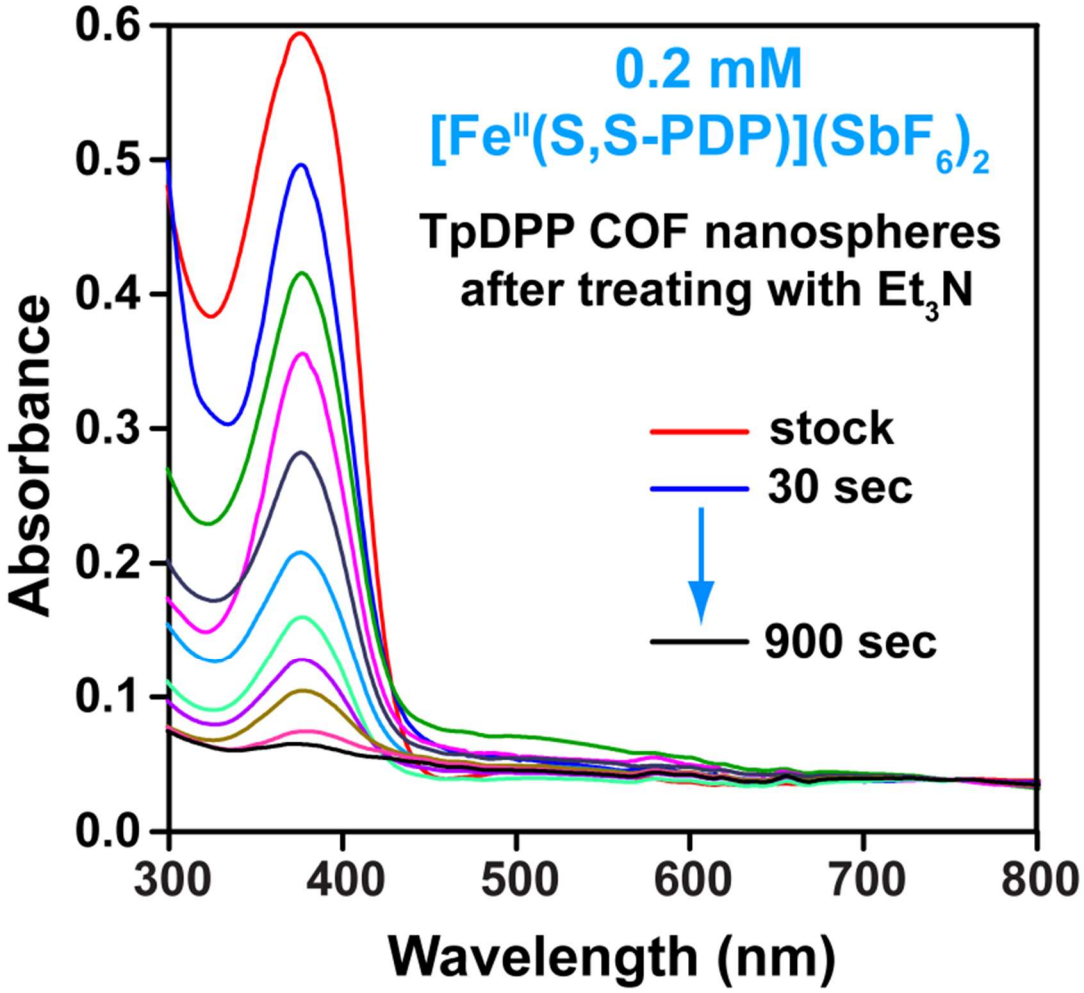


**Figure S17**. Time-dependent adsorption study of 0.2 mM [$Fe^{II}$(S,S-PDP)]$(SbF_6)_2$ catalytic solution in acetonitrile by TpDPP COF nano-spheres after treating with $Et_3N$. After 15 min the neutralized COF nano-spheres (1 mg) could able to absorb the [$Fe^{II}$(S,S-PDP)]$(SbF_6)_2$ catalyst 89% from the 1 ml 0.2 mM catalytic solution in acetonitrile. Interestingly, the neutralized COF nano-spheres (1.0 mg) could able to absorb 89% [$Fe^{II}$(S,S-PDP)]$(SbF_6)_2$ catalyst from the 0.2 mM solution (1.0 ml) in acetonitrile. The high surface area, porosity, and cation-pi interactions probably induced the adsorption.

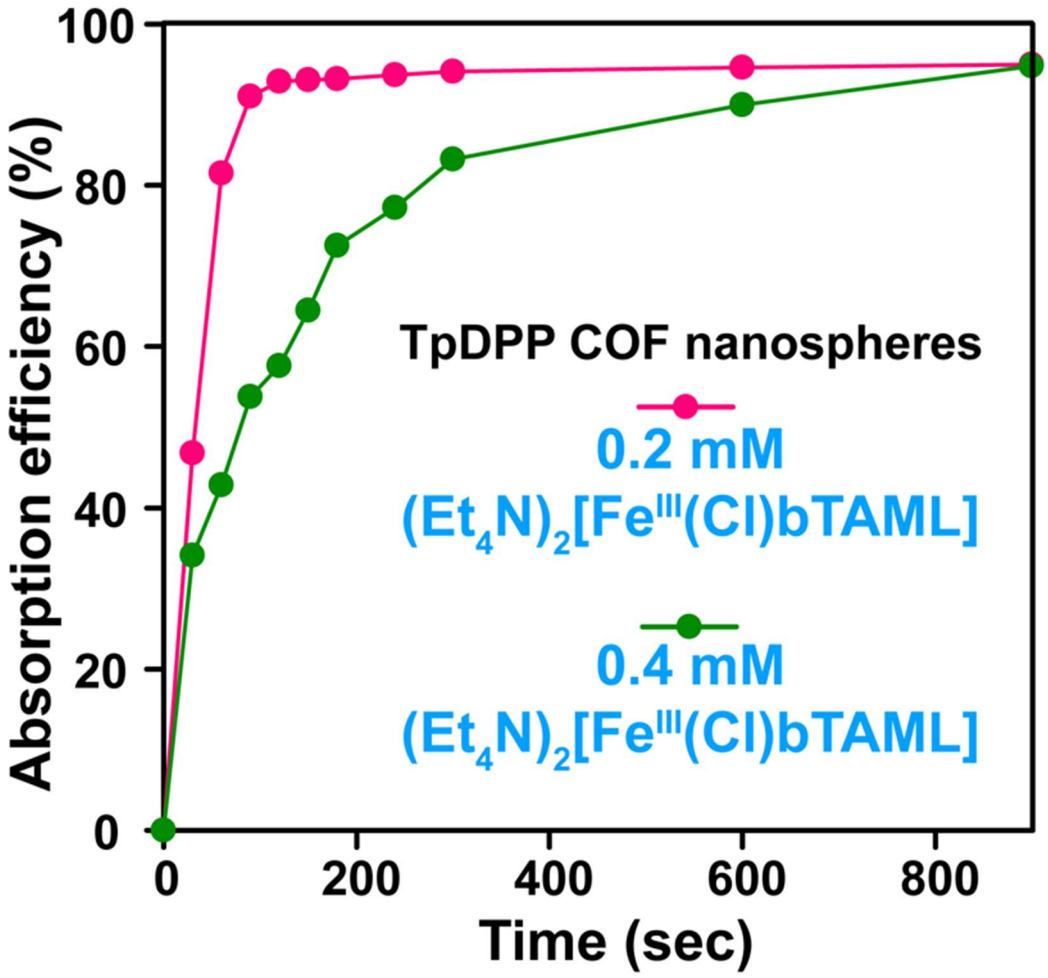


**Figure S18**. The kinetics analyses of adsorption study with 1 ml 0.2 mM and 0.4 mM $(Et_4N)_2[Fe^{III}(Cl)bTAML]$ catalytic solution in acetonitrile by as-synthesized 1 mg TpDPP COF nano-spheres.

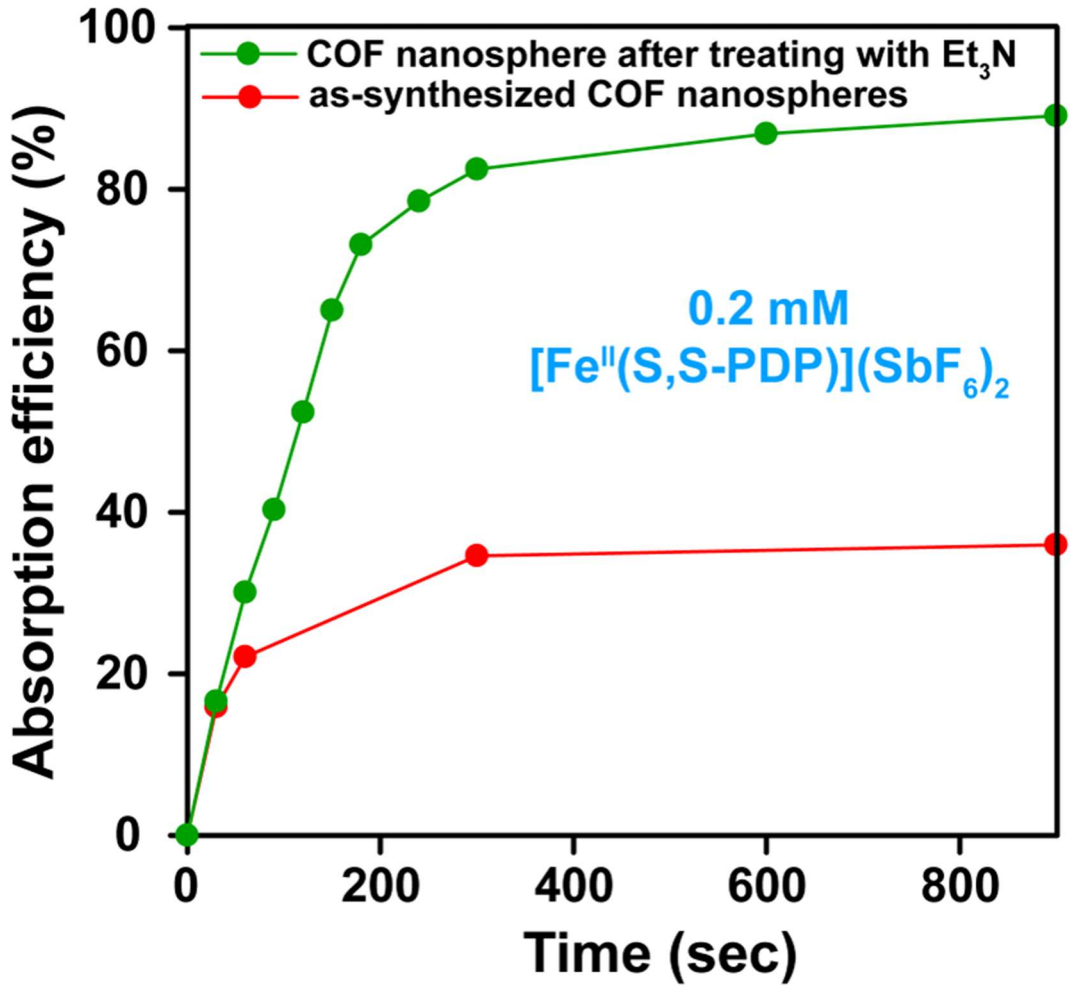


**Figure S19**. The kinetics analyses of adsorption study with 1 ml 0.2 mM $[Fe^{II}(S,S\text{-}PDP)](SbF_6)_2$ catalytic solution in acetonitrile by 1 mg of as-synthesized and neutralized TpDPP COF nano-spheres respectively.

The adsorption efficiency of the TpDPP COF nano-spheres for different concentrations of both the catalysts $(Et_4N)_2[Fe^{III}(Cl)bTAML]$ and $[Fe^{II}(S,S\text{-}PDP)](SbF_6)_2$ was measured by the following equation.

$$\text{Catalyst adsorption efficiency (\%)} = [(C_0\text{-}C_t)/C_0] \times 100$$

where $C_0$ (mmol $l^{-1}$) and $C_t$ (mmol $l^{-1}$) are the initial and residual concentration (after adsorption) of catalysts in the stock solution and filtrate, respectively.

At any time, t, if $q_t$ is the amount of catalyst adsorbed per gm of TpDPP COF nano-spheres adsorbent then

$$q_t = [(C_0\text{-}C_t) \times M_w]/m$$

where m is the amount (g) of sorbent (TpDPP COF nano-spheres) used in this study and Mw is the molar mass (g $mol^{-1}$) of the catalyst.

The rate of adsorption of the catalyst was calculated following Ho and McKay's pseudo-second-order adsorption model. The equation can be represented as:

$$t/q_t = [t/q_e] + [1 / \{k_{obs} \times (q_e)^2]$$

where $q_e$ is the amount of catalyst adsorbed (mg $g^{-1}$) at equilibrium time and $k_{obs}$ is the pseudo-second-order rate constant (g $mg^{-1}$ $min^{-1}$) of catalyst adsorption.

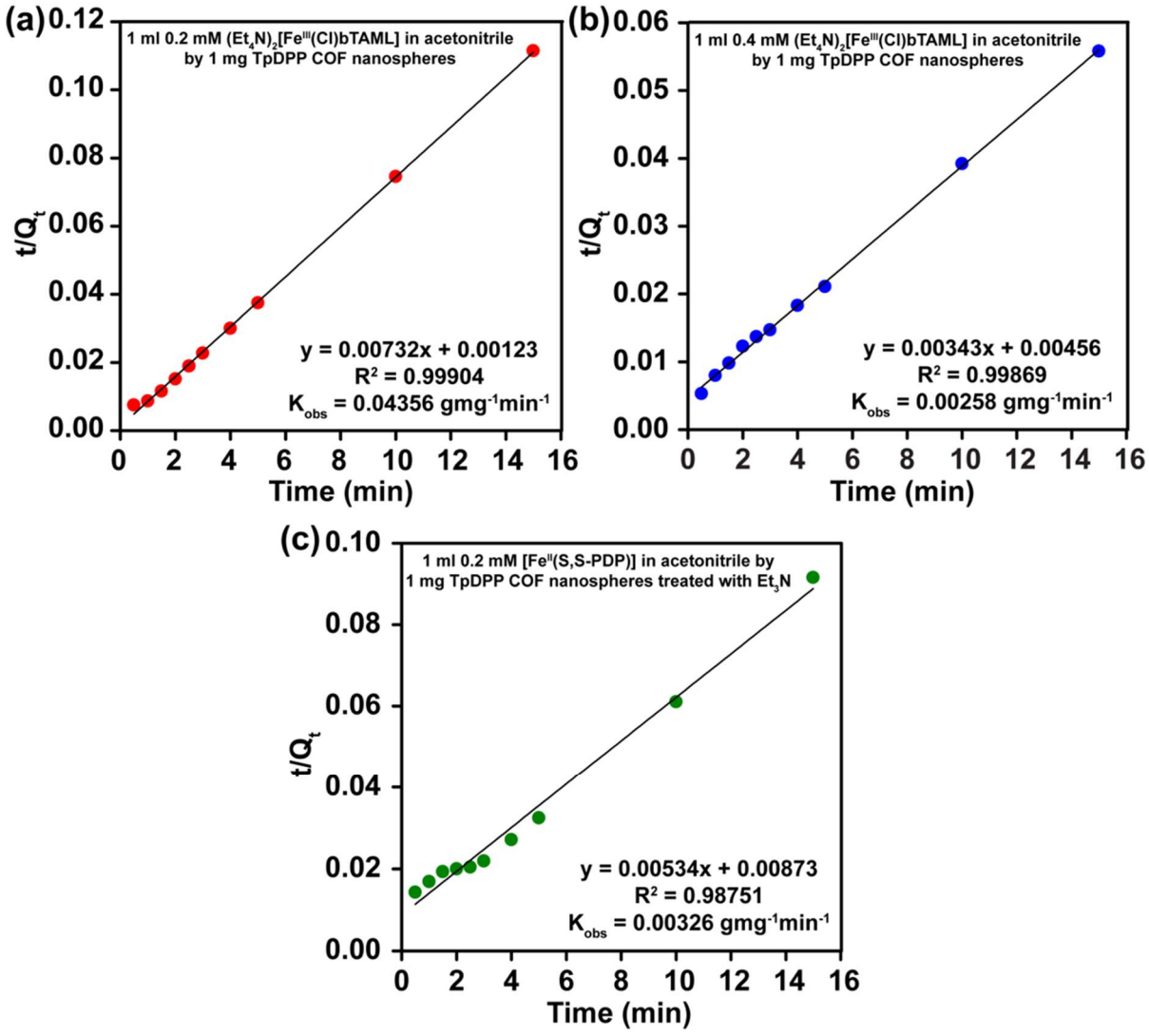


**Figure S20**. The pseudo-second-order rate constant of adsorption ($K_{obs}$) for (a) 0.2 mM $(Et_4N)_2[Fe^{III}(Cl)bTAML]$ catalytic solution in acetonitrile were found to be 0.04356 g $mg^{-1}$ $min^{-1}$ (b) 0.4 mM $[Fe^{III}(Cl)bTAML]^{2-}$catalytic solution in acetonitrile were found to be 0.00258 g $mg^{-1}$ $min^{-1}$). The maximum uptake of $(Et_4N)_2[Fe^{III}(Cl)bTAML]$ catalyst by the as-synthesized

TpDPP COF nano-spheres was found to be 378.9 mg $g^{-1}$.(c) The $K_{obs}$ for 0.2 mM [$Fe^{II}$(S,S-PDP)]$(SbF_6)_2$ catalytic solution in acetonitrile, was found 0.00326 g $mg^{-1}$ $min^{-1}$.

## Section S-7: TGA Data

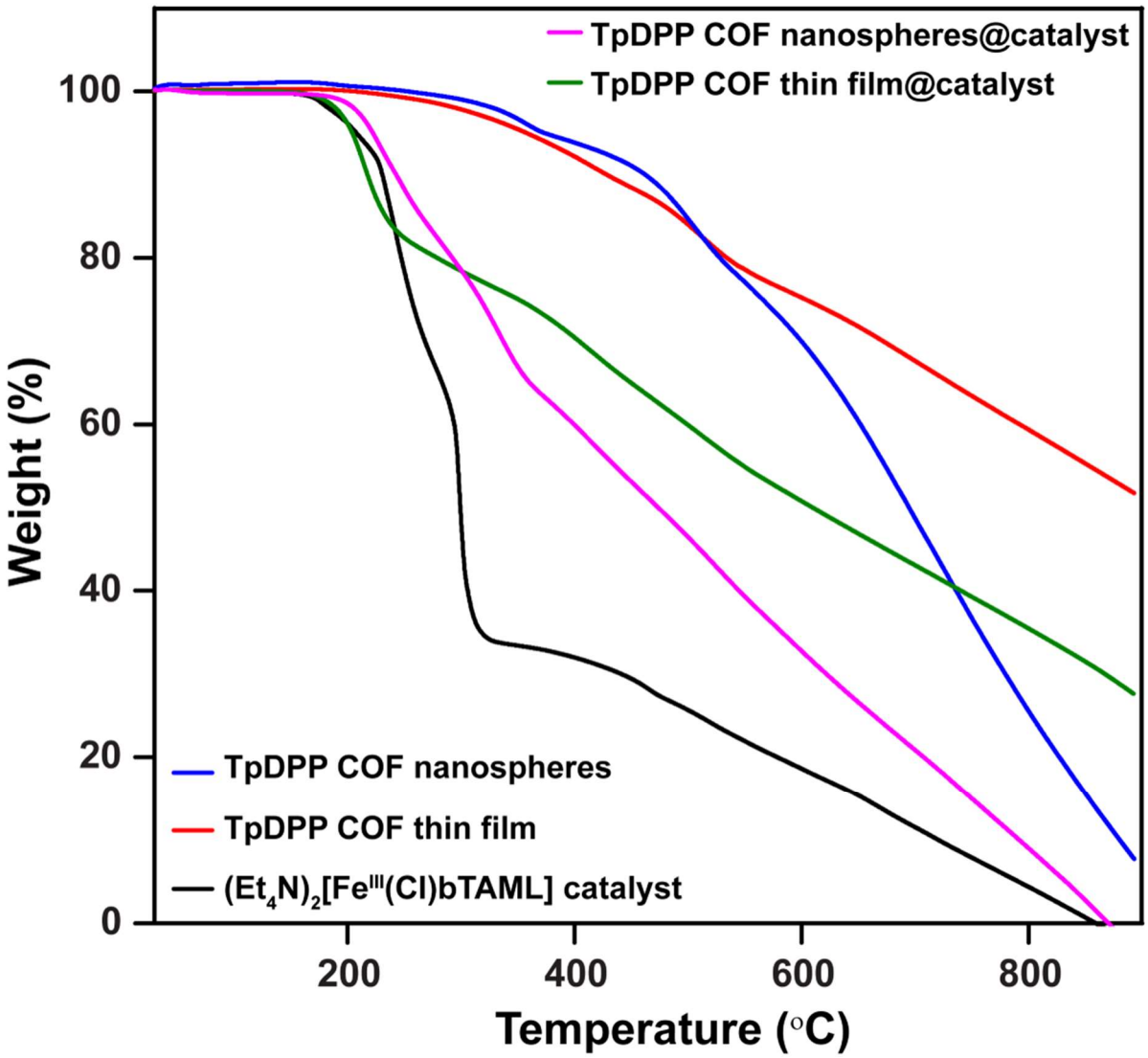


**Figure S21**. Thermogravimetric analyses of $(Et_4N)_2[Fe^{III}(Cl)bTAML]$ catalyst, as-synthesized TpDPP COF nano-spheres, TpDPP COF thin film, $[Fe^{III}(Cl)bTAML]^{2-}$@TpDPP COF nano-spheres, and $[Fe^{III}(Cl)bTAML]^{2-}$@TpDPP COF thin film. The analysis revealed the loading percentage of the $(Et_4N)_2[Fe^{III}(Cl)bTAML]$ catalyst inside the TpDPP COF nano-spheres and TpDPP COF thin film to be 23 wt% and 19 wt% respectively.

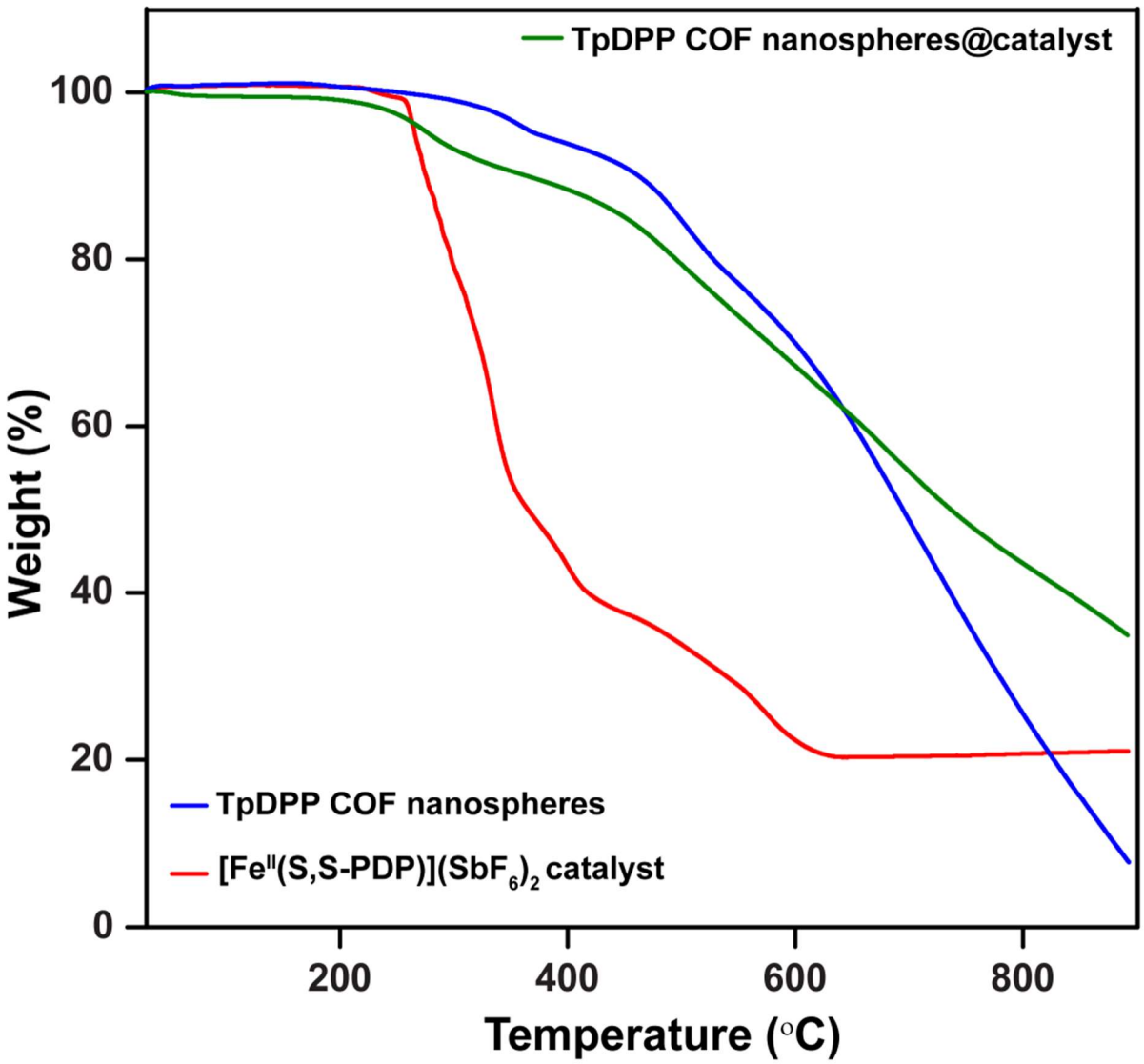


**Figure S22**. Thermogravimetric analyses of $[Fe^{II}(S,S\text{-}PDP)](SbF_6)_2$ catalyst, as-synthesized TpDPP COF nano-spheres, and $[Fe^{II}(S,S\text{-}PDP)]^{2+}$@TpDPP COF nano-spheres. The analysis revealed the loading percentage of the $[Fe^{II}(S,S\text{-}PDP)](SbF_6)_2$ catalyst inside the TpDPP COF nano-spheres to be 10 wt%.

## Section S-8: SEM Imaging

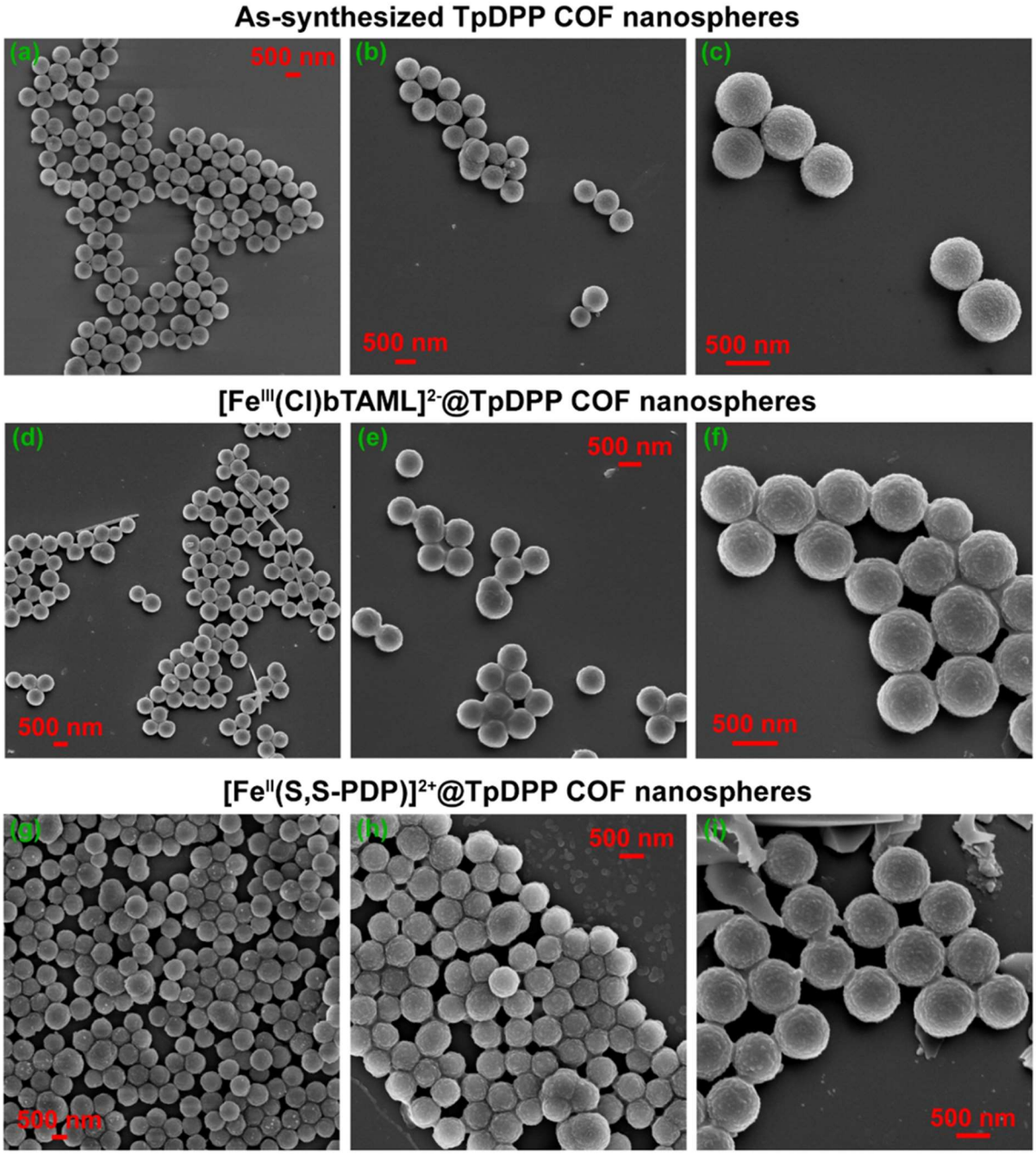


**Figure S23**. SEM images of (a-c) as-synthesized TpDPP COF nano-spheres (d-f) [Fe$^{III}$(Cl)bTAML]$^{2-}$@TpDPP COF nano-spheres (g-i) [Fe$^{II}$(S,S-PDP)]$^{2+}$@TpDPP COF nano-spheres. In the SEM analyses, the size of the nano-spheres was found to be 590-610 nm.

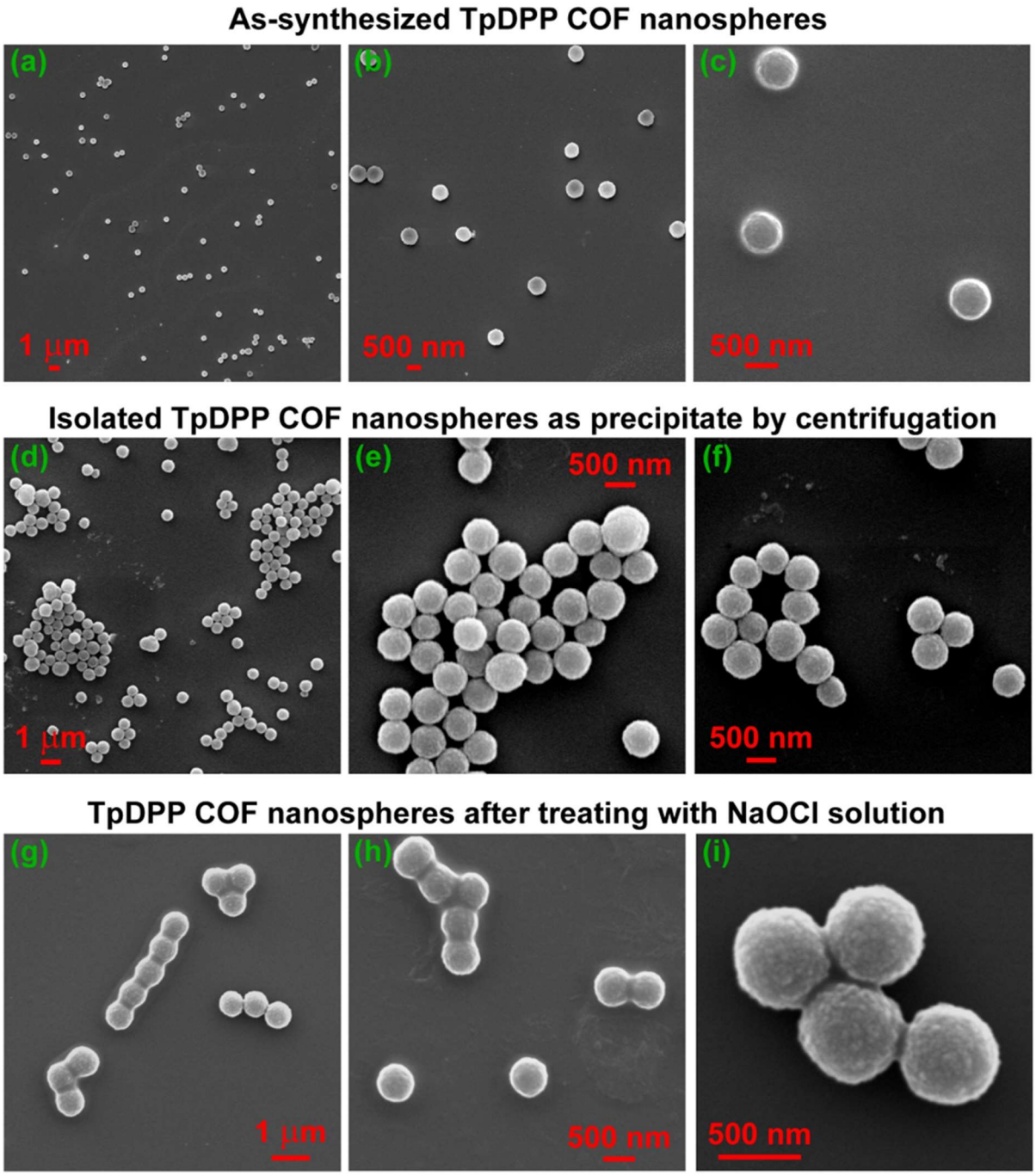


**Figure S24**. SEM images of (a-c) as-synthesized TpDPP COF nano-spheres (dispersed in DCM) were drop-casted on top of a silicon wafer at very diluted condition (d-f) Purified TpDPP COF nanosphere after the isolation as precipitate *via* centrifugation (g-i) TpDPP COF nanosphere after treating with NaOCl (which has been used in catalysis reactions as the terminal oxidant).

## Section S-9: TEM Imaging and Elemental Mapping

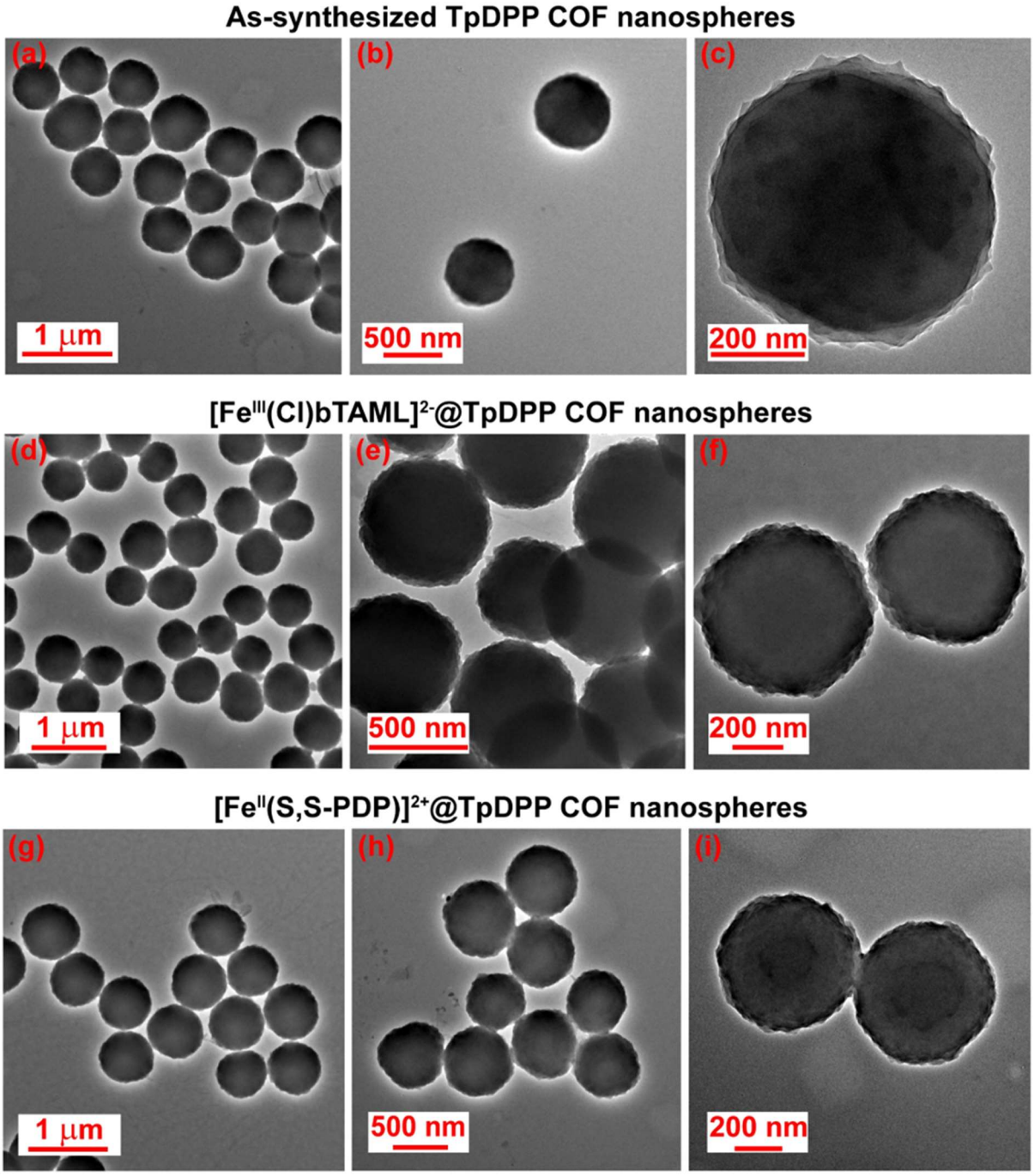


**Figure S25**. TEM images of (a-c) as-synthesized TpDPP COF nano-spheres (d-f) [$Fe^{III}$(Cl)bTAML]$^{2-}$@TpDPP COF nano-spheres (g-i) [$Fe^{II}$(S,S-PDP)]$^{2+}$@TpDPP COF nano-spheres. In the TEM analyses, the size of the nano-spheres was found to be 590-610 nm which shows excellent agreement with the SEM and DLS analyses.

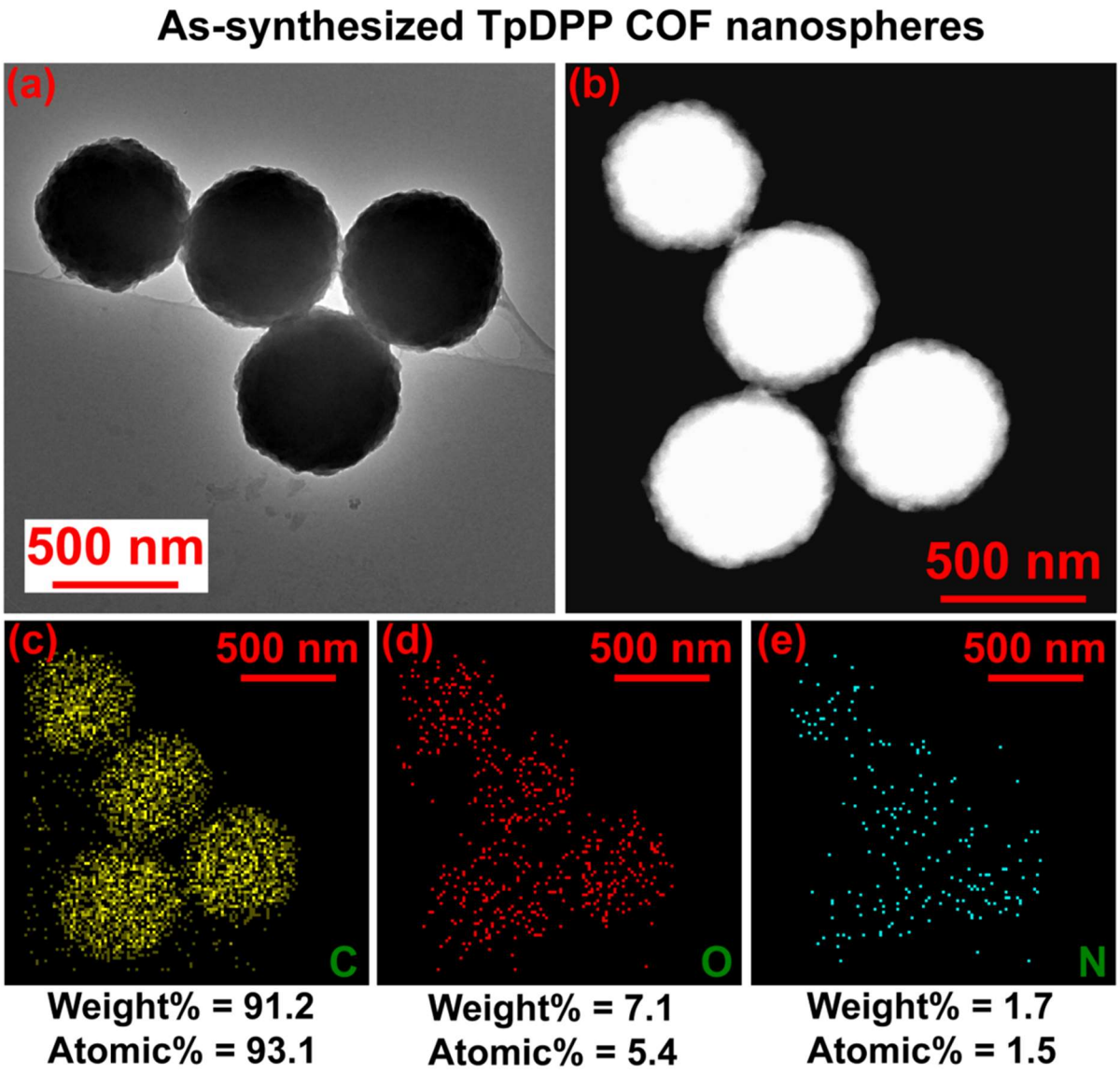


**Figure S26**. (a-e) Energy-dispersive X-ray spectrometry (EDS) elemental mapping of the as-synthesized TpDPP COF nano-spheres showcased the presence of C, O, and N as the COF structural backbone.

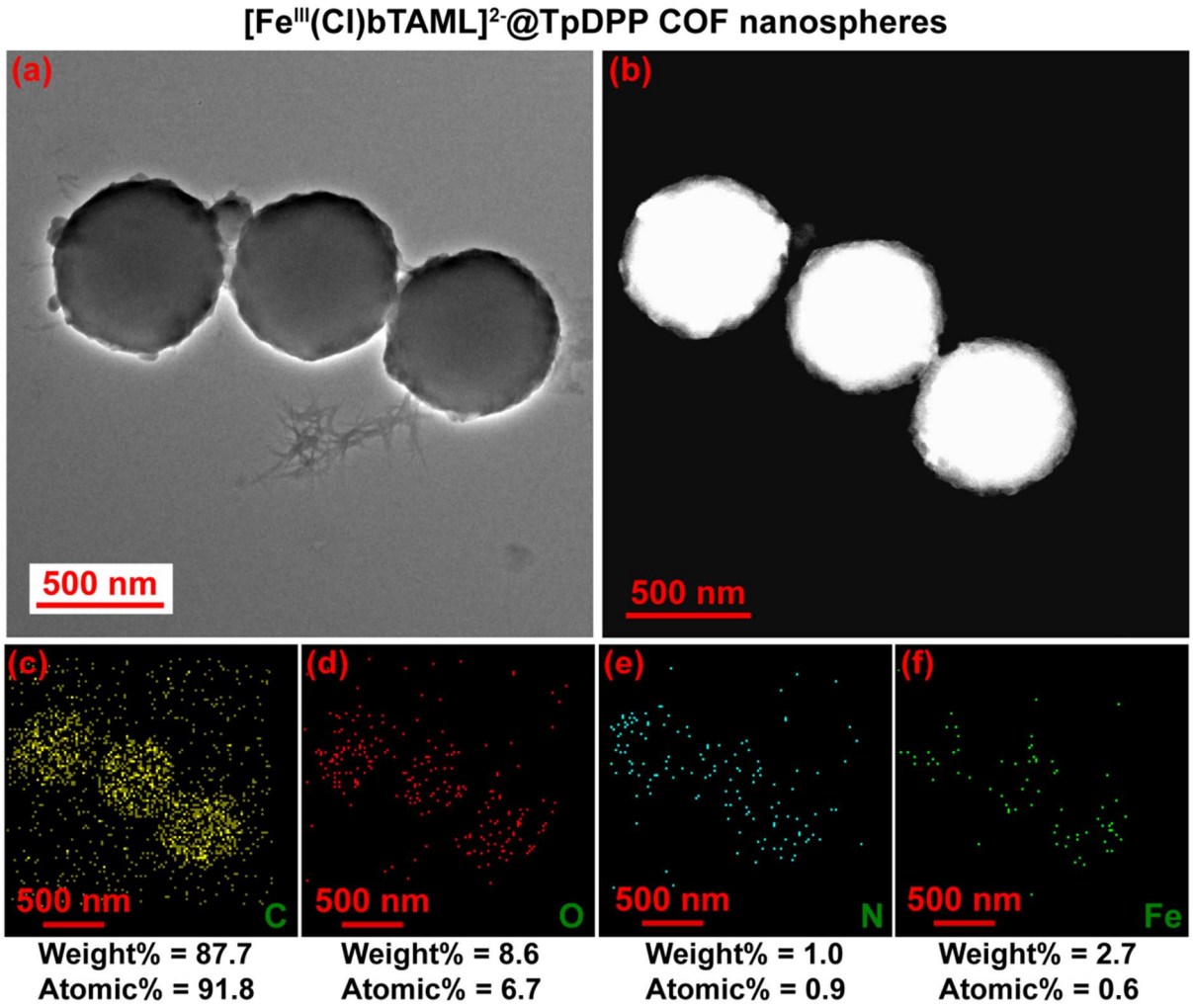


**Figure S27**. (a-e) Energy-dispersive X-ray spectrometry (EDS) elemental mapping of the $[Fe^{III}(Cl)bTAML]^{2-}$@TpDPP COF nano-spheres showcased the presence of Fe along with C, O, and N which further confirms the immobilization of $(Et_4N)_2[Fe^{III}(Cl)bTAML]$ catalyst within the TpDPP COF nano-spheres scaffold.

## Section S-10: DLS Data Analyses

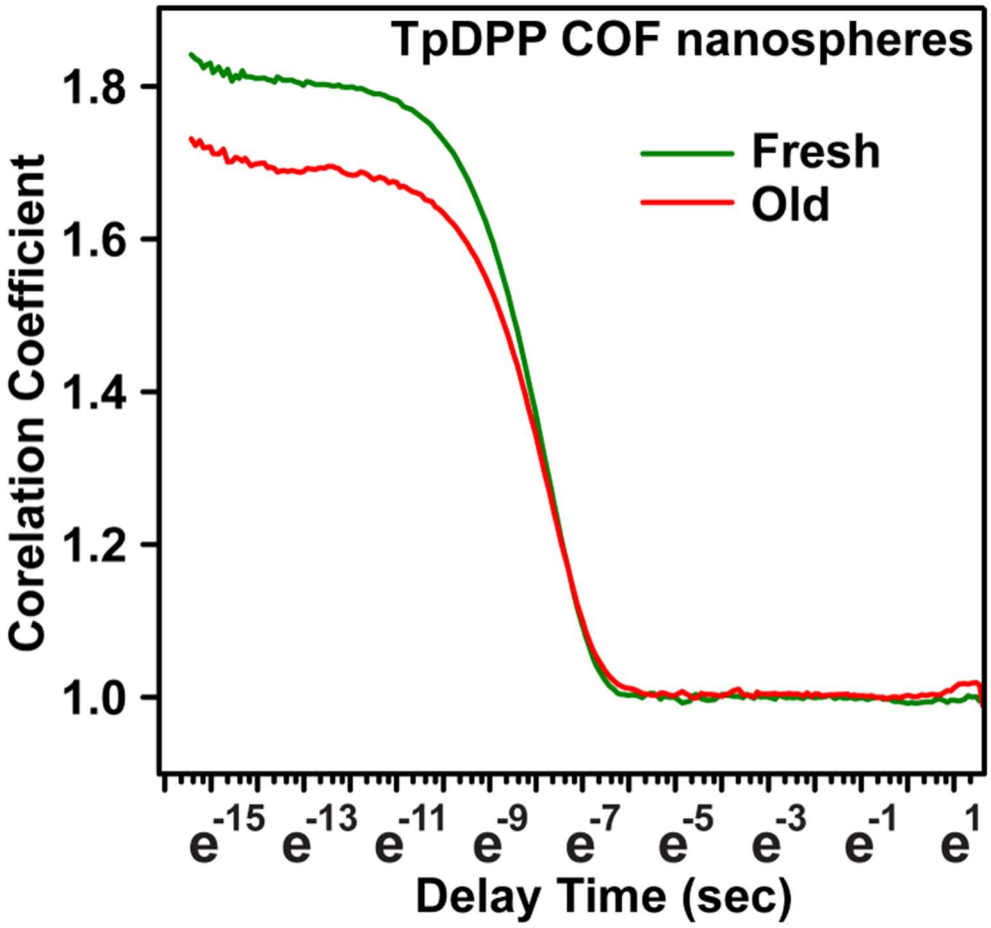


**Figure S28**. The dynamic light scattering correlation function of as-synthesized fresh TpDPP COF nano-spheres and the same TpDPP COF nano-spheres after 4 months (stored in a closed container as the colloidal solution in DCM). This revealed the stability of the colloidal TpDPP COF nano-spheres in DCM.

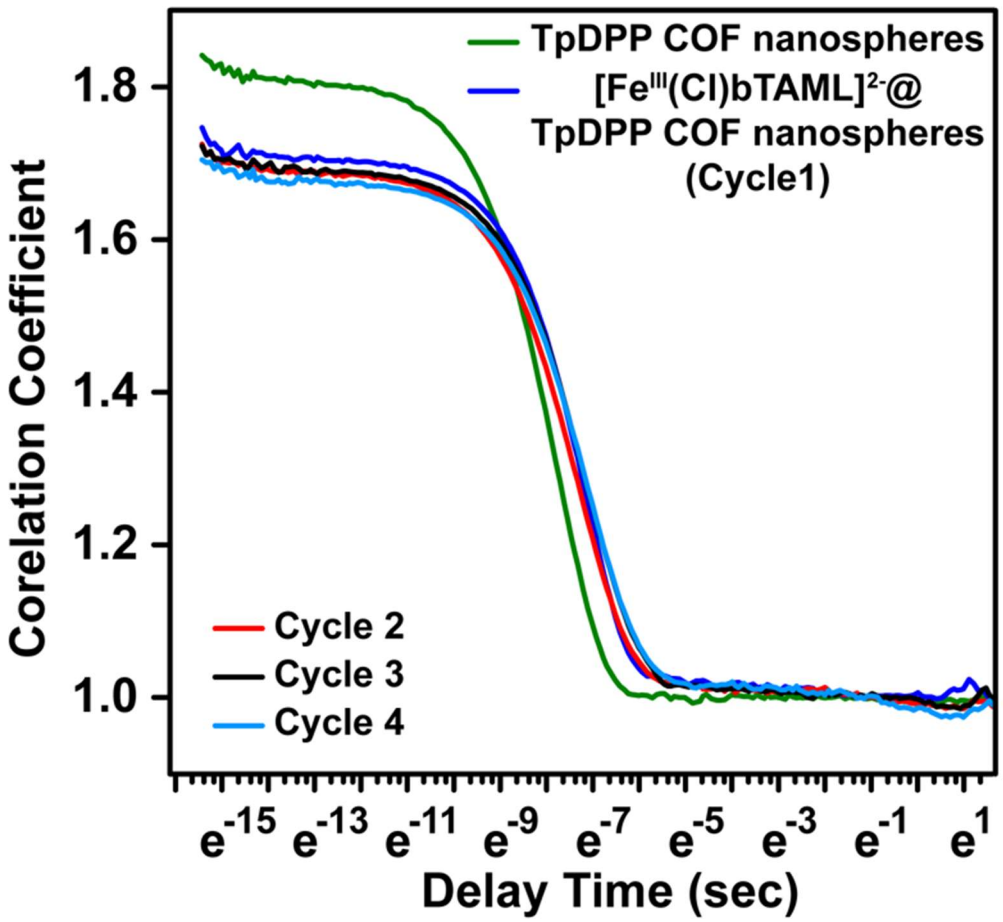


**Figure S29**. Dynamic light scattering correlation function of as-synthesized fresh TpDPP COF nano-spheres, $[Fe^{III}(Cl)bTAML]^{2-}$@TpDPP COF nano-spheres (after immobilization of the $(Et_4N)_2[Fe^{III}(Cl)bTAML]$ catalyst inside the TpDPP COF nano-spheres which was utilized as the heterogeneous catalyst in the catalytic cycle 1). By DLS analyses, after each catalytic cycle, the particle size and the corresponding correlation function of the $[Fe^{III}(Cl)bTAML]^{2-}$@TpDPP COF nano-spheres were checked. Here cycle 4 indicated the size and correlation function of the $[Fe^{III}(Cl)bTAML]^{2-}$@TpDPP COF nano-spheres after the 3$^{rd}$ catalytic cycle of recyclability which was further used in cycle 4 of the catalytic recyclability.

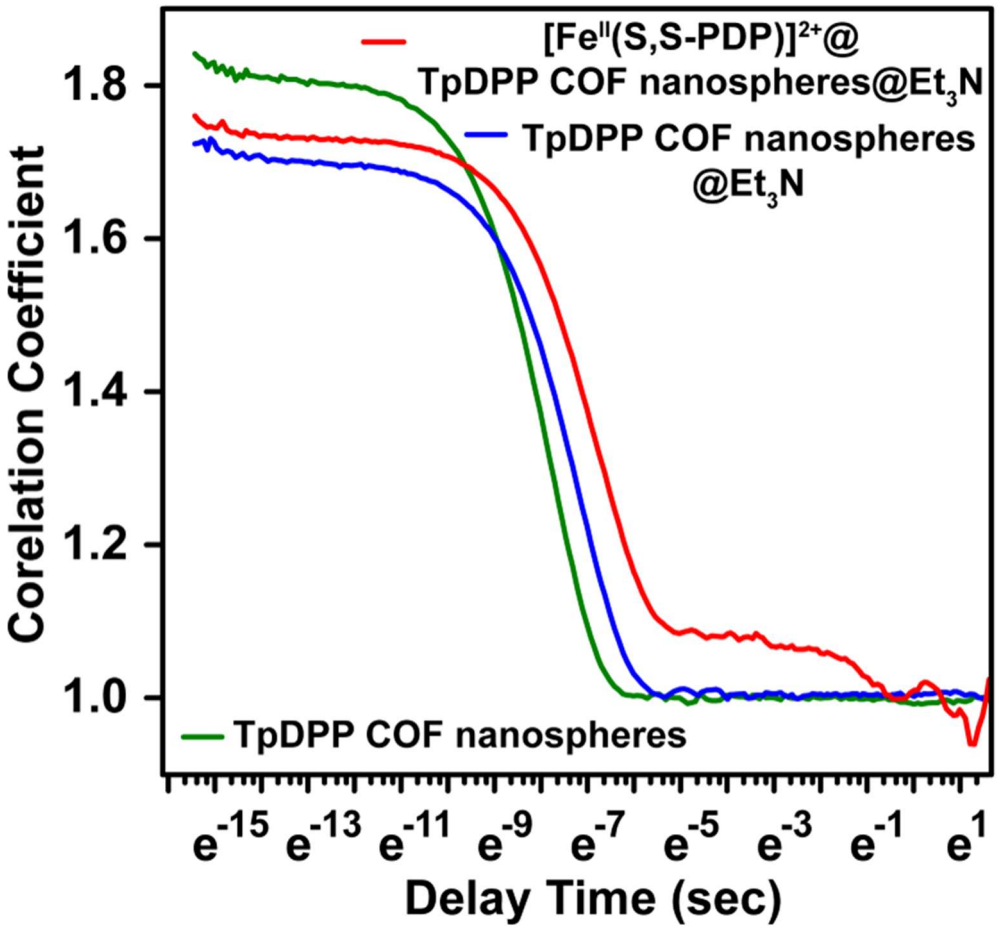


**Figure S30**. The dynamic light scattering correlation function of as-synthesized fresh TpDPP COF nano-spheres, TpDPP COF nano-spheres after treating with $Et_3N$ (to extract the proton from the COF nano-spheres scaffold), and $[Fe^{II}(S,S\text{-}PDP)]^{2+}$@TpDPP COF nano-spheres@$Et_3N$. (after immobilization of the $[Fe^{II}(S,S\text{-}PDP)](SbF_6)_2$ catalyst inside the TpDPP COF nano-spheres@$Et_3N$).

## Section S-11: Raman Spectra

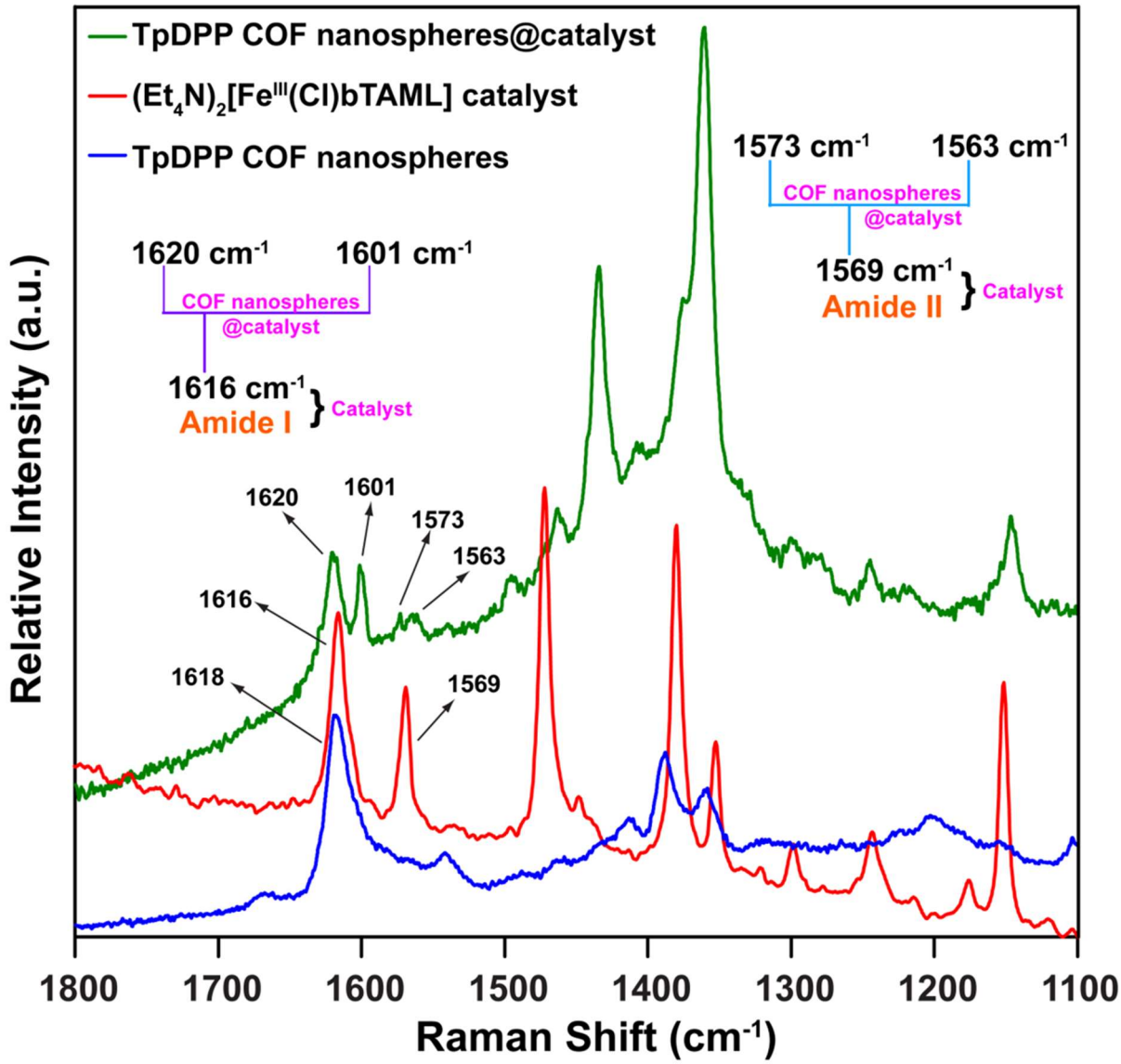


**Figure S31**. The comparison of Raman spectra of TpDPP COF nano-spheres, $(Et_4N)_2[Fe^{III}(Cl)bTAML]$ catalyst, and $[Fe^{III}(Cl)bTAML]^{2-}$@TpDPP COF nano-spheres. The Raman spectra of the $(Et_4N)_2[Fe^{III}(Cl)bTAML]$ catalyst obtained upon 785 nm excitation revealed the presence of Am I (–C=O stretch) band at 1616 $cm^{-1}$ and Am II (C–N stretch) band at 1569 $cm^{-1}$. The catalyst Am I (–C=O stretch) band red-shifted to 1601 $cm^{-1}$, and a new peak appeared at 1621 $cm^{-1}$ due to the immobilization of the catalyst inside the COF nano-spheres. Similarly, the catalyst Am II (C–N stretch) band blue-shifted to 1573 $cm^{-1}$, and a new peak appeared at1562 $cm^{-1}$. This indicated the presence of N─H···O hydrogen bonding between the free amine of the COF nanosphere and amide carbonyl of the immobilized catalyst.

## Section S-12: XPS Data Analyses

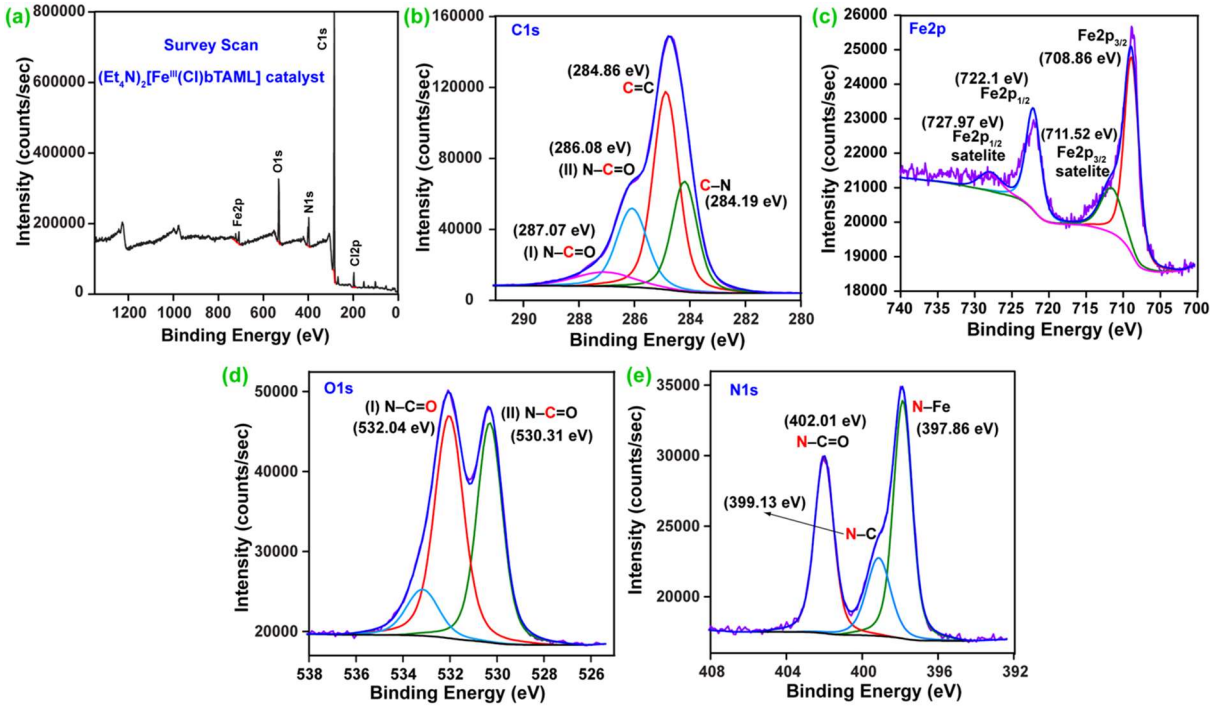


**Figure S32**. (a) The XPS survey scan of $(Et_4N)_2[Fe^{III}(Cl)bTAML]$ catalyst. (b-e) The XPS deconvoluted C1s, Fe2p, O1s, and N1s spectra of the $(Et_4N)_2[Fe^{III}(Cl)bTAML]$ catalyst. The XPS analysis of the $(Et_4N)_2[Fe^{III}(Cl)bTAML]$ catalyst revealed the deconvoluted C1s spectra, which indicates the presence of two distinct peaks at 286.1 and 287.1 eV corresponding to the amide carbon and the diamide carbon, respectively.

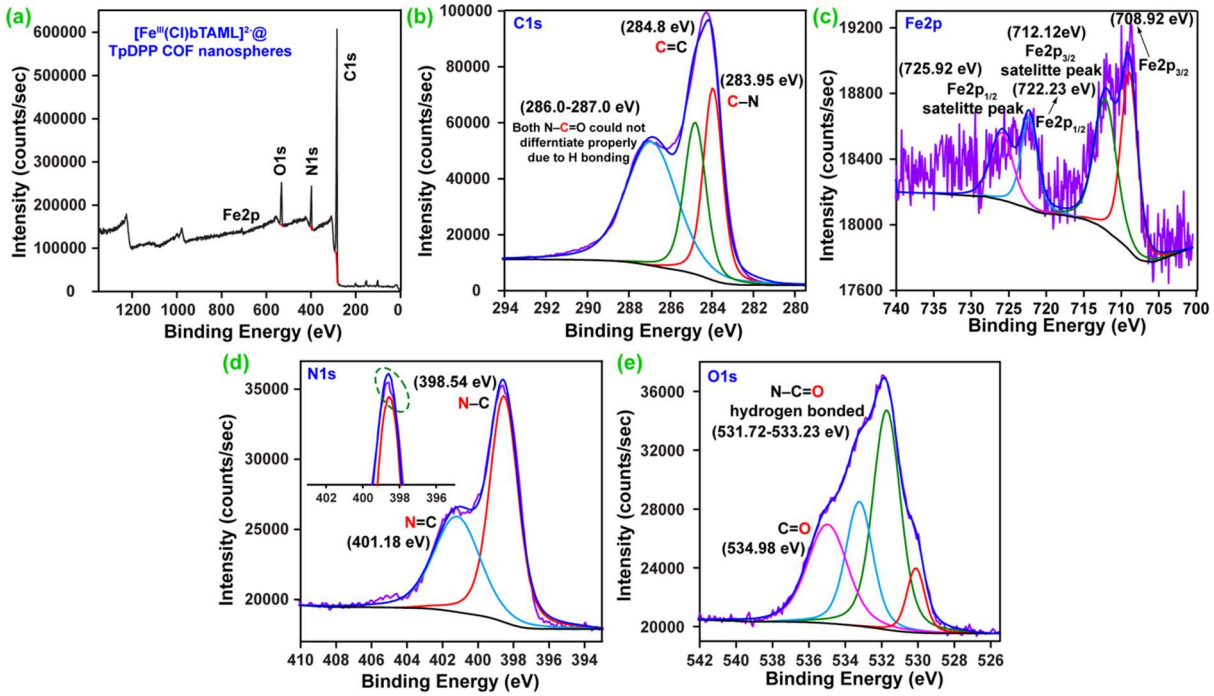

**Figure S33**. (a) The XPS survey scan of $[Fe^{III}(Cl)bTAML]^{2-}$@TpDPP COF nano-spheres (b-e) The XPS deconvoluted C1s, Fe2p, O1s, and N1s spectra of the $[Fe^{III}(Cl)bTAML]^{2-}$@TpDPP COF nano-spheres. The XPS analysis of the $[Fe^{III}(Cl)bTAML]^{2-}$@TpDPP COF nano-spheres revealed the deconvoluted C1s spectra, which indicates while immobilized inside the COF nanosphere, these two amide peaks of the catalyst appeared at almost similar regions (286.6-286.9 eV) due to the hydrogen bonding and could not be appropriately resolved.

## Section S-13: EPR Spectra

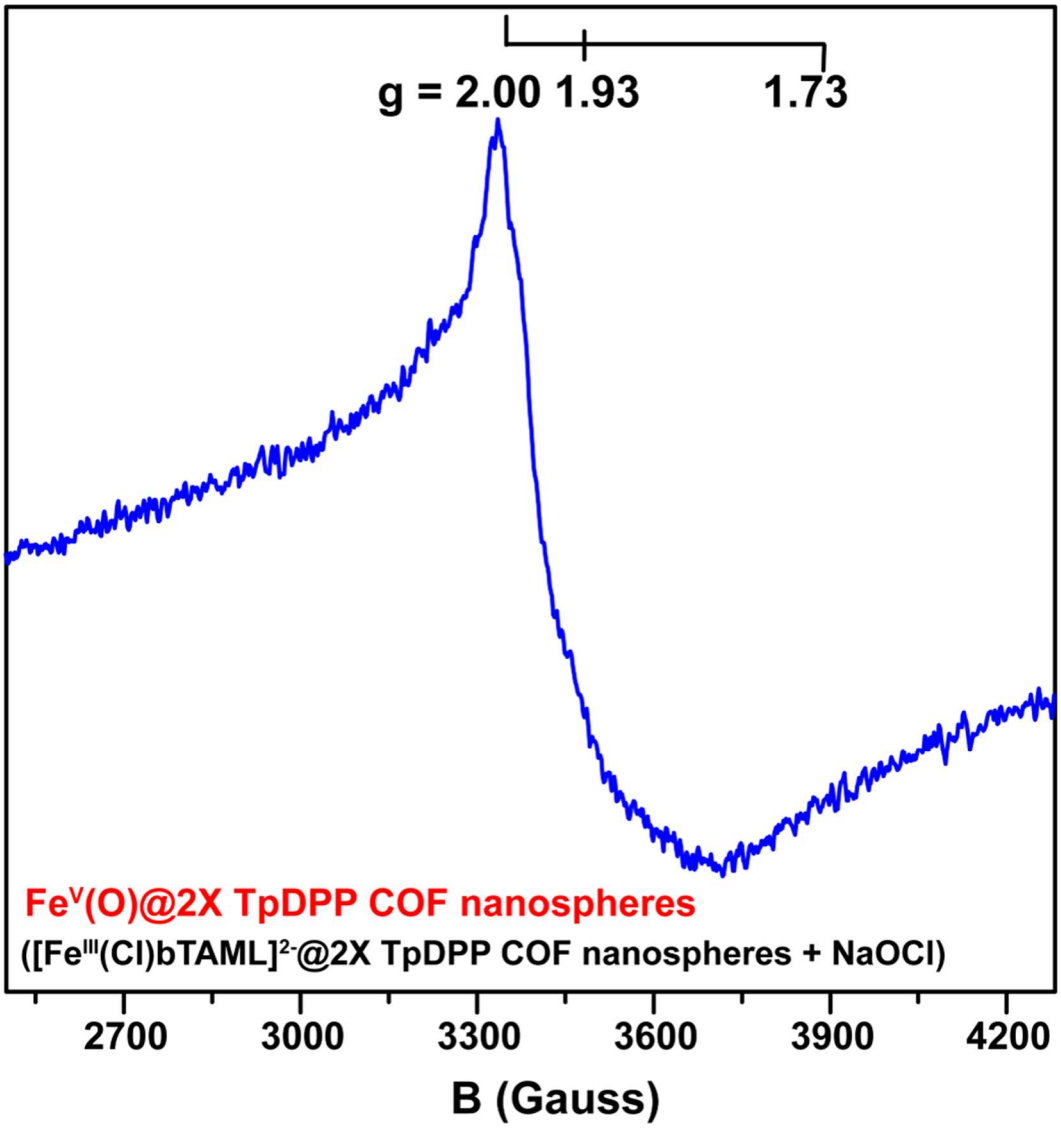


**Figure S34**. X-band EPR spectrum at 123K manifested a rhombic S= ½ species with g = 2.00, 1.93, and 1.73, which indicated that the same oxoiron(V) intermediate was generated inside the $[Fe^{III}(Cl)bTAML]^{2-}$@2X TpDPP COF nano-spheres upon addition of NaOCl, which confirms that the overall mechanism of oxidation remained unchanged upon immobilization of the catalyst.

## Section S-14: Mechanism of the Thin-Film Formation

### Covalent Self-assembly *via* Multiple Drop-casting of TpDPP COF Nano-spheres

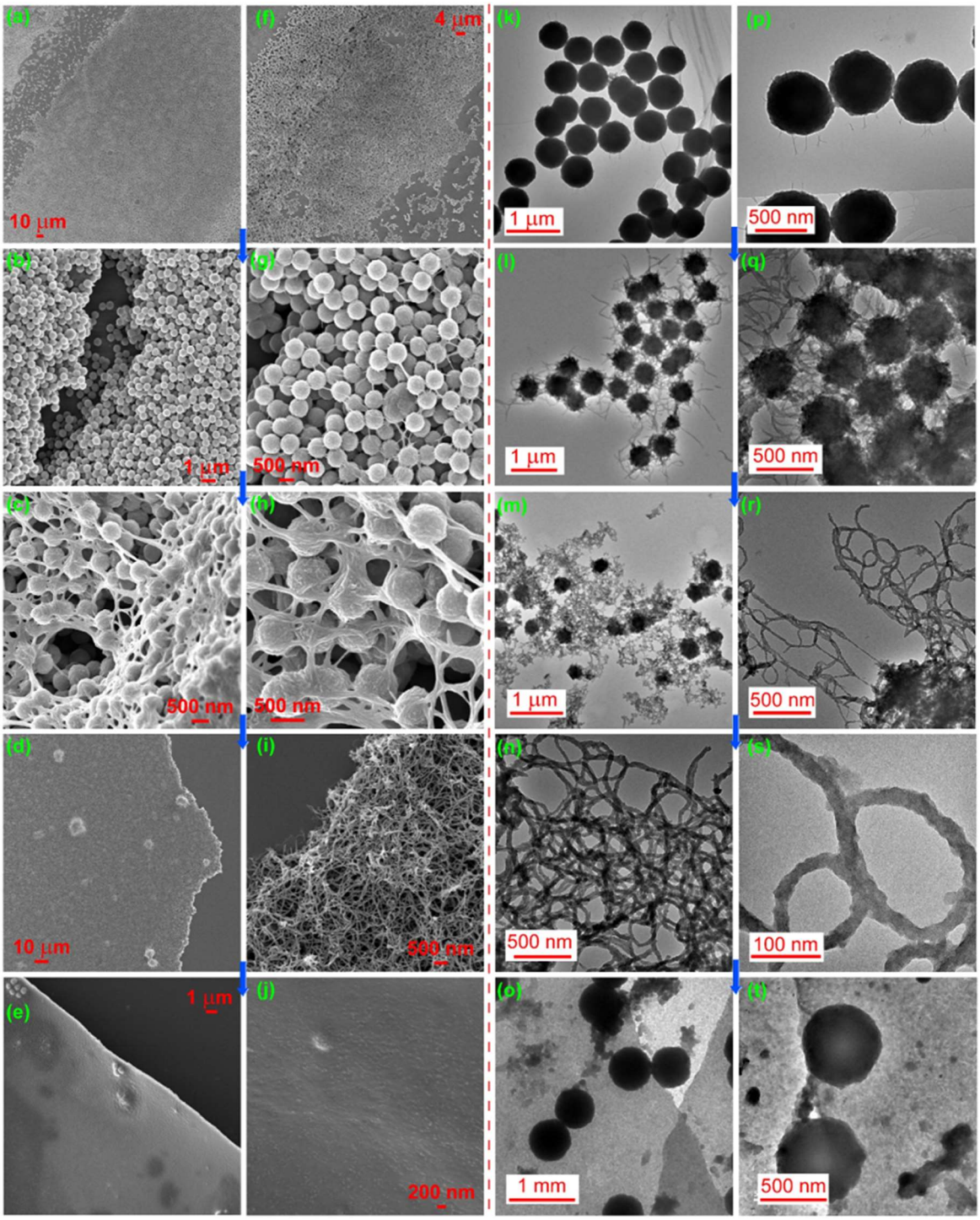


**Figure S35**. (a-e) SEM imaging revealing the mechanism of the transmutation of the COF nano-spheres → fibers → thin film. (f-j) SEM images at higher magnification during the mechanism of the transmutation of the COF nano-spheres → fibers → thin film. (k-o) TEM imaging revealing the mechanism of the transmutation of the COF nano-spheres → fibers → thin film. (p-t) TEM images at

higher magnification during the mechanism of the transmutation of the COF nano-spheres → fibers → thin film. During the multiple drop-casting of the TpDPP COF nano-spheres, the covalent self-assembly driven by the free amine and aldehyde functionality of the COF nano-spheres occurred in an unusual way that was previously unheard of. The attractive capillary forces and convective transport of the COF nano-spheres drive their self-assembly. Consequently, when two separate spheres came in contact, they started reacting *via* a reversible Schiff base reaction, which initiated the fibers/threads' protrusion at their interface. The distribution of fibers enhanced with time and the covalent self-assembly of the connected fibers accomplished the formation of COF nano-film of thicknesses of 200-300 nm after three days.

**Covalent Self-assembly of TpDPP COF Nano-spheres at the DCM-Water Interface**

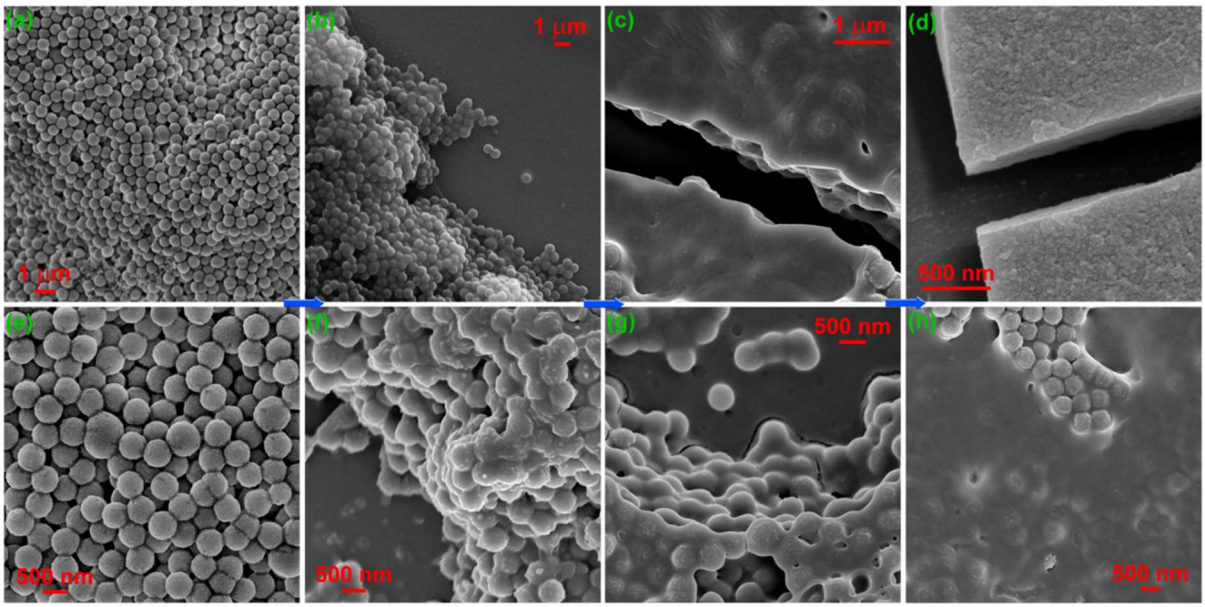


**Figure S36**. (a-d) SEM imaging revealing the mechanism of the transmutation of the COF nano-spheres → thin film. (e-h) SEM images at higher magnification during the mechanism of the transmutation of the COF nano-spheres → thin film. The covalent self-assembly at the DCM-water interface driven by the surface tension and the free amine and aldehyde functionality of the COF nano-spheres is different from the covalent self-assembly *via* multiple drop-casting method. It didn't involve the generation of fibers or threads at the interface of two COF nano-spheres although got connected *via* reversible Schiff base reaction to form uniform TpDPP COF thin film thickness of 70-90 nm.

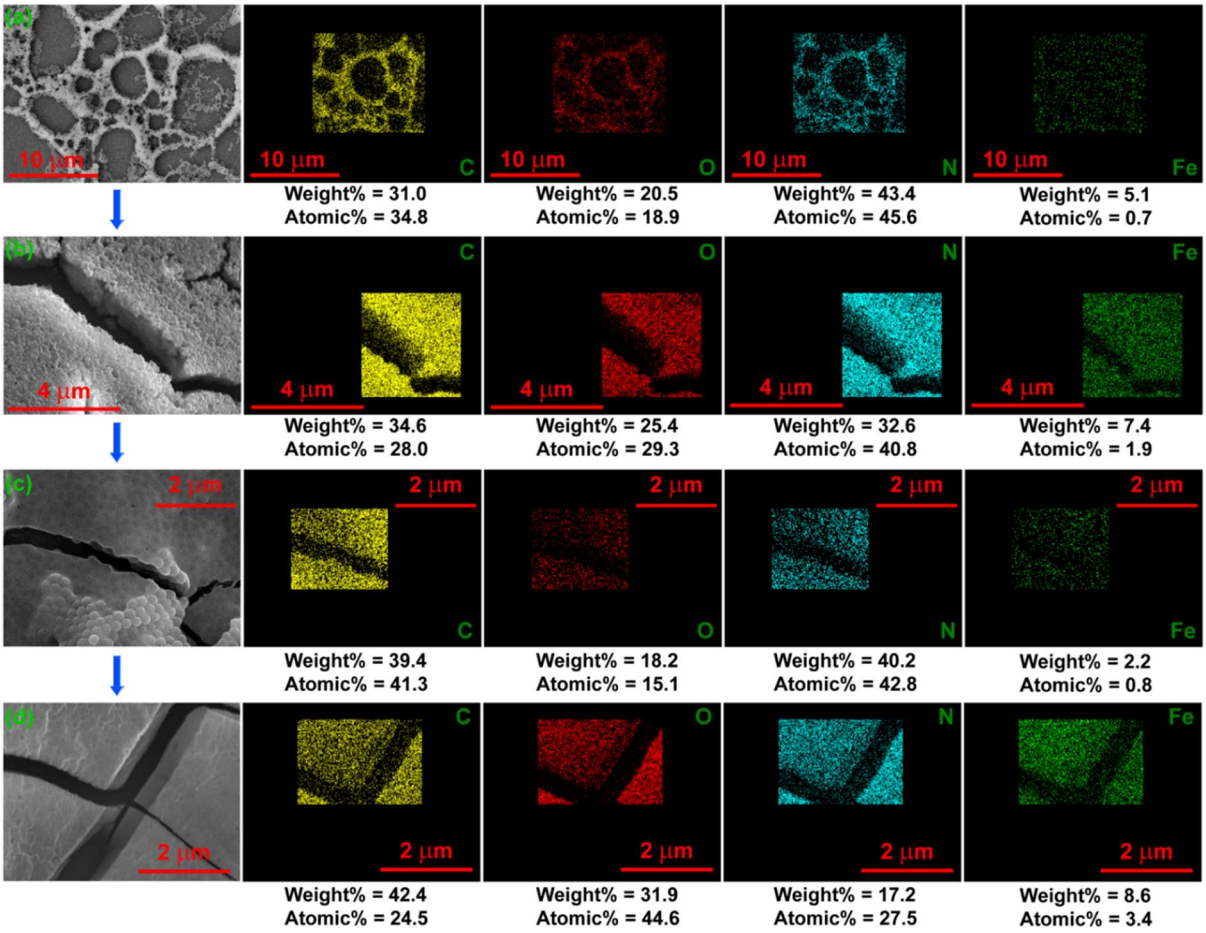


**Figure S37**. (a-d) Transmutation of the $[Fe^{III}(Cl)bTAML]^{2-}$@TpDPP COF nano-spheres into $[Fe^{III}(Cl)bTAML]^{2-}$@TpDPP COF thin film at the interface of the DCM-water bilayer. The Transmutation was monitored with energy-dispersive X-ray spectrometry (EDS) elemental mapping which showcased the stable entrapment of the $(Et_4N)_2[Fe^{III}(Cl)bTAML]$ catalyst inside the TpDPP COF scaffold and eventually generated $[Fe^{III}(Cl)bTAML]^{2-}$@TpDPP COF thin film at the interface.

## Section S-15: Confocal Imaging

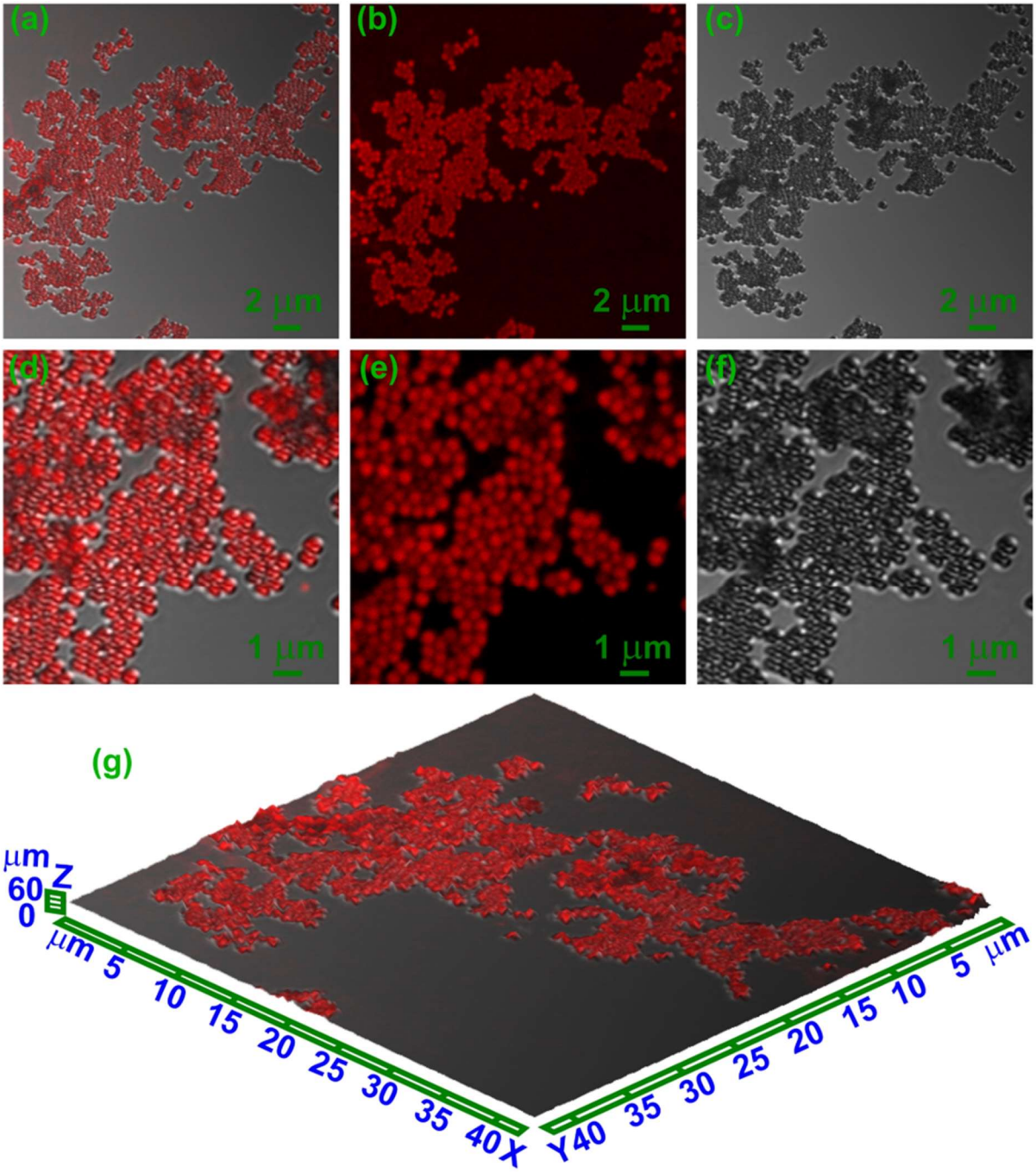


**Figure S38**. (a-c) Confocal image, fluorescence image, and optical image of the Rhodamine B@TpDPP COF nano-spheres@$Et_3N$ (d-f) Confocal, fluorescence, and optical images at higher magnification (g) 2.5D confocal imaging shows the adsorption of dyes (Rhodamine B) within the porous TpDPP COF nano-spheres.

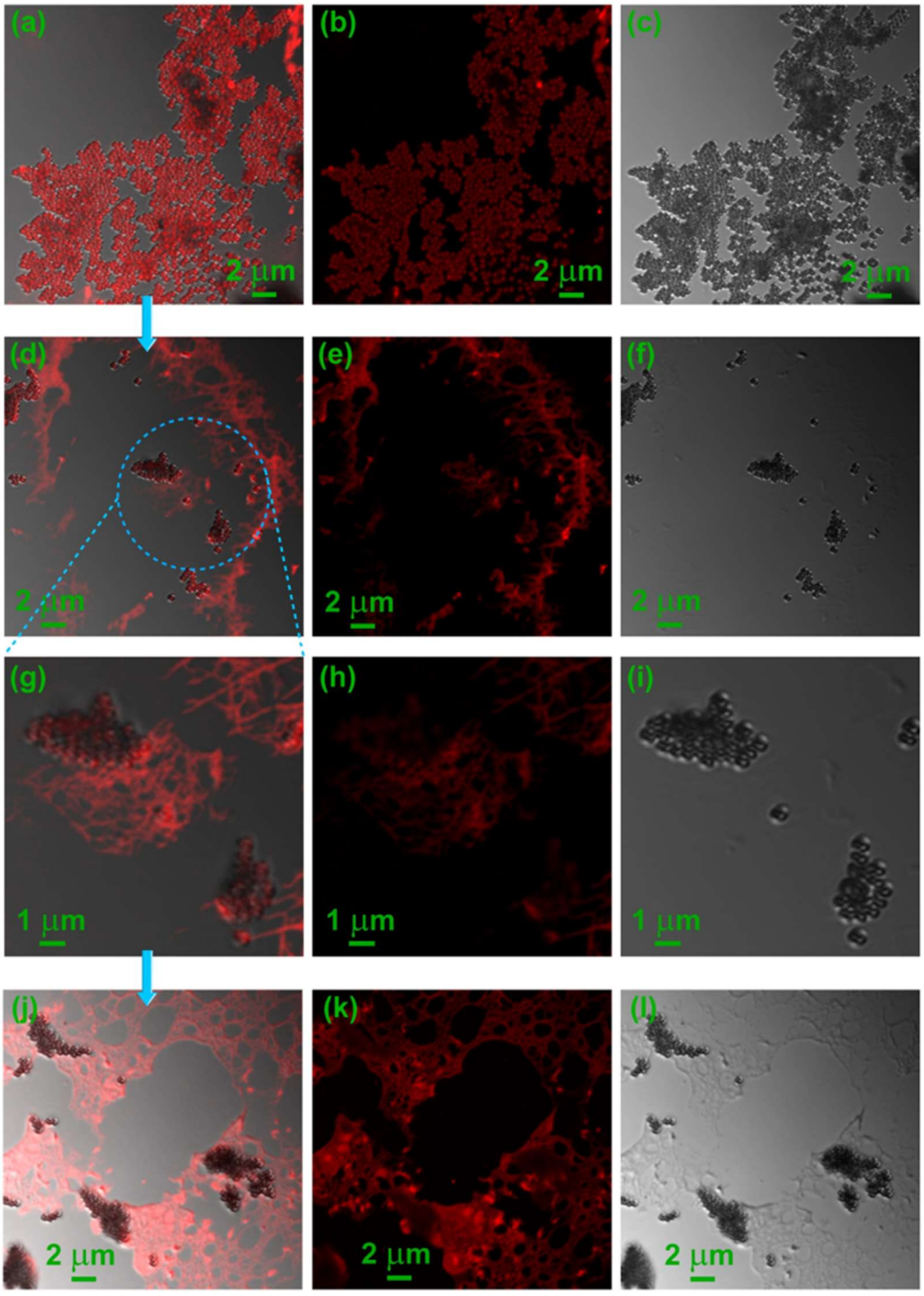


**Figure S39**. To ascertain the immobilized catalysts' enduring stability during the covalent self-assembly, we have monitored the nano-spheres → fibers → thin film transmutation with confocal imaging. The confocal imaging (a, d, g, and j) revealed the uniform adsorption and distribution of (Rhodamine B) dye molecules inside the COF nano-spheres and COF fibers, which manifested their high and stable porosity and adsorption capacity.

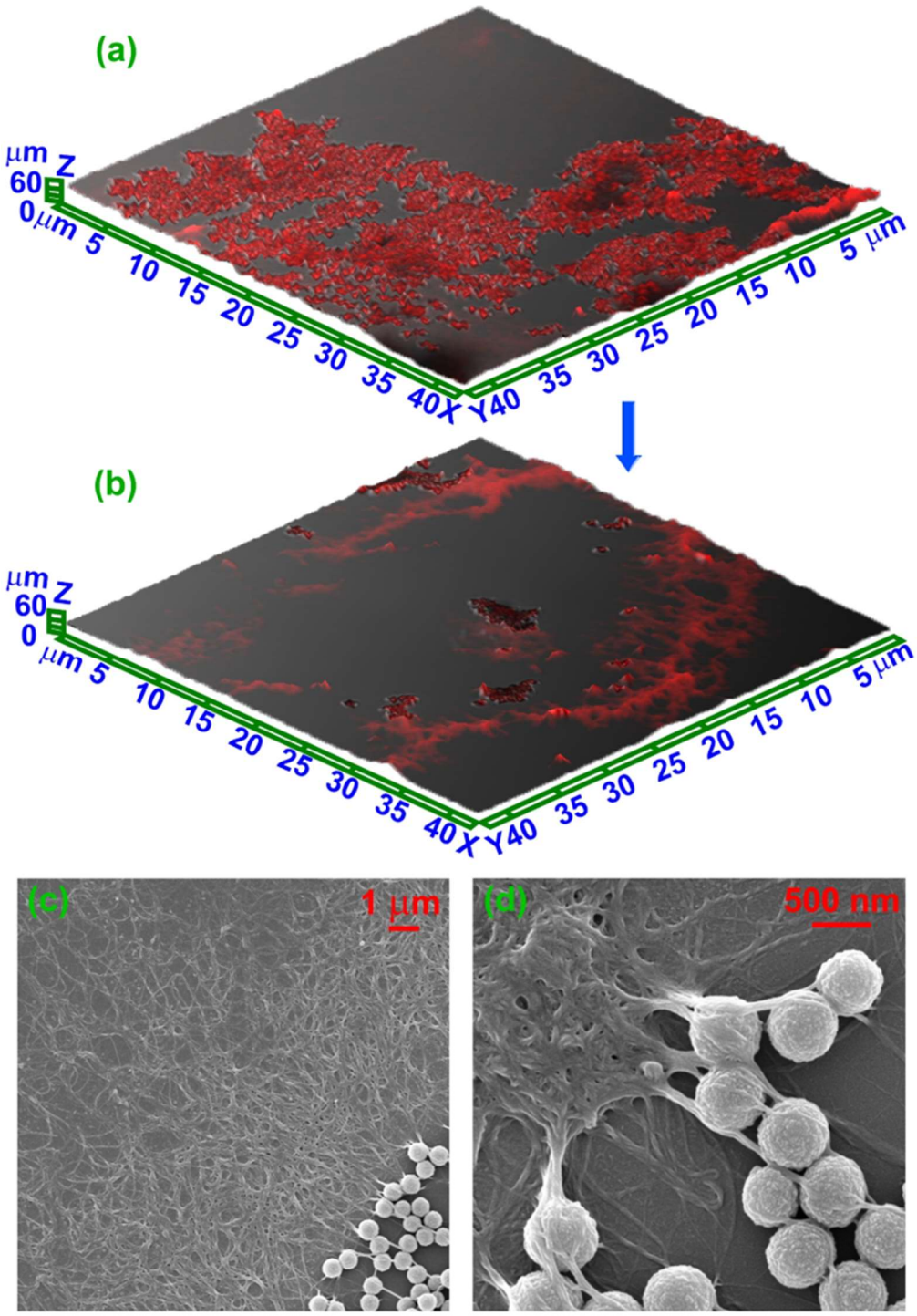


**Figure S40**. (a) 2.5 D confocal imaging of the Rhodamine B@TpDPP COF nano-spheres at the very beginning of the transmutation from nano-spheres to the thin film via the formation of fibers/threads as intermediates. (b) 2.5 D confocal image showcasing the protrusion of the porous fibers/threads at the interface of two nano-spheres transmuting the spheres into films. (c-d) SEM images supporting the observations in confocal images of protrusion of the porous fibers/threads at the interface of two nano-spheres.

## Section S-16: Contact Angle Measurement

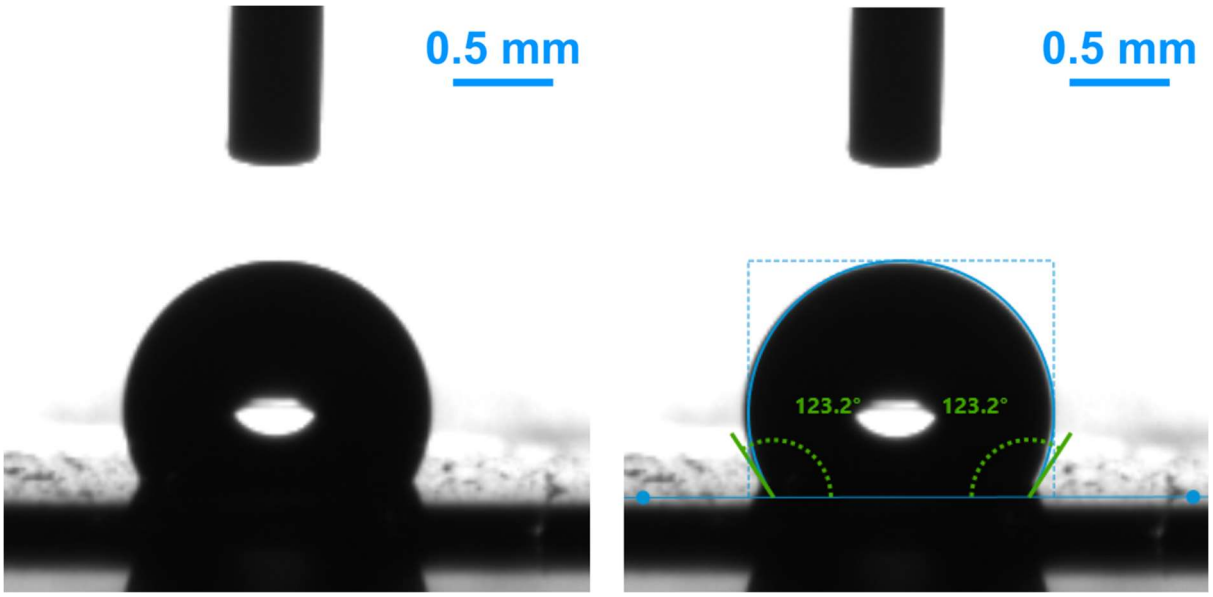


**Figure S41**. (a) Side view of a sessile drop of water on a $[Fe^{III}(Cl)bTAML]^{2-}$@TpDPP COF thin film surface (b) The baseline is shown in turquoise blue. The green lines show the fitting result. The contact angle measurement of the catalyst immobilized TpDPP COF thin film revealed the hydrophobic nature of the film having a contact angle of 123.2°.

## Section S-17: Time-Dependent pH Measurement

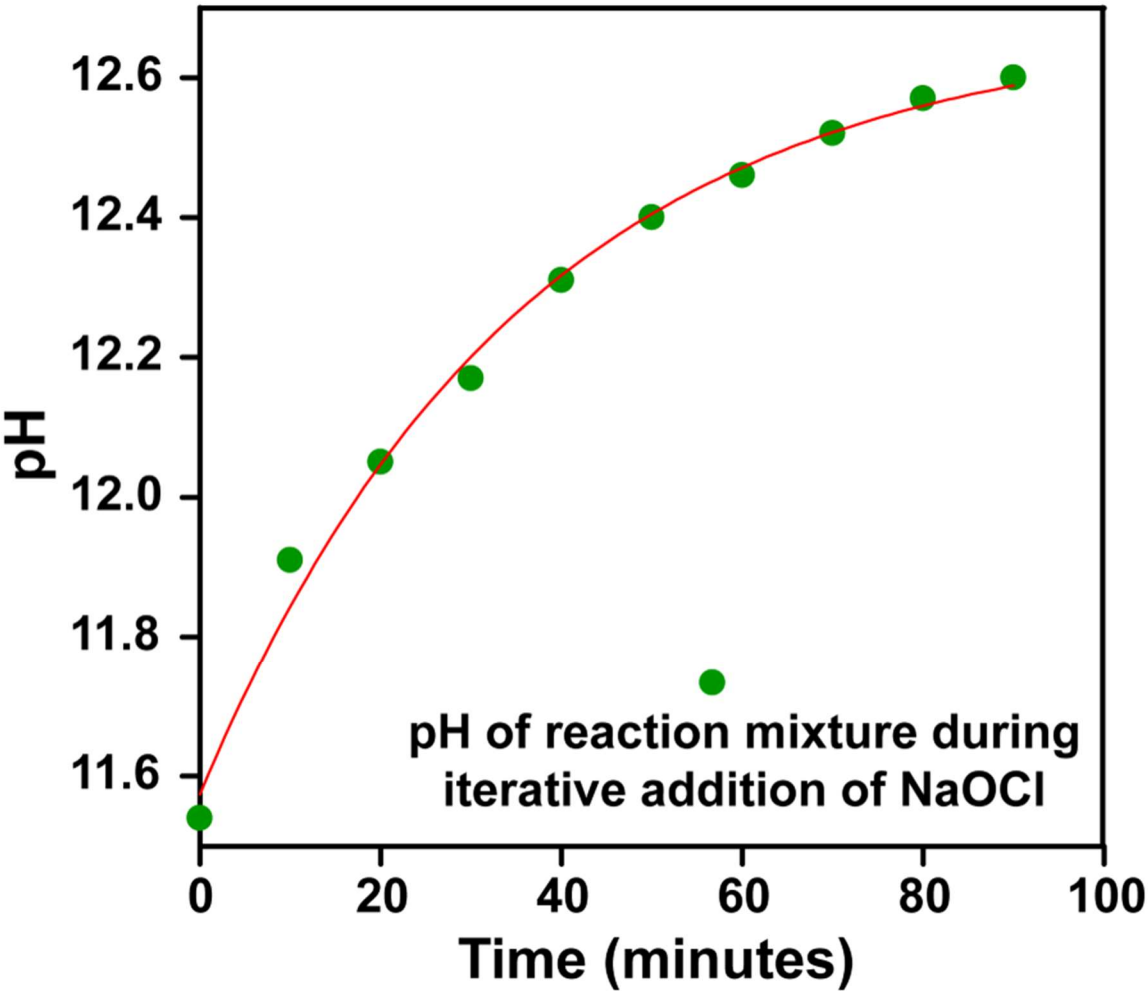


**Figure S42**. Time-dependent pH measurement of the catalytic reaction mixture due to the iterative (10 µl x 20 times maintaining the time interval of the addition of 5 minutes) addition of 0.6 M aqueous solution of NaOCl as the terminal oxidant. The final pH of the reaction mixture was measured as 12.60. The pH of Sodium hypochlorite solution about 4% w/v available chlorine was measured to be 13.24 at 25°C where the pH of the Milli-Q water was measured to be 6.9 at 25°C.

## Section S-18: C-H Functionalization in Flow

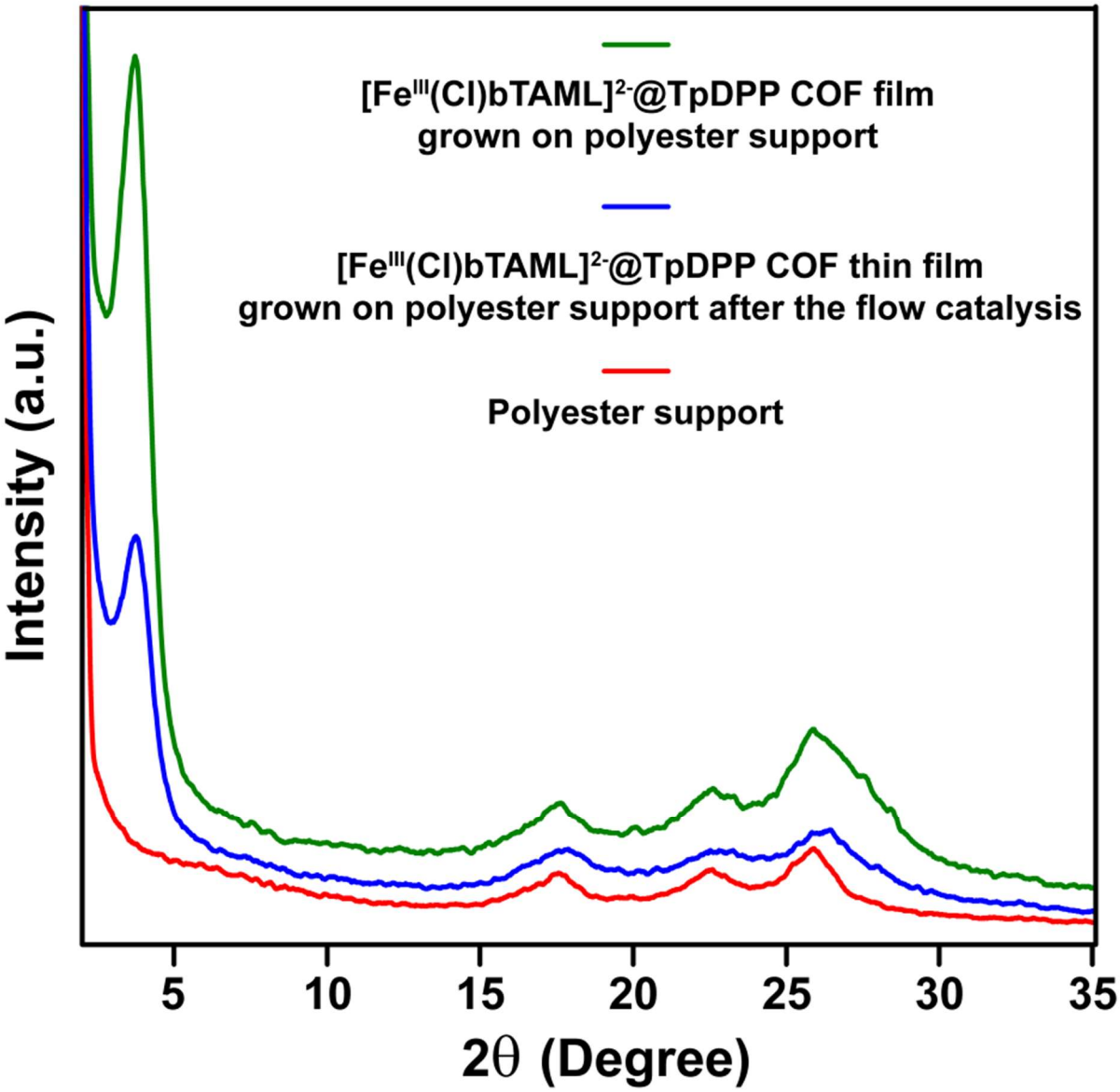


**Figure S43**. PXRD of the polyester support, [Fe$^{III}$(Cl)bTAML]$^{2-}$@TpDPP COF thin film grown on top of the polyester support, and the same [Fe$^{III}$(Cl)bTAML]$^{2-}$@TpDPP COF thin film after the completion of the floe catalysis.

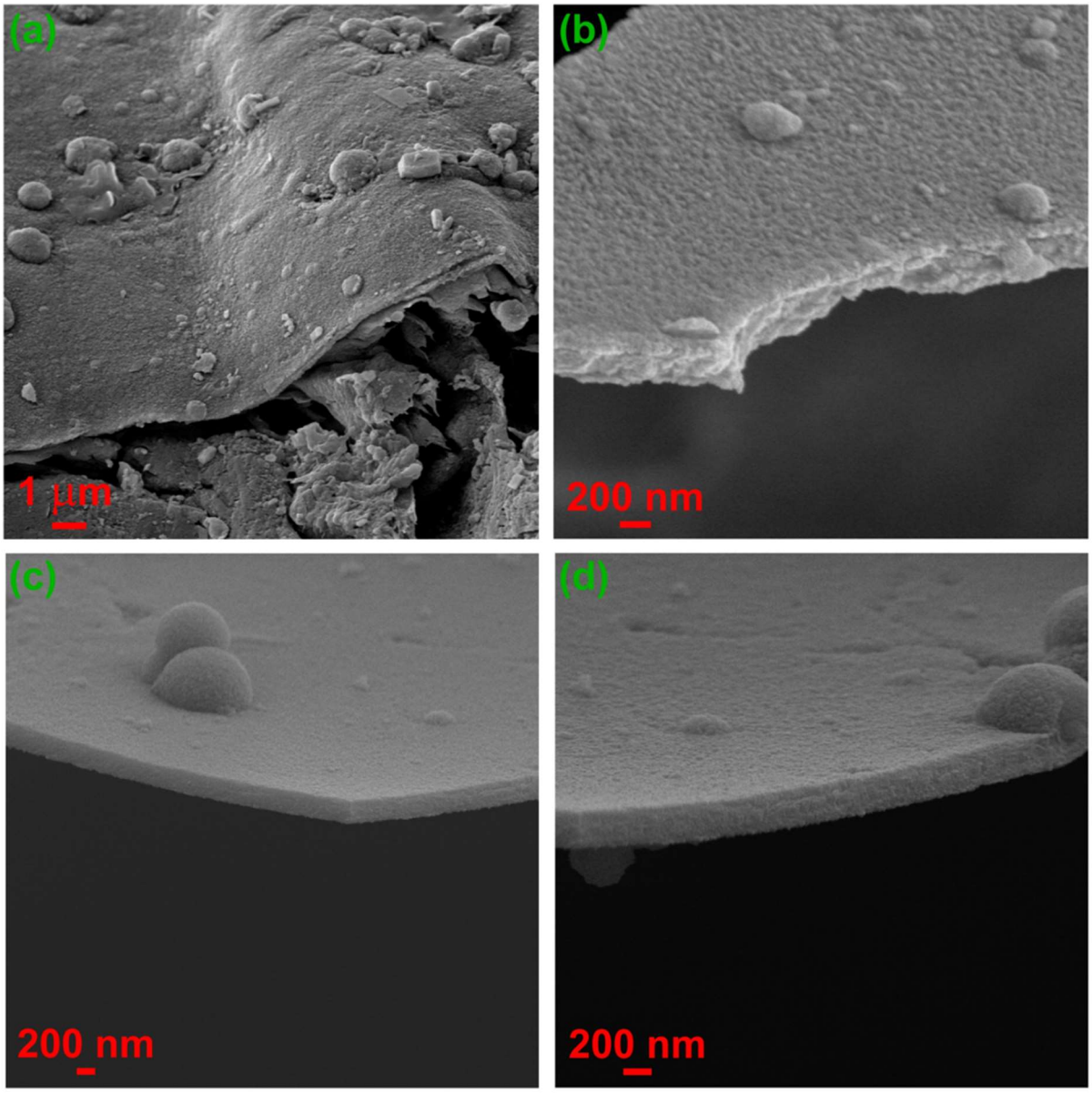


**Figure S44**. (a-b) SEM images showing the formation of $[Fe^{III}(Cl)bTAML]^{2-}$@TpDPP COF thin film grown on top of polyester support *via* the multiple drop-casting of the $[Fe^{III}(Cl)bTAML]^{2-}$@TpDPP COF nano-spheres (c-d) After the completion of the formation of $[Fe^{III}(Cl)bTAML]^{2-}$@TpDPP COF thin film showcasing the thickness around 250-270 nm.

# Section S-19: GC-MS data

**Product identification and quantification (in GC-MS)**

All the products formed by alkane and alkene oxidation reactions were analyzed by gas chromatography-mass spectrometry (GC-MS). After each electrolysis, 500 µl of the reaction mixture was taken out from the electrochemical cell and diluted with 2000 µl of acetonitrile. The 5-fold diluted solution was analyzed by GC-MS. An internal standard (bromobenzene) was used for all the reactions. The yield and conversion were estimated using the response factor of authentic substrates and products. The concentration of substrate (8 x $10^{-3}$ M), internal standard (8 x $10^{-3}$ M), catalyst (4 x $10^{-4}$ M), and terminal oxidant (12 x $10^{-2}$ M) were maintained all the substrate scope.

We measured the GC-MS trace of adamantane, 1-adamantanol, and 2-adamantanone of concentration 1.6 x $10^{-3}$ M using the internal standard (bromobenzene) of similar concentration to estimate their respective response factor. As an example, we found the response factor of adamantane, 1-adamantanol, and 2-adamantanone to be 1.5, 0.7. and 0.8 using bromobenzene as the internal standard.[5]

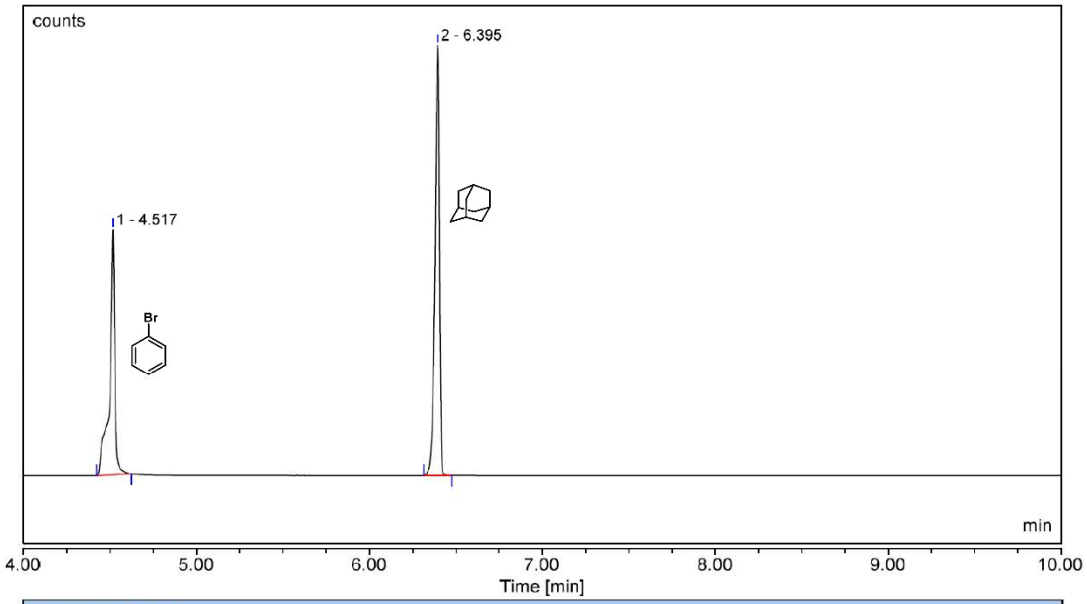


Integration Results

| No. | Peak Name | Retention Time min | Area counts*min | Height counts | Relative Area % | Relative Height % | Amount n.a. |
|---|---|---|---|---|---|---|---|
| 1 | | 4.517 | 24788989.699 | 732239011.896 | 38.99 | 36.37 | n.a. |
| 2 | | 6.395 | 38793014.338 | ########### | 61.01 | 63.63 | n.a. |
| **Total:** | | | **63582004.036** | **###########** | **100.00** | **100.00** | |

**Figure S45**. GC-MS traces for adamantane in acetonitrile using bromobenzene as the internal standard of the same concentration as adamantane.

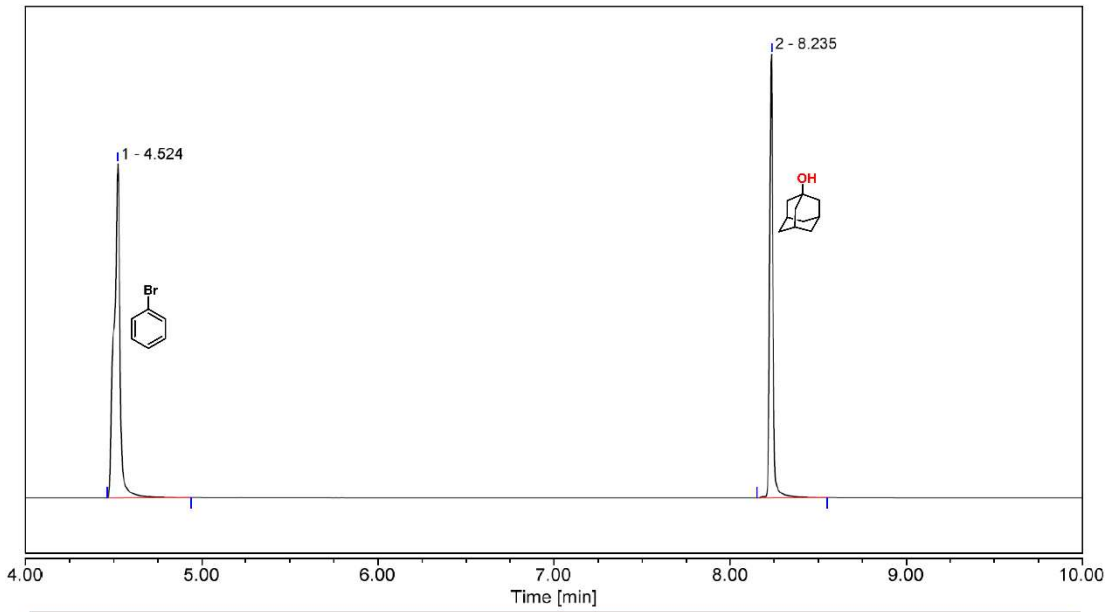


**Integration Results**

| No. | Peak Name | Retention Time min | Area counts*min | Height counts | Relative Area % | Relative Height % | Amount n.a. |
|---|---|---|---|---|---|---|---|
| 1 | | 4.524 | 24125409.881 | 611256676.751 | 57.89 | 42.95 | n.a. |
| 2 | | 8.235 | 17548908.386 | 811841229.805 | 42.11 | 57.05 | n.a. |
| **Total:** | | | **41674318.267** | **##########** | **100.00** | **100.00** | |

**Figure S46**. GC-MS traces for 1-adamantanol in acetonitrile using bromobenzene as the internal standard of the same concentration as 1-adamantanol.

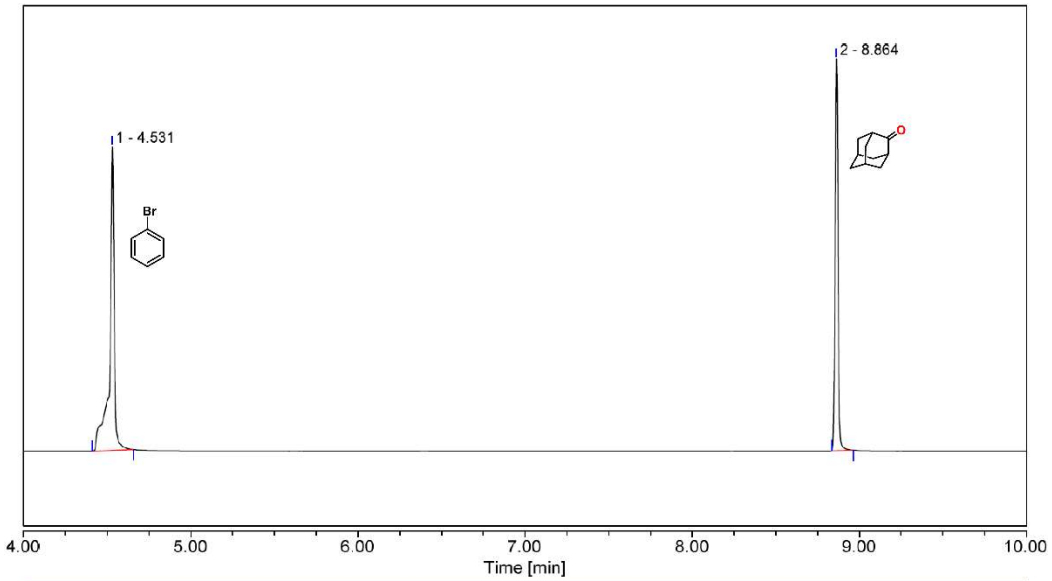


**Integration Results**

| No. | Peak Name | Retention Time min | Area counts*min | Height counts | Relative Area % | Relative Height % | Amount n.a. |
|---|---|---|---|---|---|---|---|
| 1 | | 4.531 | 25705424.548 | 816499063.948 | 55.13 | 43.65 | n.a. |
| 2 | | 8.864 | 20923039.533 | ########## | 44.87 | 56.35 | n.a. |
| **Total:** | | | **46628464.081** | **##########** | **100.00** | **100.00** | |

**Figure S47**. GC-MS traces for 2-adamantanone in acetonitrile using bromobenzene as the internal standard of the same concentration as 2-adamantanone.

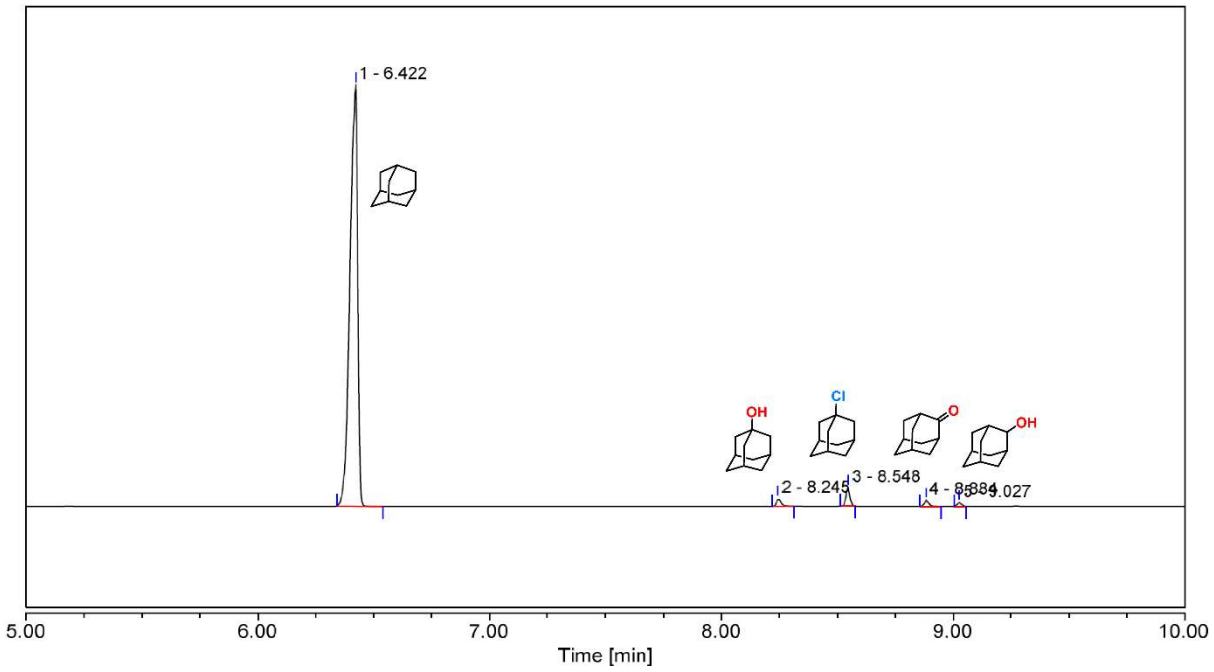


**Figure S48**. GC-MS traces for the oxidation of adamantane in the control experiment (Adamantane+NaOCl) in acetonitrile in absence of TpDPP COF nano-spheres and $(Et_4N)_2[Fe^{III}(Cl)bTAML]$ catalyst.

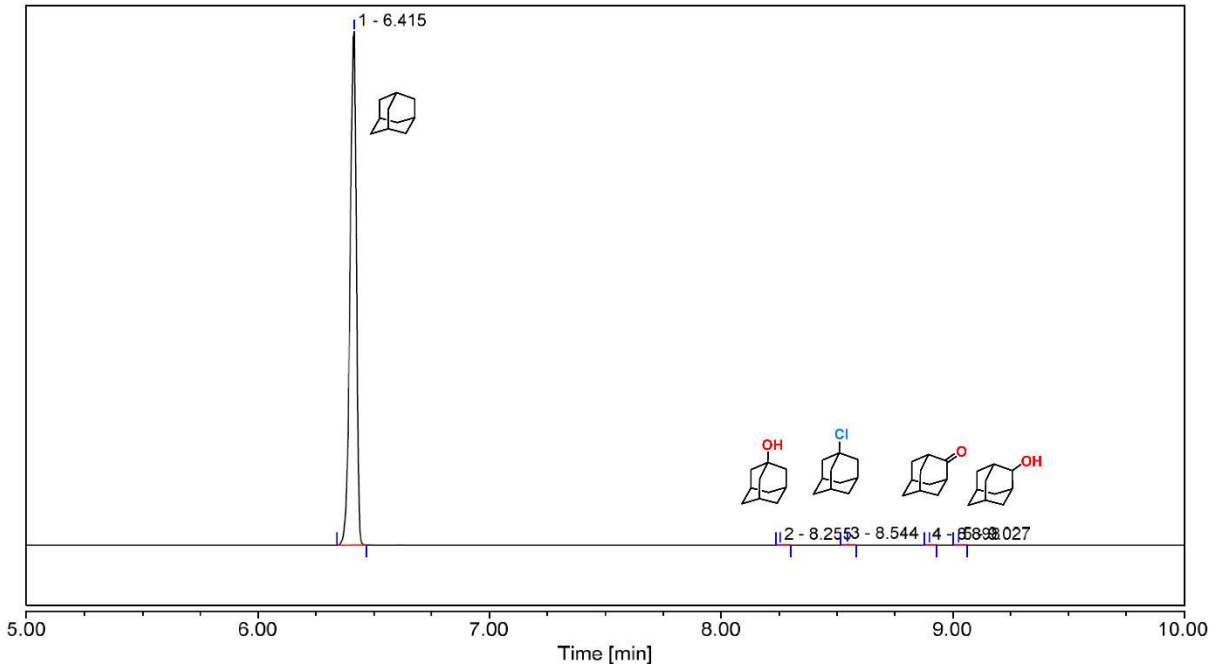


**Figure S49**. GC-MS traces for the oxidation of adamantane in the control experiment (Adamantane+NaOCl+TpDPP COF nano-spheres) in acetonitrile in absence of $(Et_4N)_2[Fe^{III}(Cl)bTAML]$ catalyst.

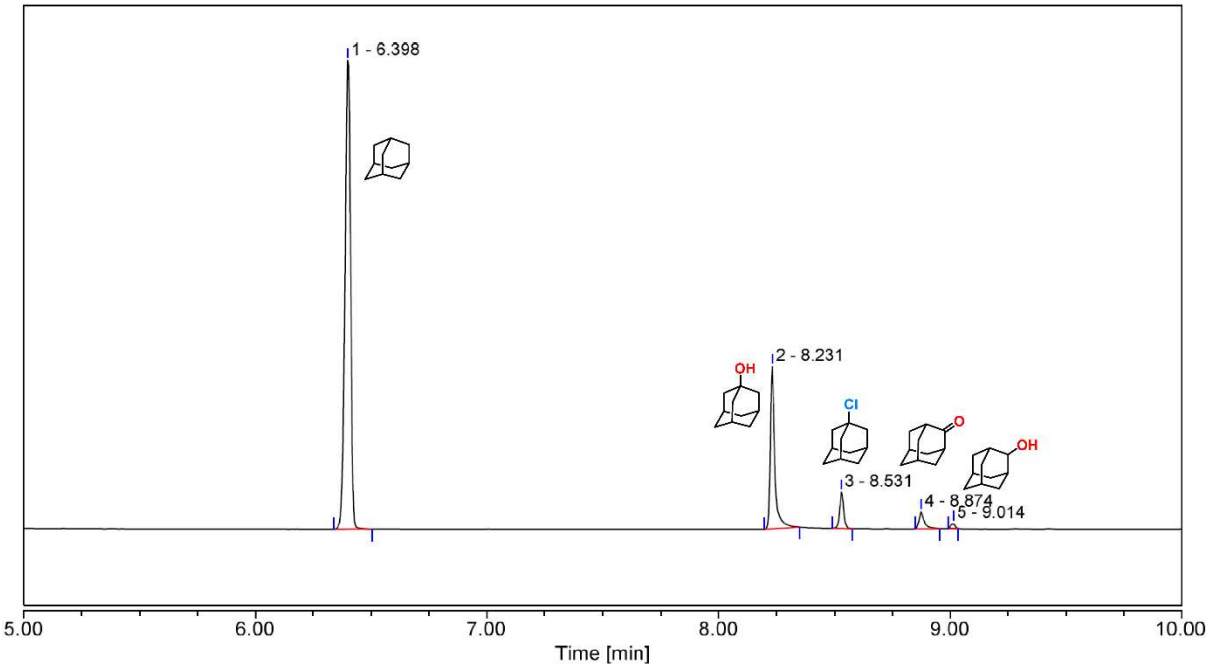


**Figure S50**. GC-MS traces for the oxidation of adamantane (Adamantane+NaOCl+$(Et_4N)_2[Fe^{III}(Cl)bTAML]$ catalyst) in acetonitrile in absence of TpDPP COF nano-spheres (Homogeneous Reaction).

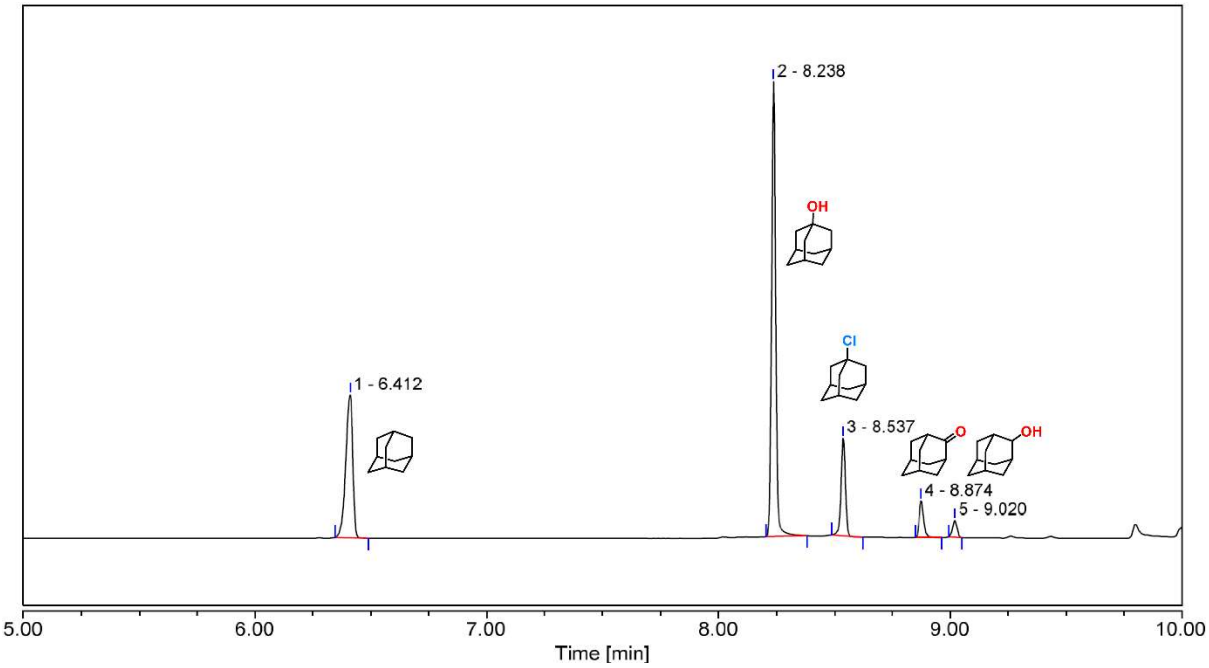


**Figure S51**. GC-MS traces for the oxidation of adamantane in acetonitrile by $[Fe^{III}(Cl)bTAML]^{2-}$@1X TpDPP COF nano-spheres and NaOCl.

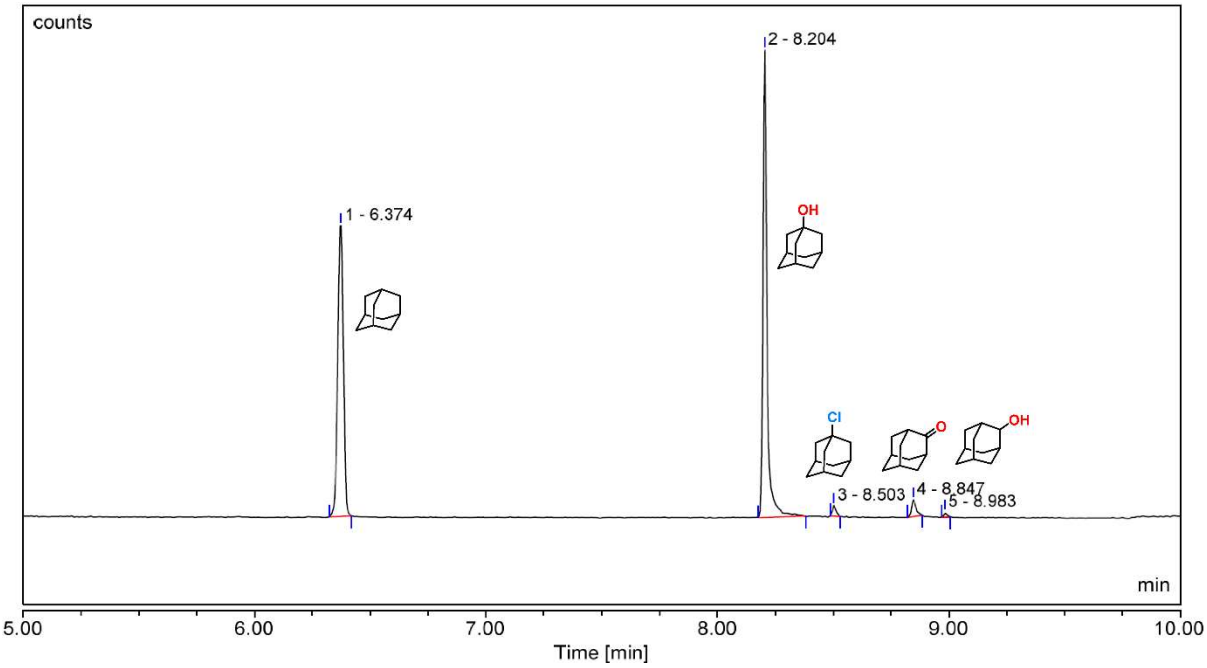


**Figure S52**. GC-MS traces for the oxidation of adamantane in acetonitrile by $[Fe^{III}(Cl)bTAML]^{2-}$@2X TpDPP COF nano-spheres and NaOCl (**cycle – 1**).

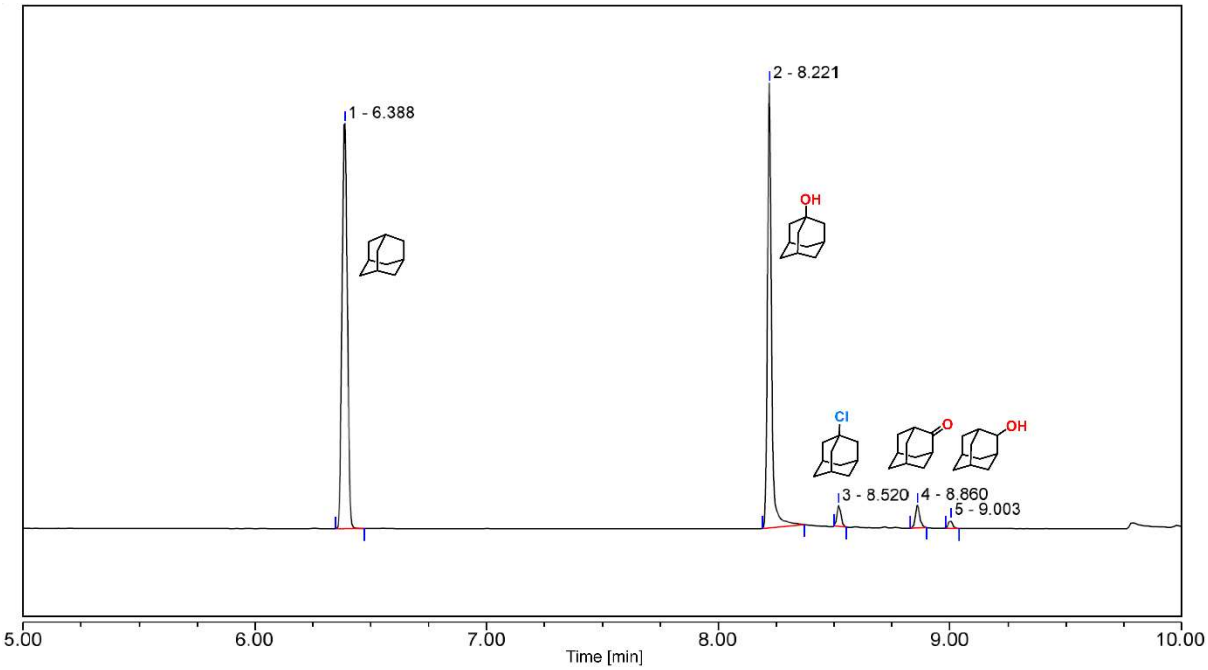


**Figure S53**. GC-MS traces for the oxidation of adamantane in acetonitrile by $[Fe^{III}(Cl)bTAML]^{2-}$@3X TpDPP COF nano-spheres and NaOCl.

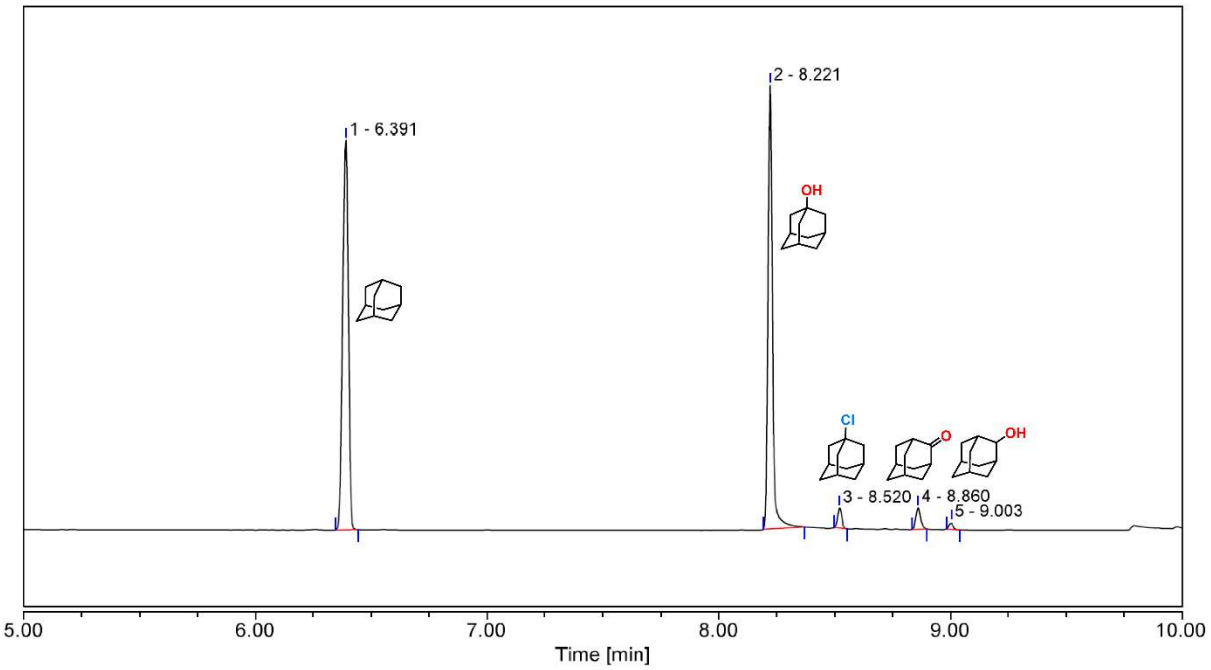


**Figure S54**. GC-MS traces for the oxidation of adamantane in acetonitrile by $[Fe^{III}(Cl)bTAML]^{2-}$@4X TpDPP COF nano-spheres and NaOCl.

## Optimization of catalytical TpDPP COF nano-spheres

**$[Fe^{III}(Cl)bTAML]^{2-}$@1X TpDPP COF nano-spheres:** $(Et_4N)_2[Fe^{III}(Cl)bTAML]$ catalyst immobilized from 1 ml 0.4 mM acetonitrile solution by 1 mg of COF nano-spheres. Loading of the catalyst by as-synthesized TpDPP COF nano-spheres is 21.2 wt% (considering the adsorption of the catalyst molecules from the solution by TpDPP COF nano-spheres 94.8% as measures in UV-vis spectrometer). Loading/immobilization of the catalyst molecules inside the TpDPP COF nano-spheres could also be quantified as 270 mg $g^{-1}$.

**$[Fe^{III}(Cl)bTAML]^{2-}$@2X TpDPP COF nano-spheres:** $(Et_4N)_2[Fe^{III}(Cl)bTAML]$ catalyst immobilized from 1 ml 0.4 mM acetonitrile solution by 2 mg of COF nano-spheres. Loading of the catalyst by as-synthesized TpDPP COF nano-spheres is 12.3 wt% (the adsorption of the catalyst molecules from the solution by TpDPP COF nano-spheres ~100%). Loading/immobilization of the catalyst molecules inside the TpDPP COF nano-spheres could also be quantified as 140 mg $g^{-1}$.

**$Fe^{III}(Cl)bTAML]^{2-}$@3X TpDPP COF nano-spheres:** $(Et_4N)_2[Fe^{III}(Cl)bTAML]$ catalyst immobilized from 1 ml 0.4 mM acetonitrile solution by 3 mg of COF nano-spheres. Loading of the catalyst by as-synthesized TpDPP COF nano-spheres is 8.5 wt%. Loading/immobilization of the catalyst molecules inside the TpDPP COF nano-spheres could also be quantified as 93 mg $g^{-1}$.

**$Fe^{III}$(Cl)bTAML]$^{2-}$@4X TpDPP COF nano-spheres:** $(Et_4N)_2[Fe^{III}(Cl)bTAML]$ catalyst immobilized from 1 ml 0.4 mM acetonitrile solution by 4 mg of COF nano-spheres. Loading of the catalyst by as-synthesized TpDPP COF nano-spheres is 6.5 wt%. Loading/immobilization of the catalyst molecules inside the TpDPP COF nano-spheres could also be quantified as 70 mg $g^{-1}$.

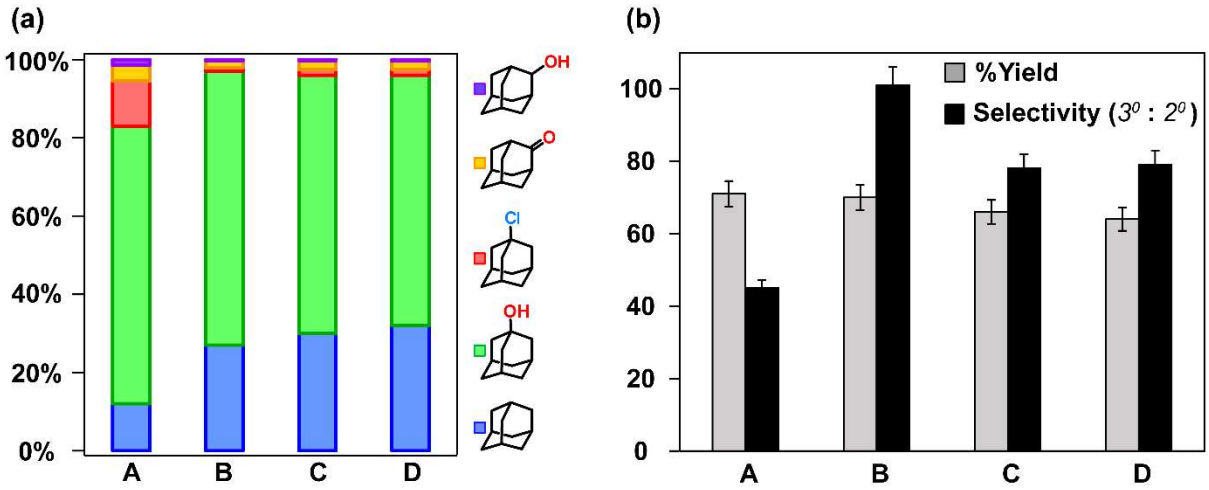


(c)

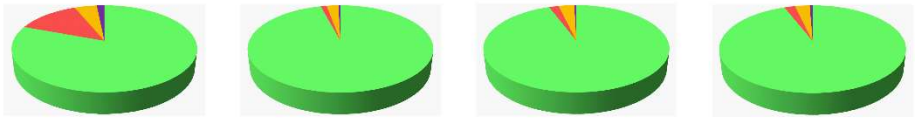

(d)

| | A | B | C | D |
|---|---|---|---|---|
| | [$Fe^{III}$(Cl)bTAML]$^{2-}$@ 1X TpDPP COF NPs + NaOCl | [$Fe^{III}$(Cl)bTAML]$^{2-}$@ 2X TpDPP COF NPs + NaOCl | [$Fe^{III}$(Cl)bTAML]$^{2-}$@ 3X TpDPP COF NPs + NaOCl | [$Fe^{III}$(Cl)bTAML]$^{2-}$@ 4X TpDPP COF NPs + NaOCl |
| %Conversion | 88 | 73 | 70 | 68 |
| %yield | 71 | 70 | 66 | 64 |
| Selectivity ($3^0$ : $2^0$) | 45:1 | 101:1 | 78:1 | 79:1 |

**Figure S55**. (a) Optimization for the oxidation of adamantane in acetonitrile by 4 different catalytic TpDPP COF nano-spheres [$Fe^{III}$(Cl)bTAML]$^{2-}$@1X TpDPP COF nano-spheres (**A**), [$Fe^{III}$(Cl)bTAML]$^{2-}$@2X TpDPP COF nano-spheres (**B**), [$Fe^{III}$(Cl)bTAML]$^{2-}$@3X TpDPP COF nano-spheres (**C**), and [$Fe^{III}$(Cl)bTAML]$^{2-}$@4X TpDPP COF nano-spheres (**D**) and NaOCl. (b) Bar chart representing the comparison of the catalytic yield and selectivity (3°:2°) using the previously mentioned catalytic TpDPP COF nano-spheres. (c) Pie chart and (d) table representing the comparison of the catalytic conversion, yield, and selectivity (3°:2°) using previously mentioned catalytic TpDPP COF nano-spheres in detail. Using the catalytic experiments for optimization, we found that [$Fe^{III}$(Cl)bTAML]$^{2-}$@2X TpDPP COF nano-spheres could able to oxidize adamantane to 1-adamantanol with the highest degree of

selectivity (3°:2°=101:1) with 70% catalytic yield. As a consequence, we had carried out the catalytical heterogeneous C-H functionalization for all the other substrates using $[Fe^{III}(Cl)bTAML]^{2-}$@2X TpDPP COF nano-spheres and NaOCl.

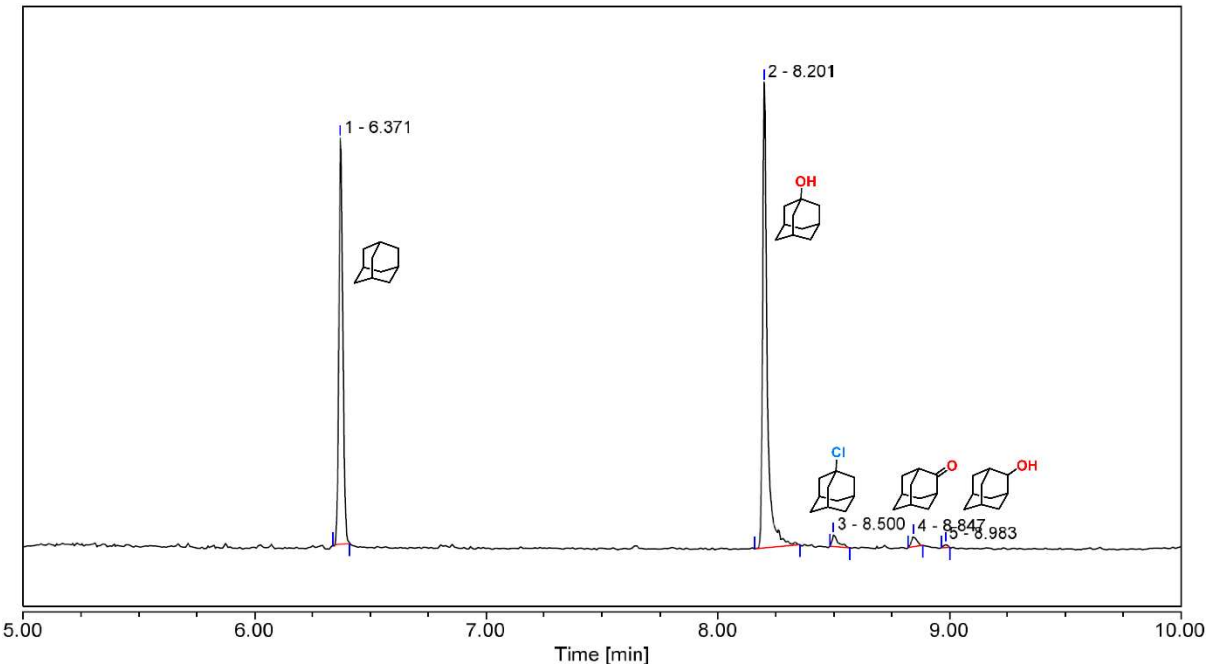


**Figure S56.** GC-MS traces for the oxidation of adamantane in acetonitrile by recyclable $[Fe^{III}(Cl)bTAML]^{2-}$@2X TpDPP COF nano-spheres and NaOCl (**cycle – 2**).

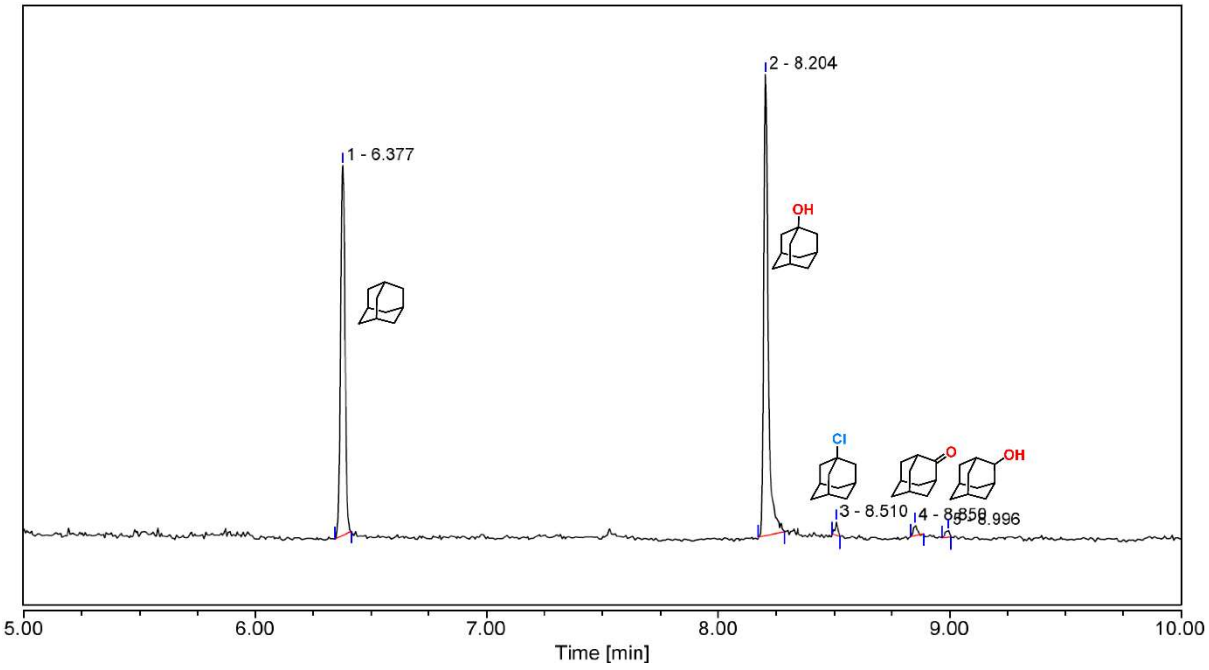


**Figure S57.** GC-MS traces for the oxidation of adamantane in acetonitrile by recyclable $[Fe^{III}(Cl)bTAML]^{2-}$@2X TpDPP COF nano-spheres and NaOCl (**cycle – 3**).

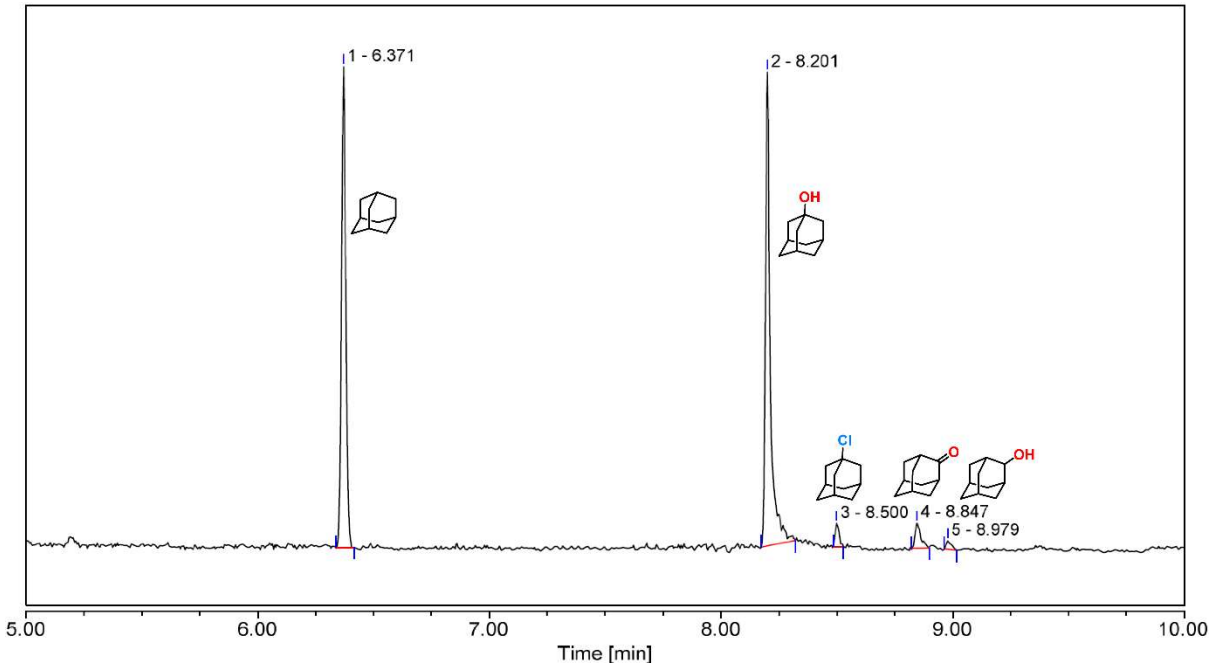


**Figure S58.** GC-MS traces for the oxidation of adamantane in acetonitrile by recyclable $[Fe^{III}(Cl)bTAML]^{2-}$@2X TpDPP COF nano-spheres and NaOCl (**cycle – 4**).

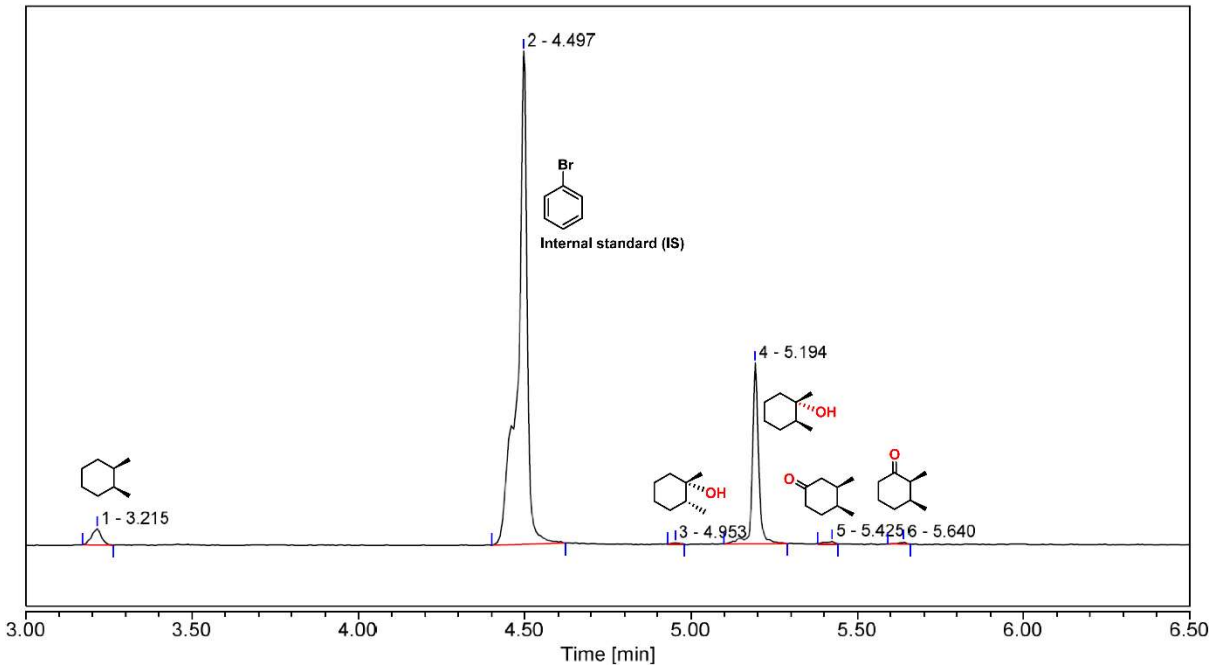


**Figure S59**. GC-MS traces for the oxidation of *cis*-dimethylcyclohexane in acetonitrile by $[Fe^{III}(Cl)bTAML]^{2-}$@2X TpDPP COF nano-spheres and NaOCl.

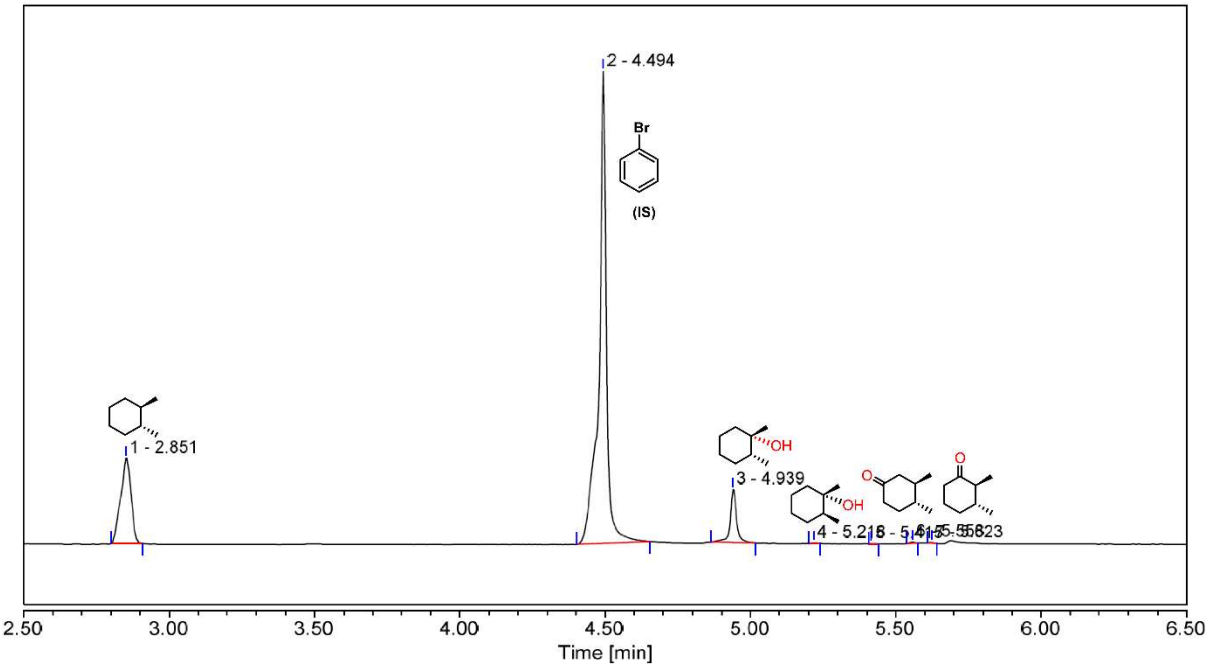


**Figure S60**. GC-MS traces for the oxidation of *trans*-dimethylcyclohexane in acetonitrile by $[Fe^{III}(Cl)bTAML]^{2-}$@2X TpDPP COF nano-spheres and NaOCl.

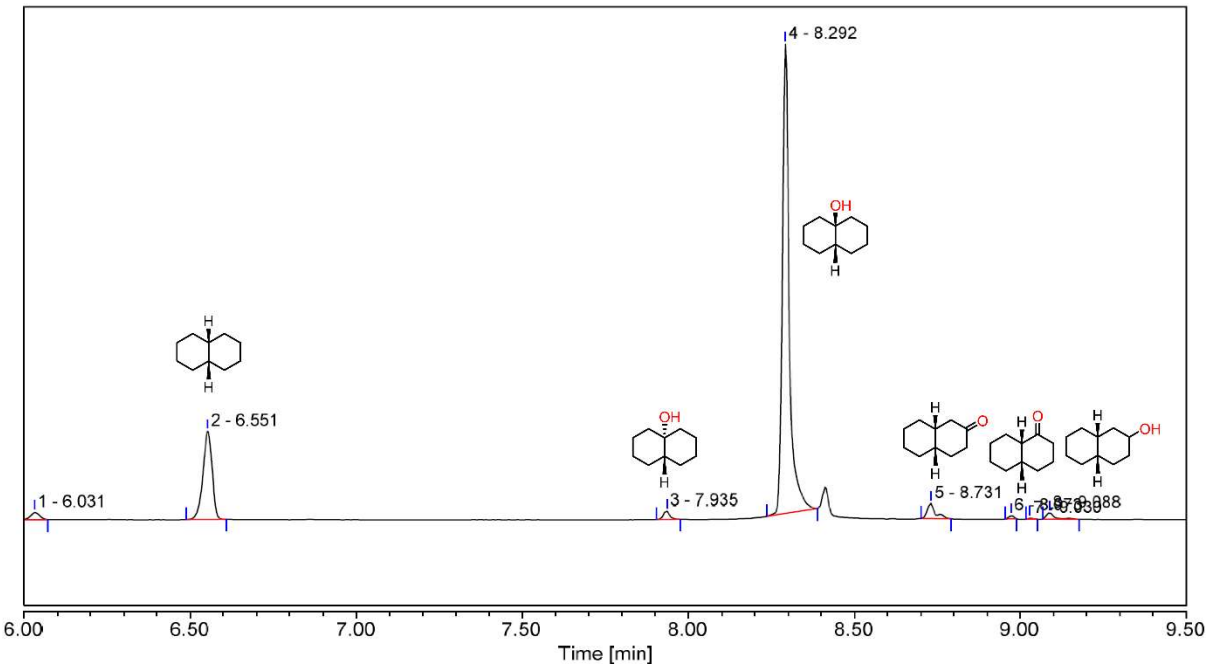


**Figure S61**. GC-MS traces for the oxidation of *cis*-dihydroanthracene in acetonitrile by $[Fe^{III}(Cl)bTAML]^{2-}$@2X TpDPP COF nano-spheres and NaOCl.

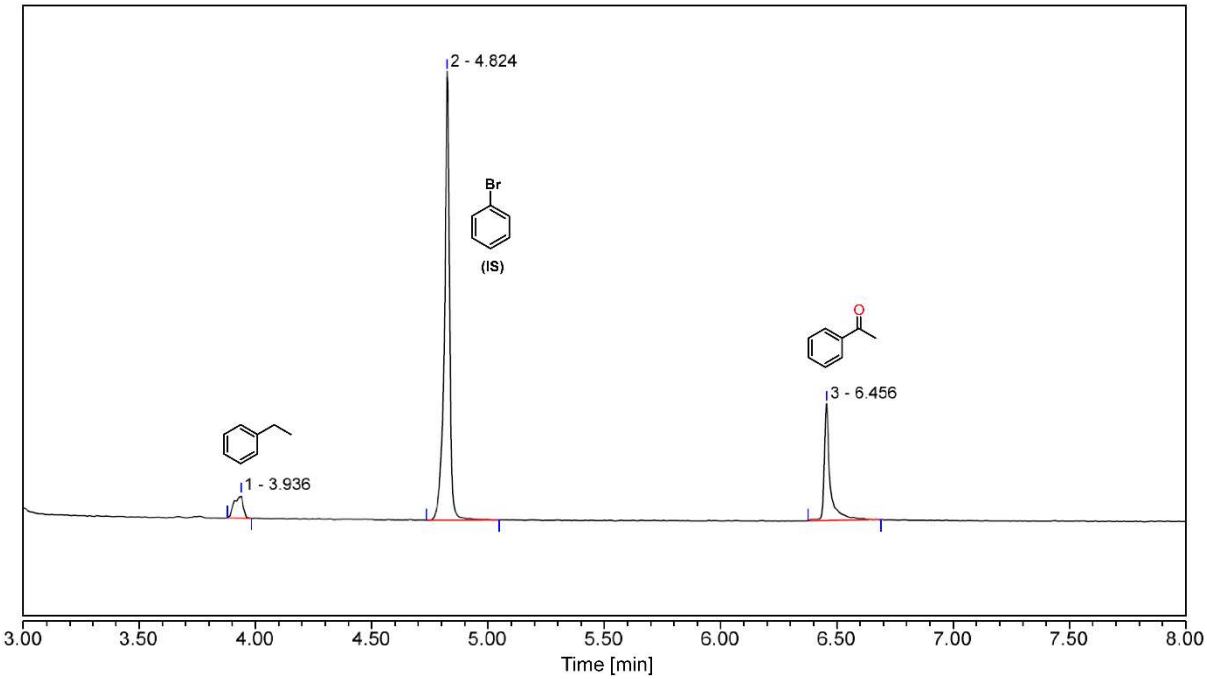


**Figure S62**. GC-MS traces for the oxidation of ethylbenzene in acetonitrile by $[Fe^{III}(Cl)bTAML]^{2-}$@2X TpDPP COF nano-spheres and NaOCl.

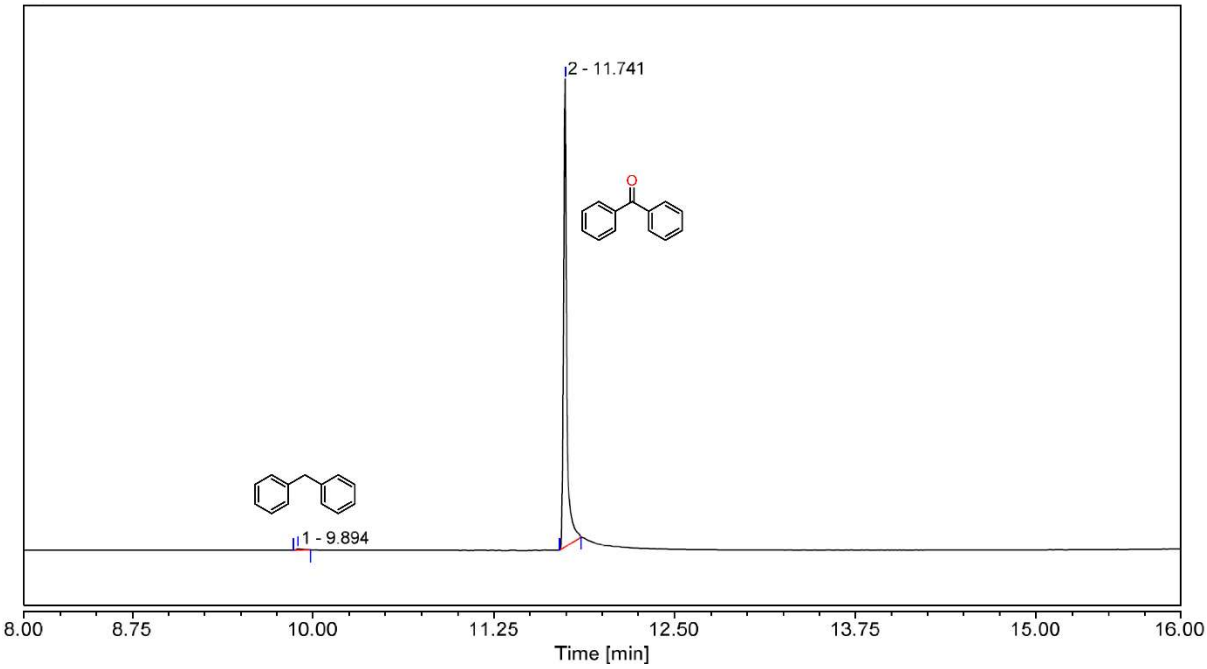


**Figure S63**. GC-MS traces for the oxidation of diphenylmethane in acetonitrile by $[Fe^{III}(Cl)bTAML]^{2-}$@2X TpDPP COF nano-spheres and NaOCl.

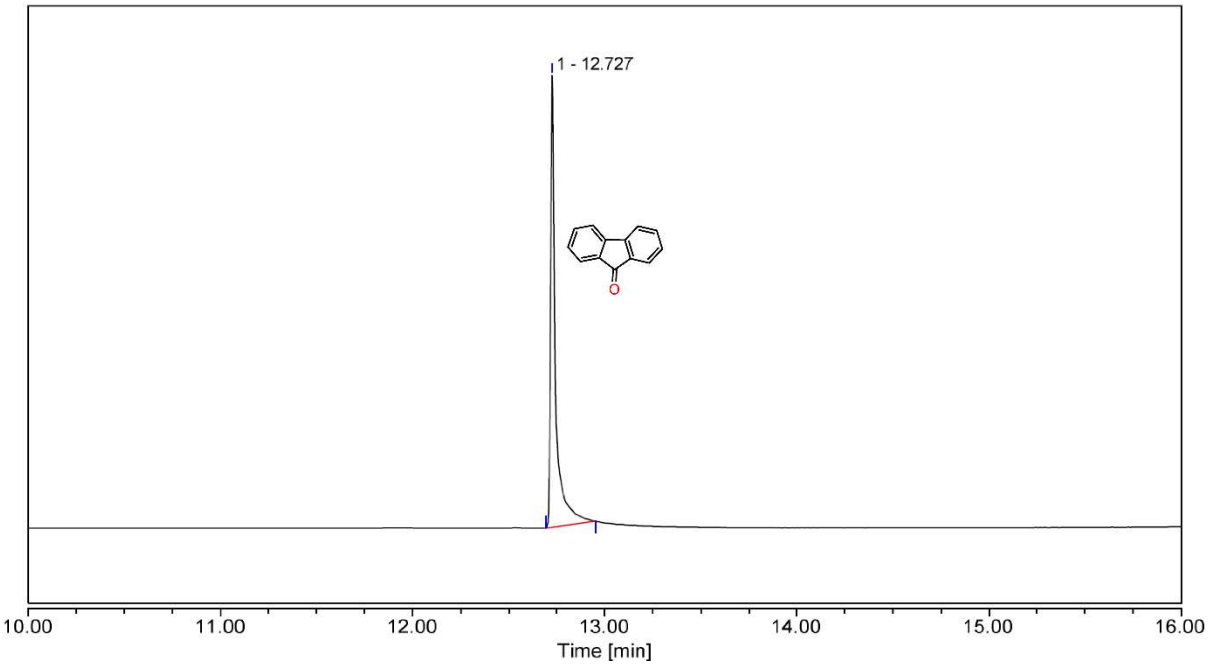


**Figure S64**. GC-MS traces for the oxidation of fluorene in acetonitrile by $[Fe^{III}(Cl)bTAML]^{2-}$@2X TpDPP COF nano-spheres and NaOCl.

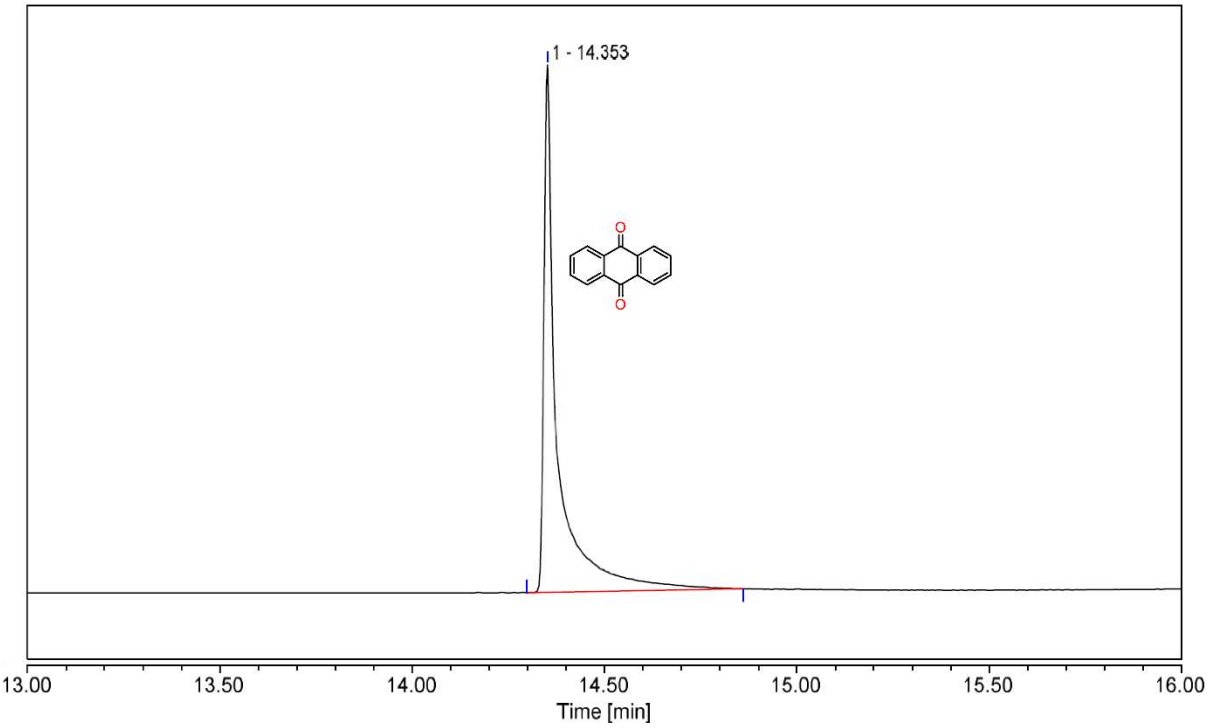


**Figure S65**. GC-MS traces for the oxidation of 9, 10-dihydroanthracene in acetonitrile by $[Fe^{III}(Cl)bTAML]^{2-}$@2X TpDPP COF nano-spheres and NaOCl.

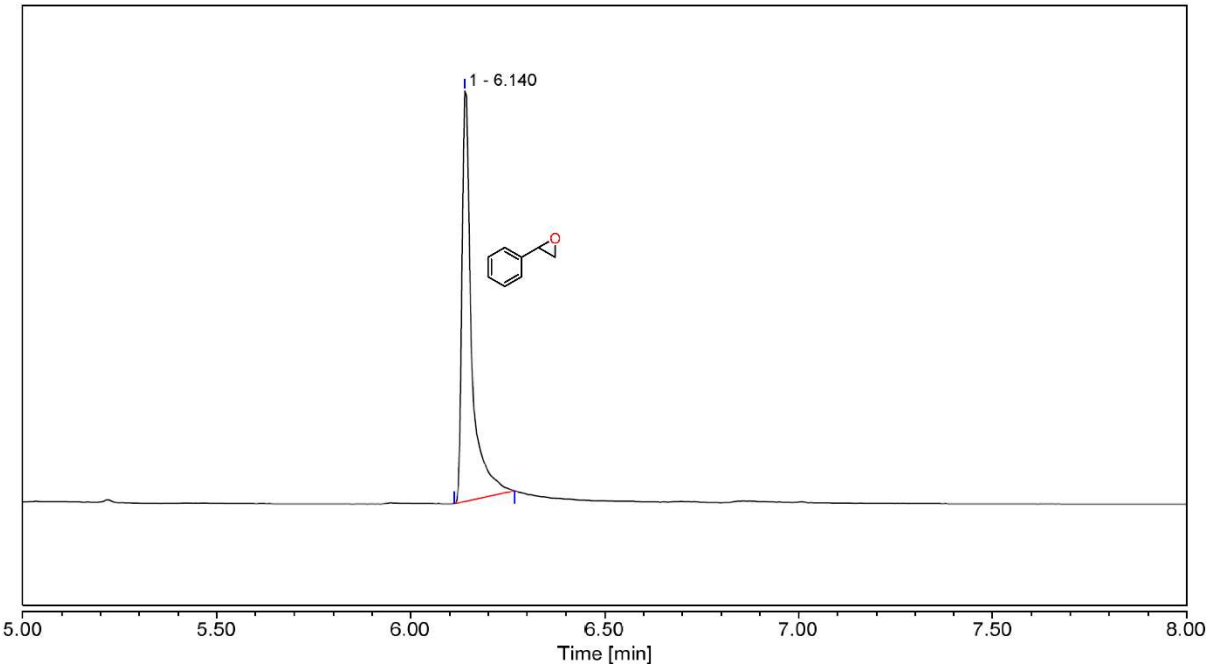


**Figure S66**. GC-MS traces for the oxidation of styrene in acetonitrile by $[Fe^{III}(Cl)bTAML]^{2-}$@2X TpDPP COF nano-spheres and NaOCl.

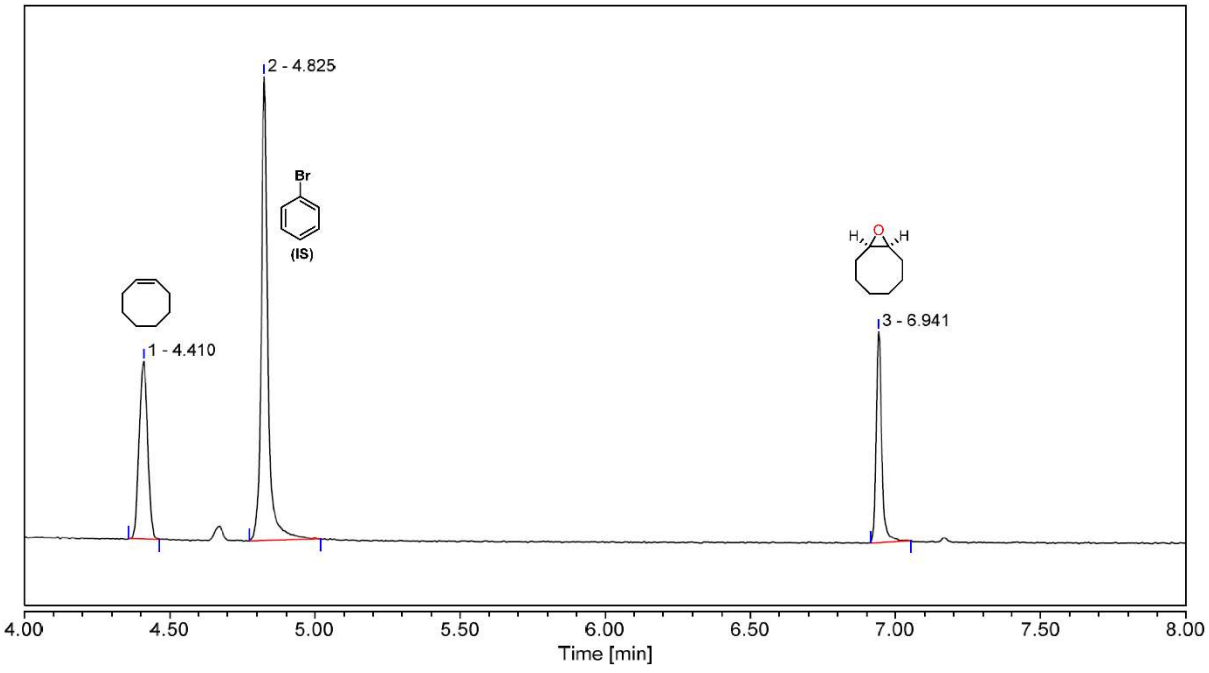


**Figure S67**. GC-MS traces for the oxidation of *cis*-cyclooctene in acetonitrile by $[Fe^{III}(Cl)bTAML]^{2-}$@2X TpDPP COF nano-spheres and NaOCl.

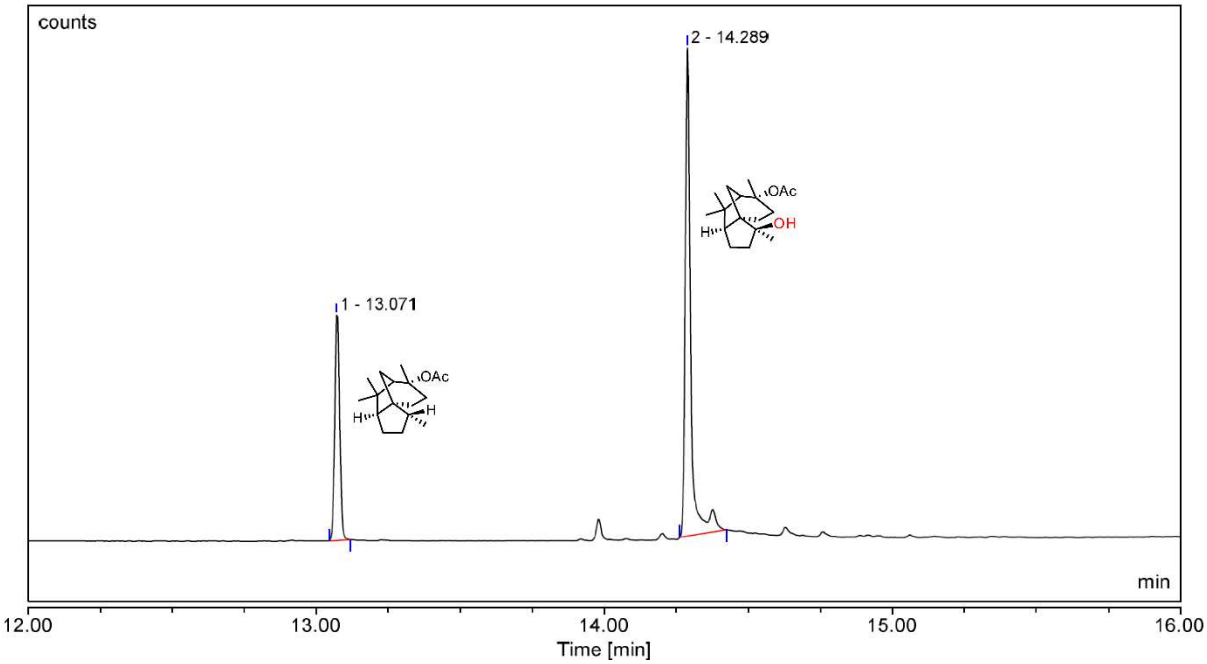


**Figure S68**. GC-MS traces for the oxidation of cedryl acetate in acetonitrile by $[Fe^{III}(Cl)bTAML]^{2-}$@2X TpDPP COF nano-spheres and NaOCl.

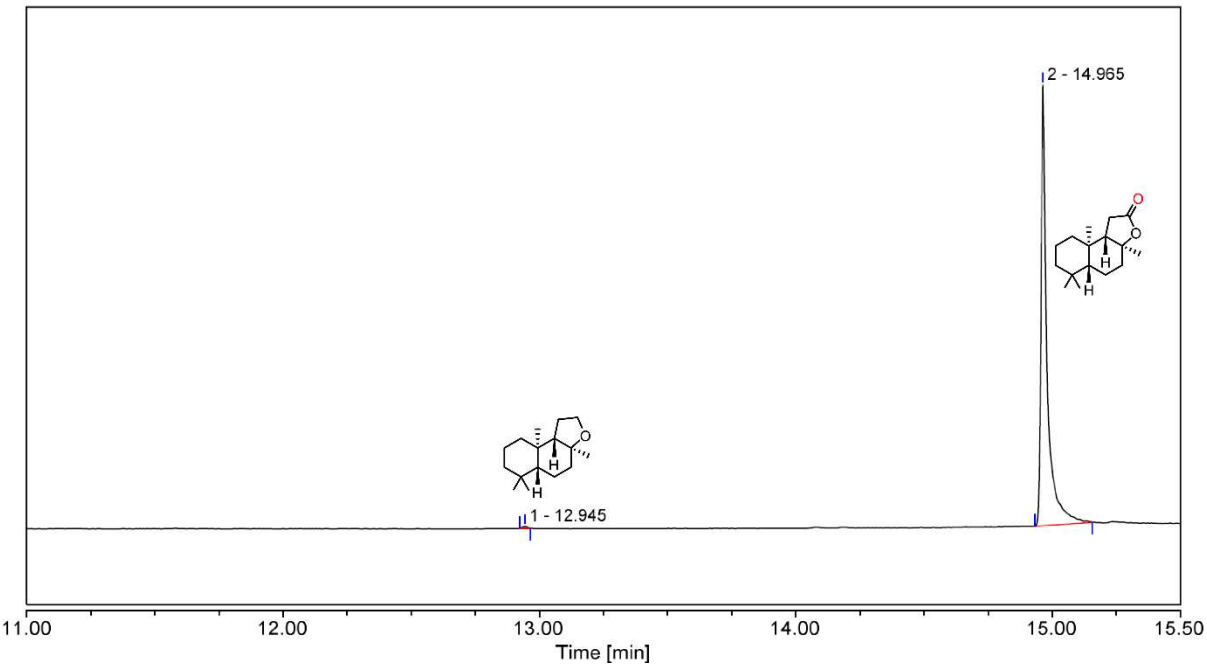


**Figure S69**. GC-MS traces for the oxidation of ambroxide in acetonitrile by $[Fe^{III}(Cl)bTAML]^{2-}$@2X TpDPP COF nano-spheres and NaOCl.

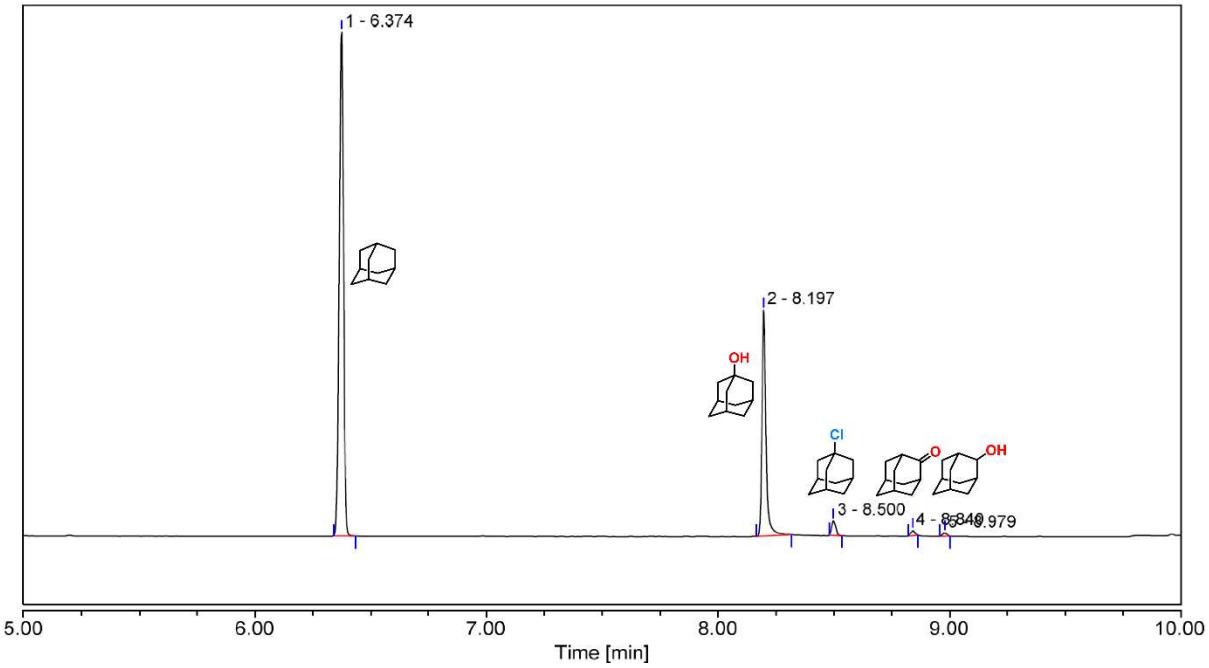


**Figure S70**. GC-MS traces for the oxidation of adamantane in water by $[Fe^{III}(Cl)bTAML]^{2-}$@TpDPP COF film and NaOCl.

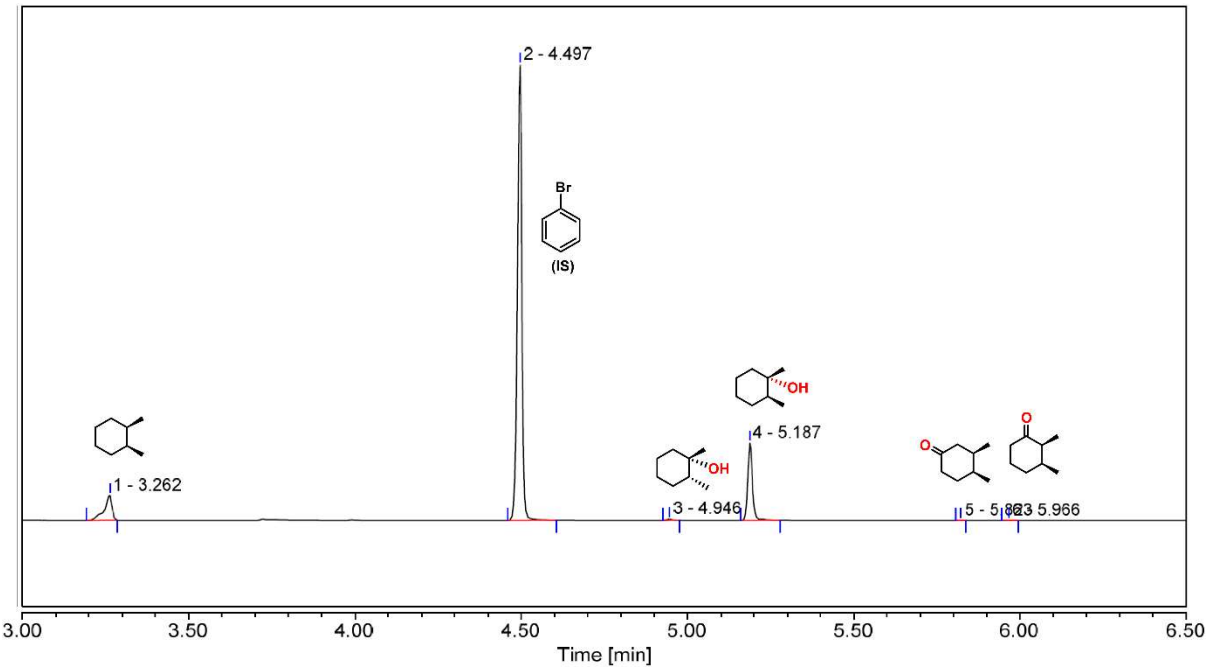


**Figure S71**. GC-MS traces for the oxidation of *cis*-dimethylcyclohexane in water by $[Fe^{III}(Cl)bTAML]^{2-}$@TpDPP COF film and NaOCl (**cycle – 1**).

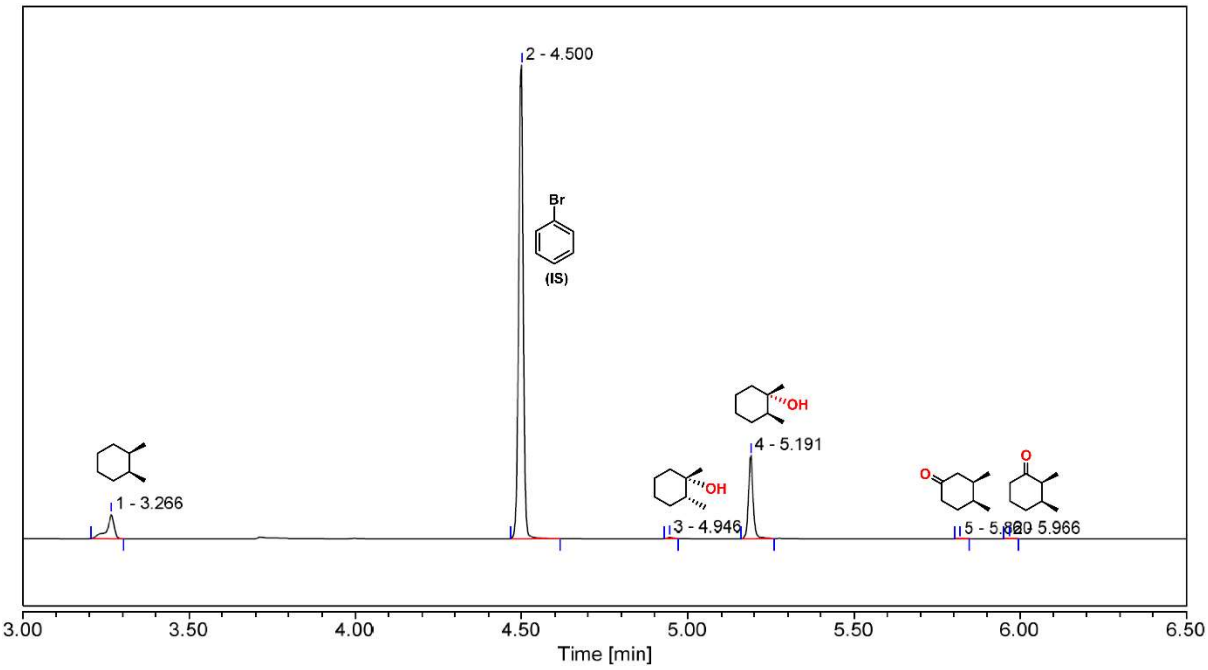


**Figure S72**. GC-MS traces for the oxidation of *cis*-dimethylcyclohexane in water by recyclable $[Fe^{III}(Cl)bTAML]^{2-}$@TpDPP COF film and NaOCl (**cycle – 2**).

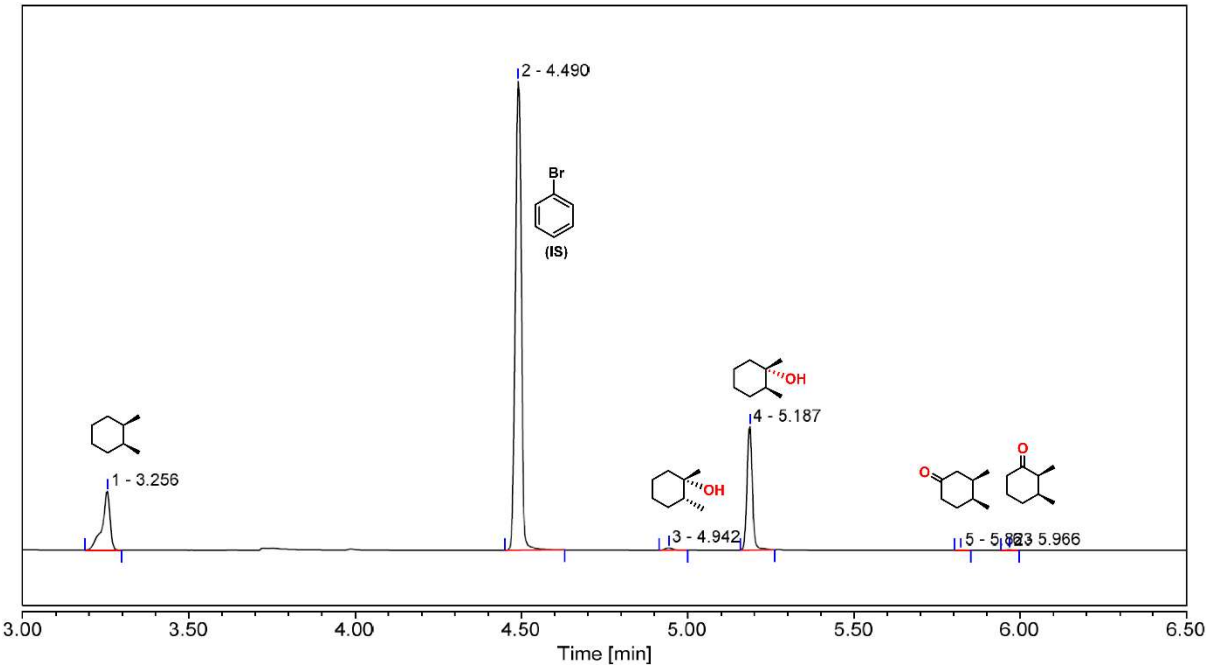


**Figure S73**. GC-MS traces for the oxidation of *cis*-dimethylcyclohexane in water by recyclable $[Fe^{III}(Cl)bTAML]^{2-}$@TpDPP COF film and NaOCl (**cycle – 3**).

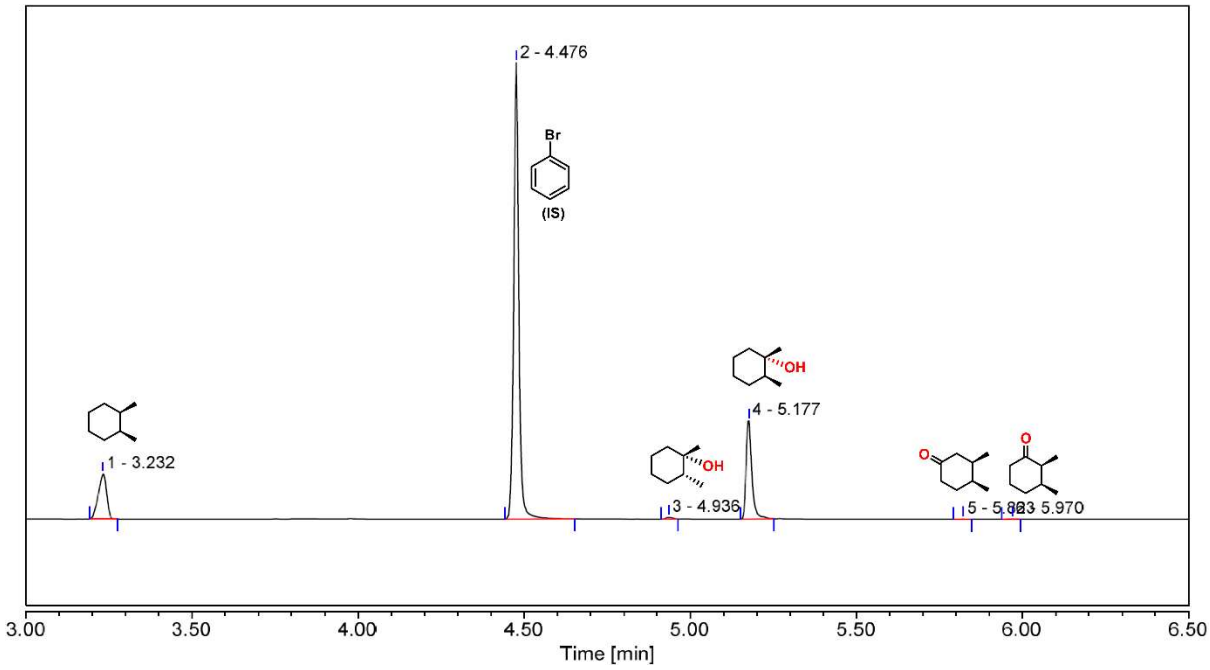


**Figure S74**. GC-MS traces for the oxidation of *cis*-dimethylcyclohexane in water by recyclable $[Fe^{III}(Cl)bTAML]^{2-}$@TpDPP COF film and NaOCl (**cycle – 4**).

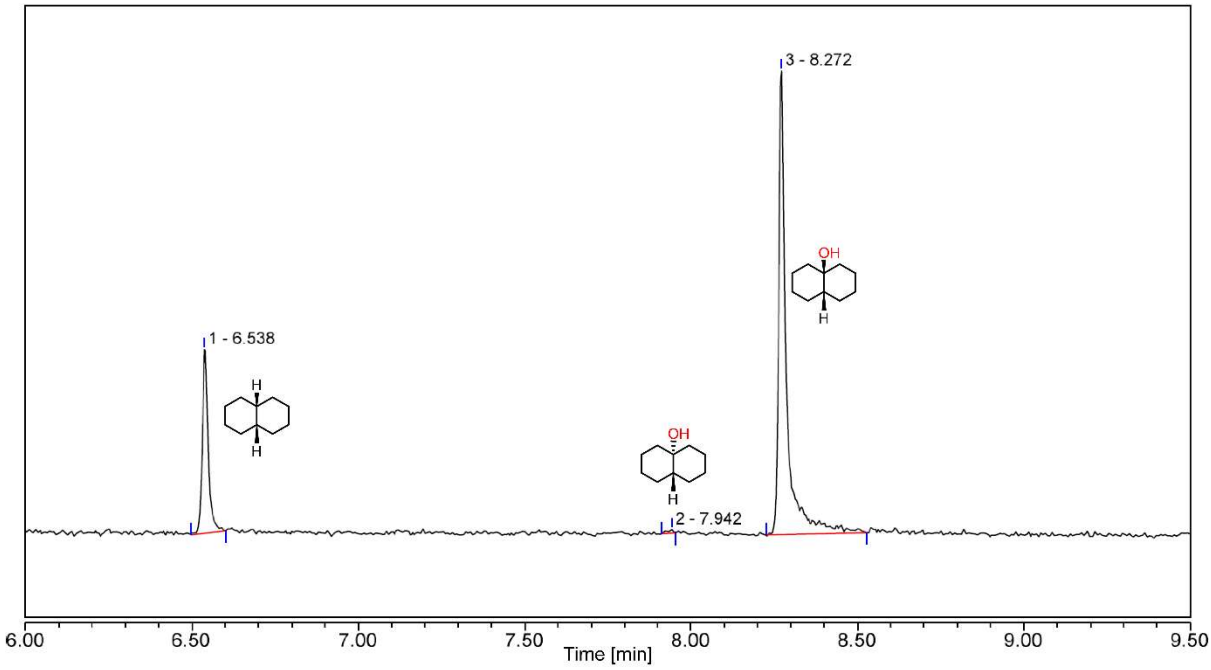


**Figure S75**. GC-MS traces for the oxidation of *cis*-dihydroanthracene in water by $[Fe^{III}(Cl)bTAML]^{2-}$@TpDPP COF film and NaOCl.

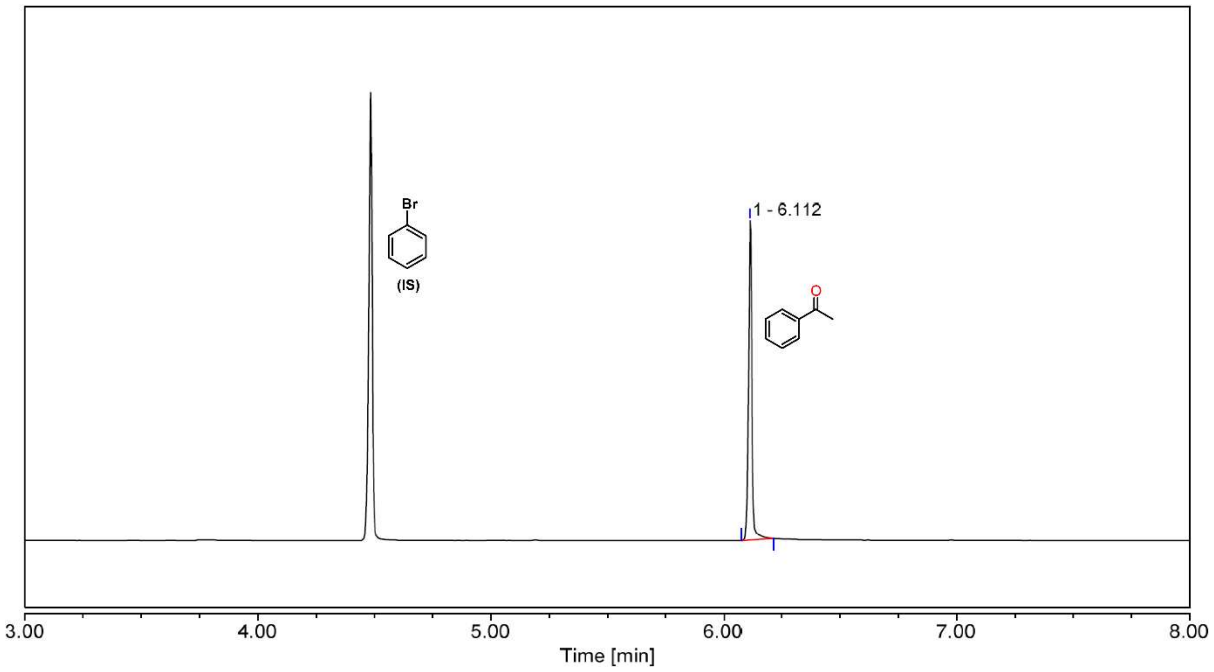


**Figure S76**. GC-MS traces for the oxidation of ethylbenzene in water by $[Fe^{III}(Cl)bTAML]^{2-}$@TpDPP COF film and NaOCl.

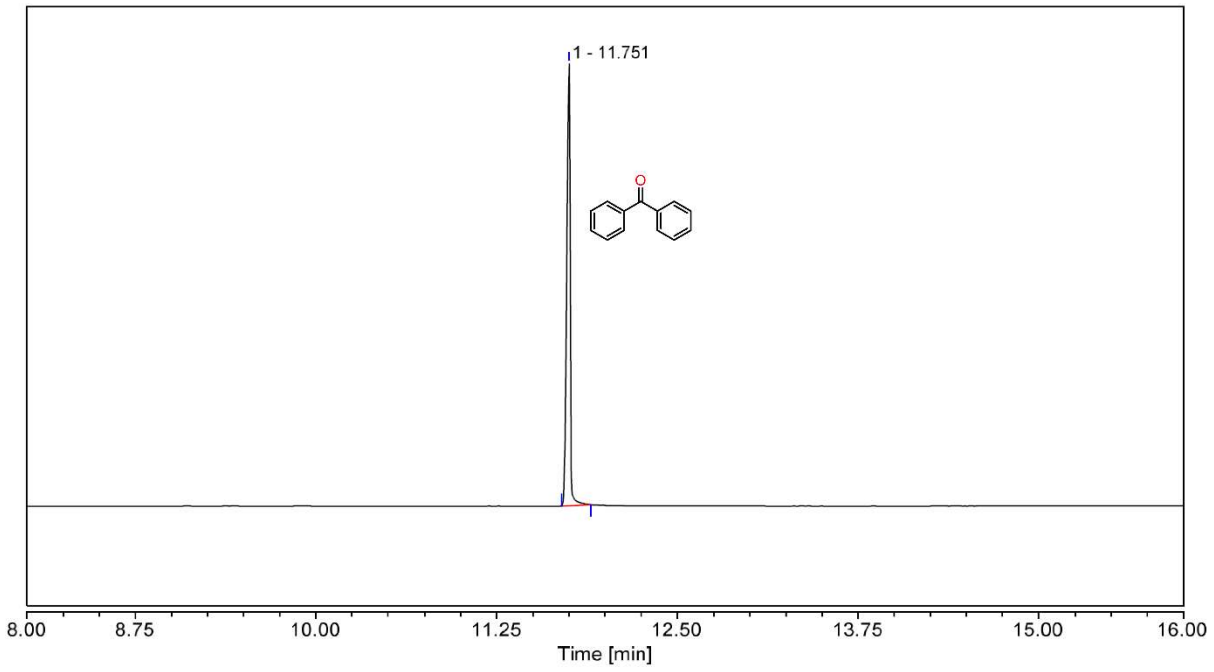


**Figure S77**. GC-MS traces for the oxidation of diphenylmethane in water by $[Fe^{III}(Cl)bTAML]^{2-}$@TpDPP COF film and NaOCl.

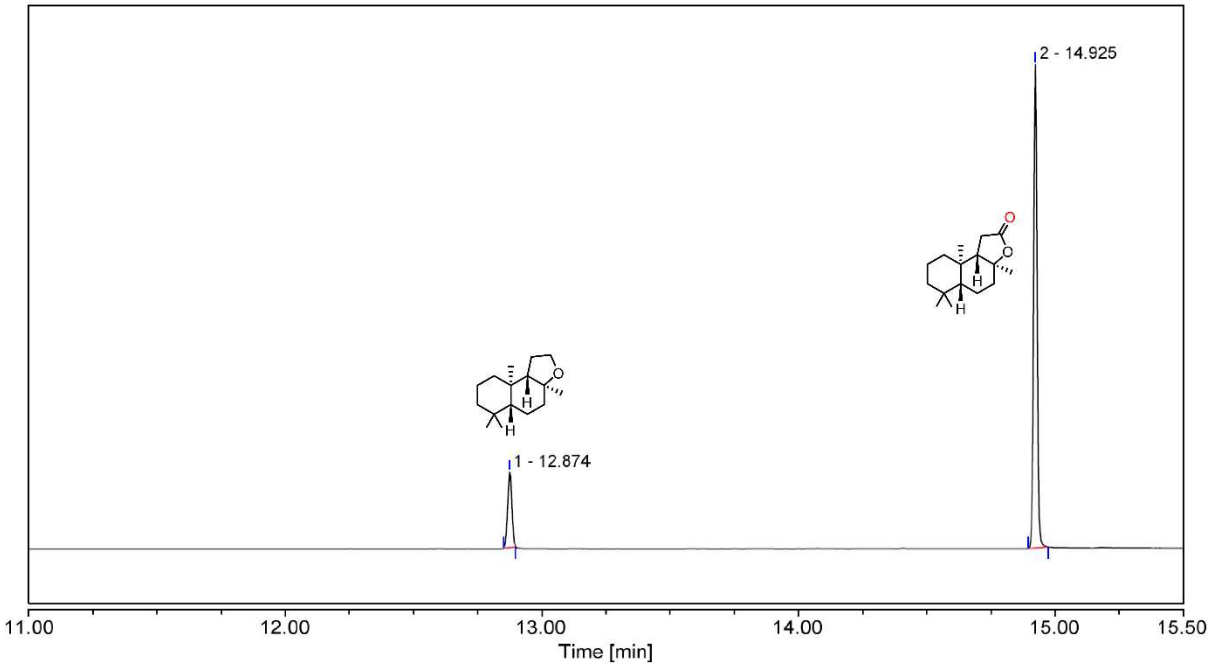


**Figure S78**. GC-MS traces for the oxidation of ambroxide in water by $[Fe^{III}(Cl)bTAML]^{2-}$ @TpDPP COF film and NaOCl.

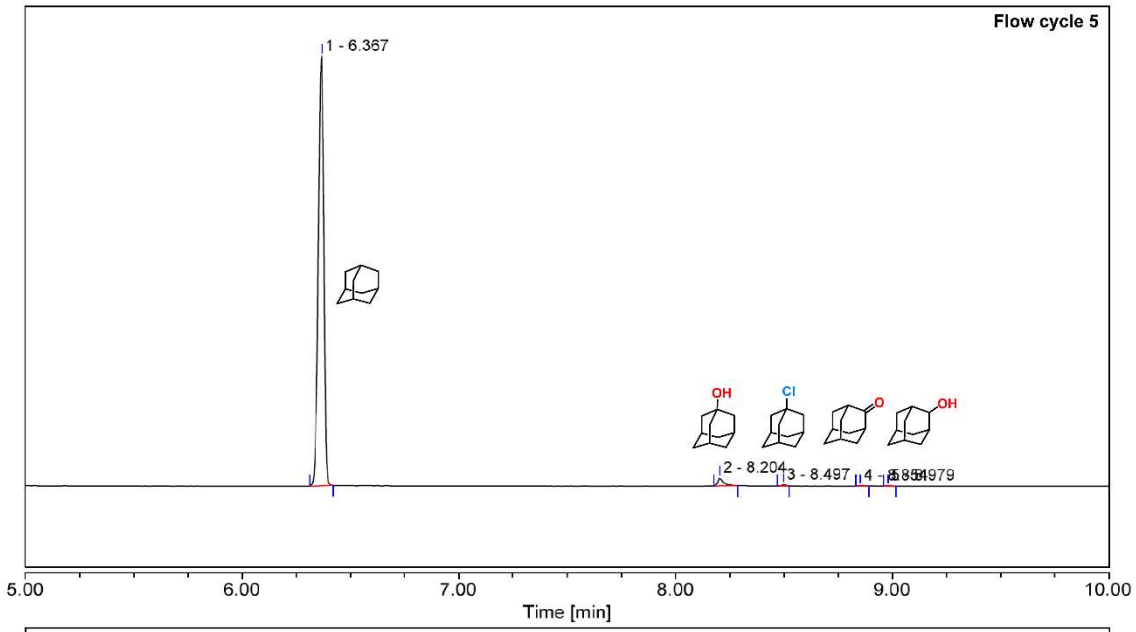
Flow cycle 5
1 - 6.367
OH
Cl
O
OH
2 - 8.204
3 - 8.497
5.00
6.00
7.00
8.00
9.00
10.00
Time [min]

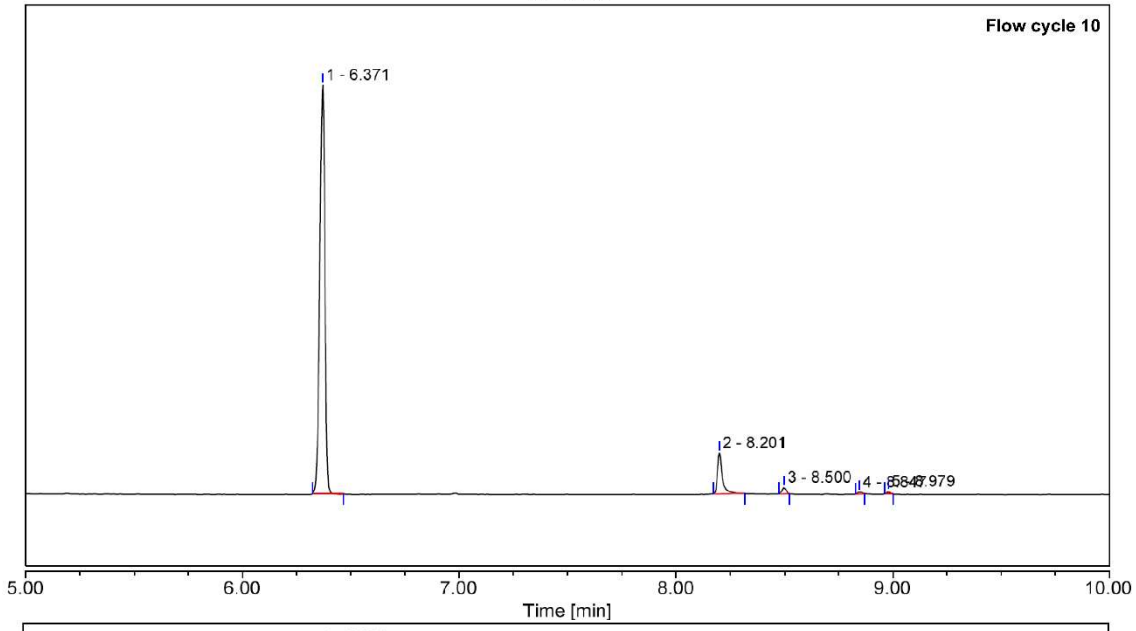
Flow cycle 10
1 - 6.371
2 - 8.201
3 - 8.500
5.00
6.00
7.00
8.00
9.00
10.00
Time [min]

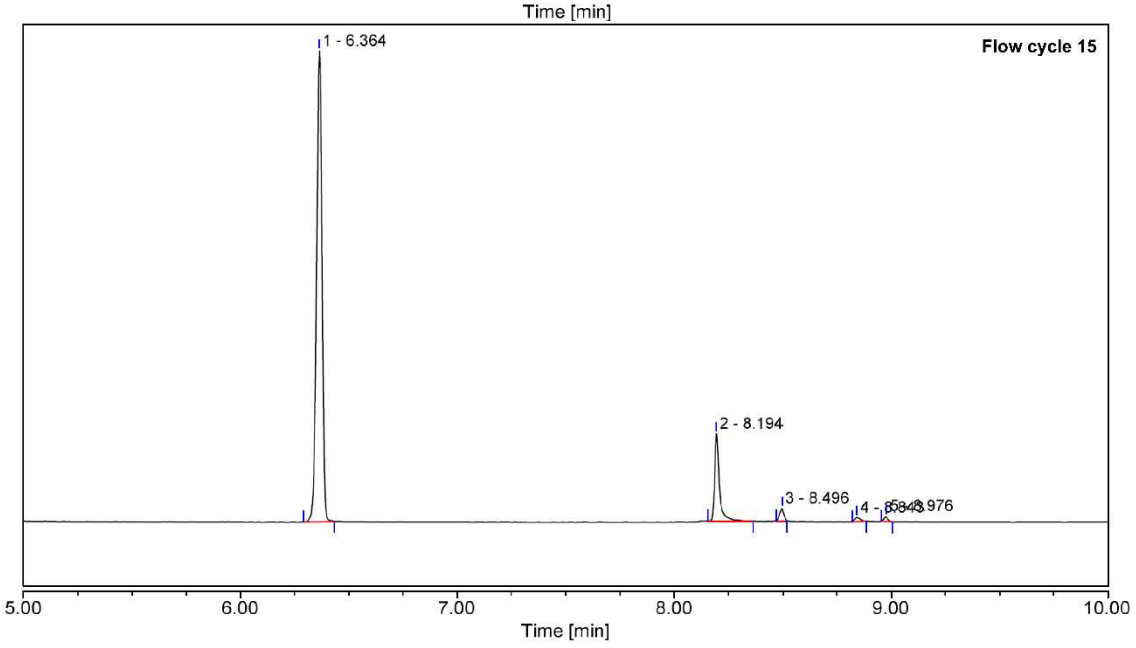
Flow cycle 15
1 - 6.364
2 - 8.194
3 - 8.496
5.00
6.00
7.00
8.00
9.00
10.00
Time [min]

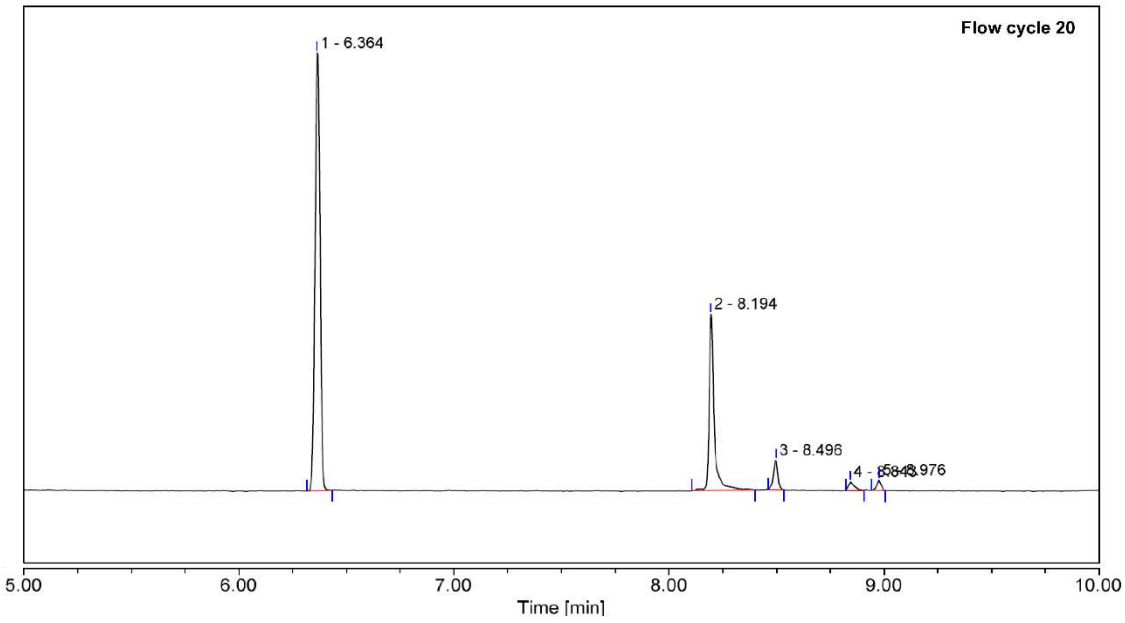
Flow cycle 20
1 - 6.364
2 - 8.194
3 - 8.496
5.00
6.00
7.00
8.00
9.00
10.00
Time [min]

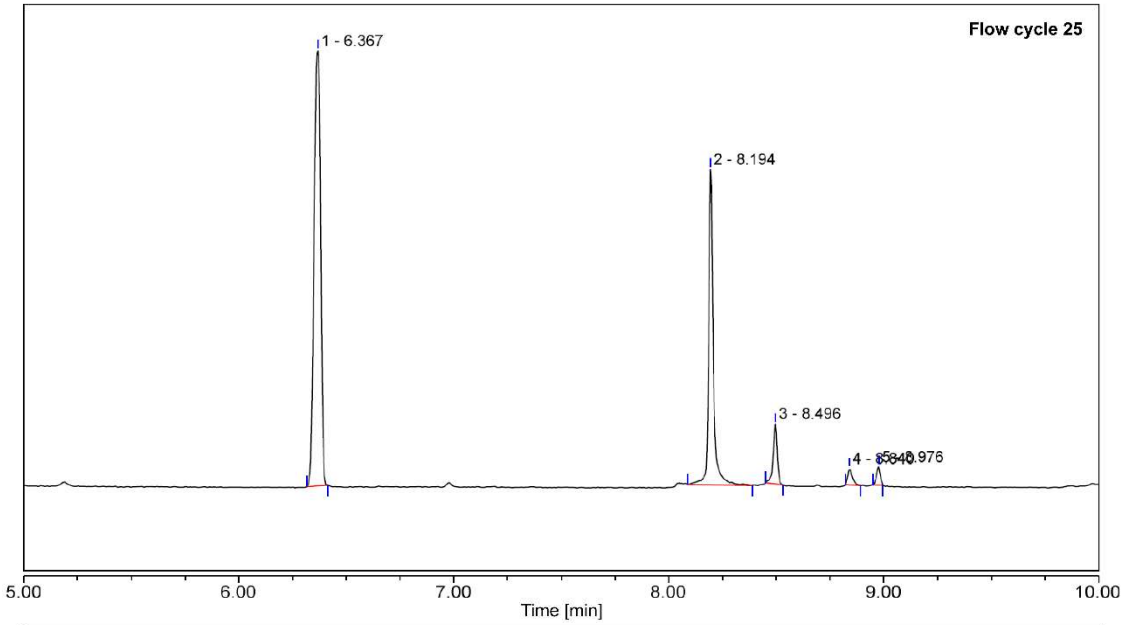
Flow cycle 25
1 - 6.367
2 - 8.194
3 - 8.496
5.00
6.00
7.00
8.00
9.00
10.00
Time [min]

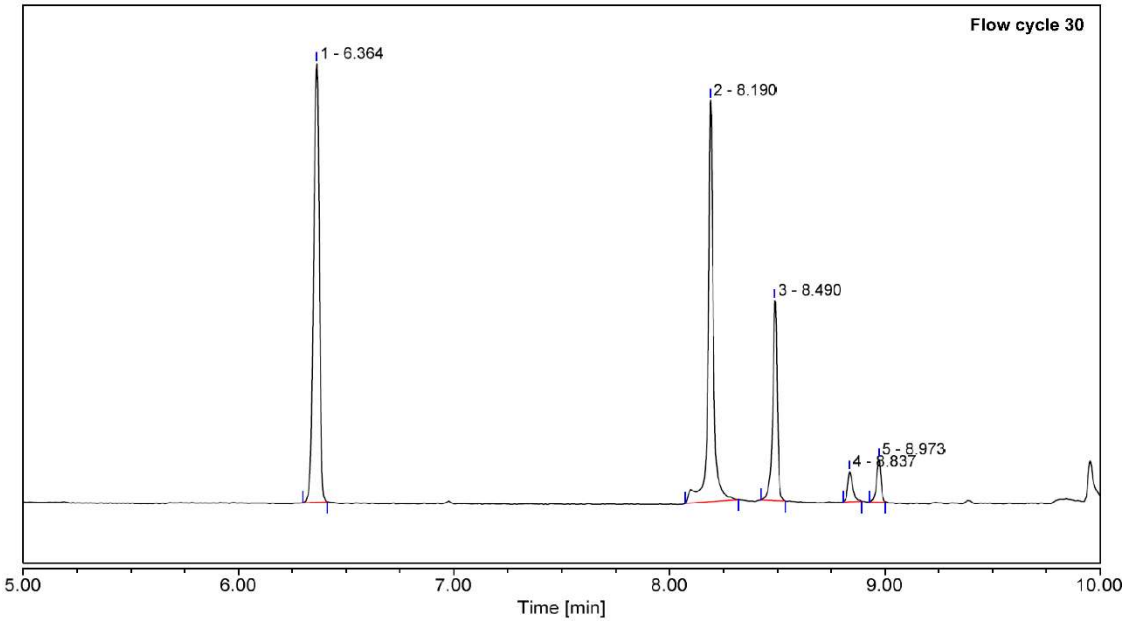
Flow cycle 30
1 - 6.364
2 - 8.190
3 - 8.490
4 - 8.837
5 - 8.973
5.00
6.00
7.00
8.00
9.00
10.00
Time [min]

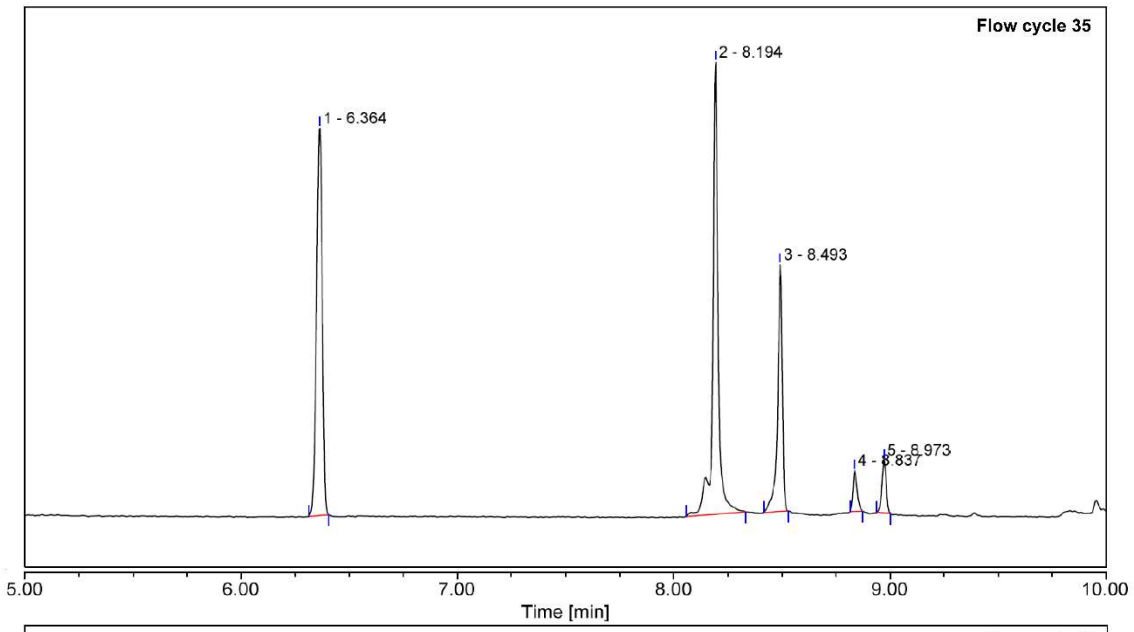
Flow cycle 35
1 - 6.364
2 - 8.194
3 - 8.493
4 - 8.837
5 - 8.973
5.00
6.00
7.00
8.00
9.00
10.00
Time [min]

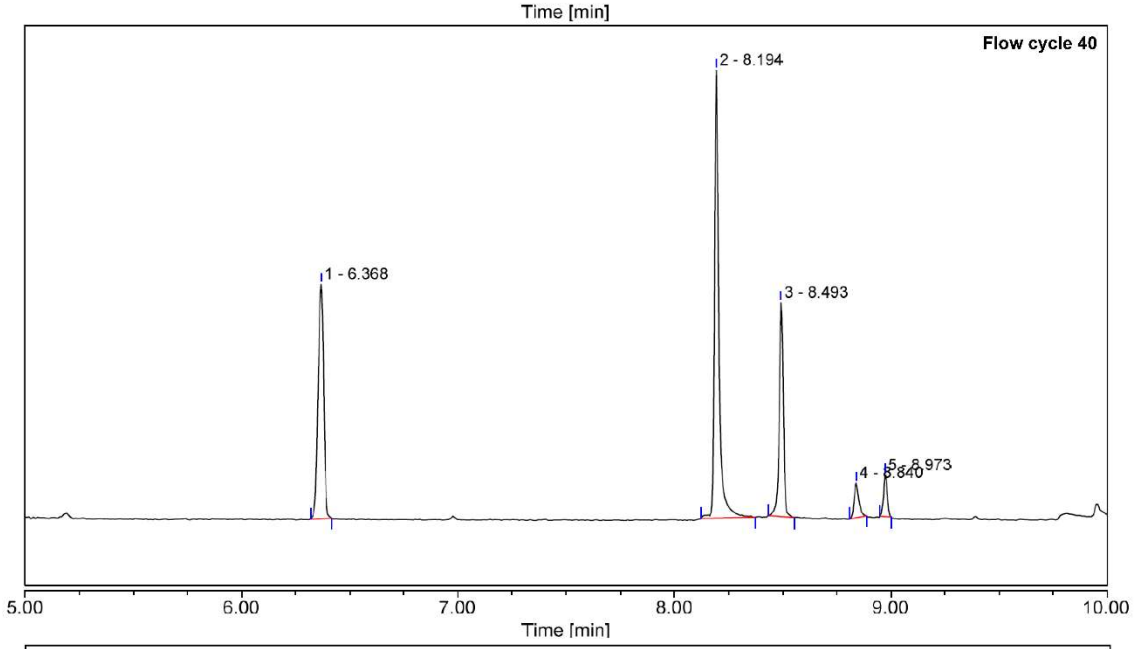
Flow cycle 40
1 - 6.368
2 - 8.194
3 - 8.493
4 - 8.840
5 - 8.973
5.00
6.00
7.00
8.00
9.00
10.00
Time [min]

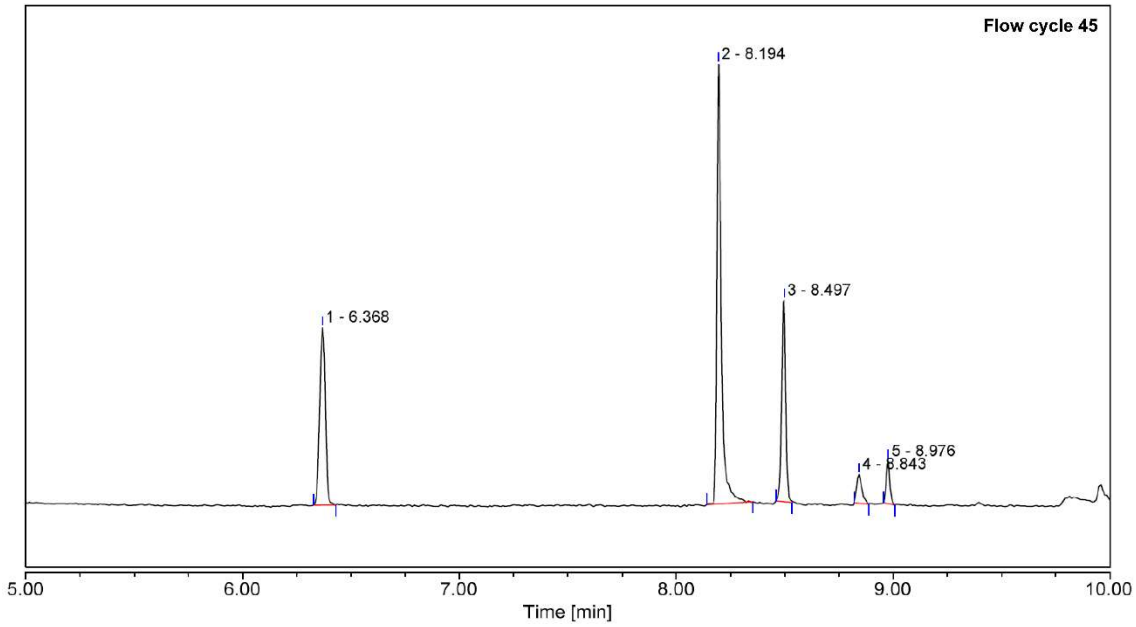
Flow cycle 45
1 - 6.368
2 - 8.194
3 - 8.497
4 - 8.843
5 - 8.976
5.00
6.00
7.00
8.00
9.00
10.00
Time [min]

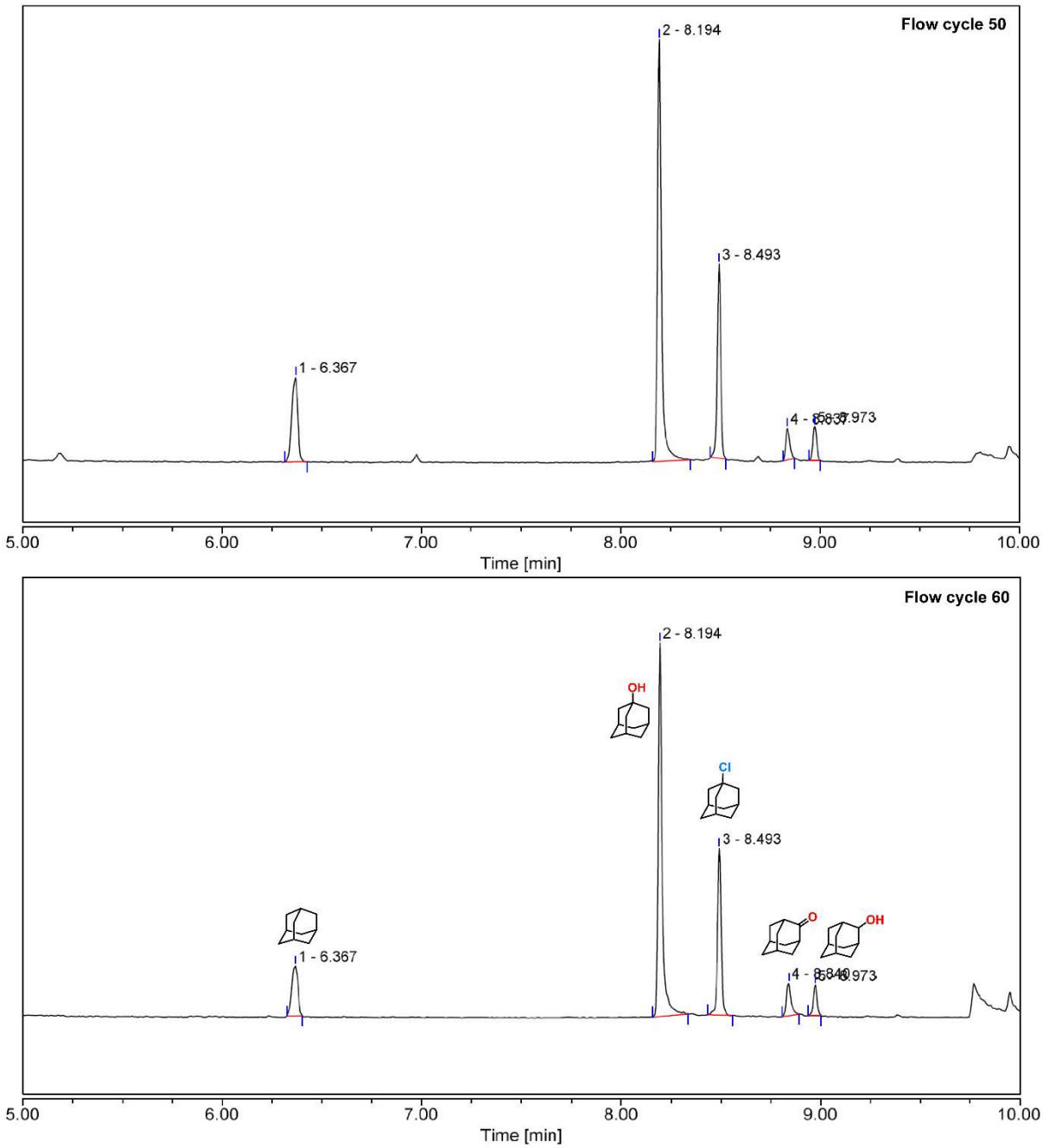


**Figure S79**. GC-MS traces for the oxidation of adamantane in acetonitrile by $[Fe^{III}(Cl)bTAML]^{2-}$@TpDPP COF film and NaOCl in flow catalysis up to 60 cycles.

We performed flow catalysis using catalyst immobilized COF thin films on a macroporous solid polymeric support to establish this C–H functionalization approach's generality. 90 mg (0.66 millimoles) adamantane was dissolved in 25 ml $CH_3CN$ (0.66 millimoles of bromobenzene as internal standard). It was passed through ~5 mg of $[Fe^{III}(Cl)bTAML]^{2-}$@TpDPP COF thin film (19wt% catalyst loading) for several cycles with iterative addition of NaOCl (0.06 M). After the 60th cycle, this inflow catalysis showcased the 72% catalytic yield

of 1-adamantanol with selectivity (3°:2°=32:1) and with an excellent turnover number of 355±5. The average rate of flow during the catalysis was measured as 4.5 ml $min^{-1}$.

## Section S-20: References


1. Kandambeth, S. et al. *J. Am. Chem. Soc*. **134,** 19524-19527 (2012).
2. Ghosh, M. et al. *J. Am. Chem. Soc.* **136,** 9524-9527 (2014).
3. Sasmal, H.S. et al. Covalent Self-Assembly in Two Dimensions: Connecting Covalent Organic Framework nano-spheres into crystalline and porous thin films. *J. Am. Chem. Soc.* **141,** 20371–20379 (2019).
4. Lukose, B., Kuc, A. & Heine, T. *Chem.Eur. J.* **17,** 2388-2392 (2011).
5. Chandra, B., Helllan, K. M., Pattanayak, S. & Gupta, S. S. Oxoiron(V) mediated selective electrochemical oxygenation of unactivated C-H and C=C bonds using water as oxygen source. *Chem. Sci.* **11,** 11877-11885 (2020).